UNIVERSITY OF CALIFORNIA
RIVERSIDE

Understanding and Engineering Alcohol-O-acetyl/acyltransferase in Yeast

A Dissertation submitted in partial satisfaction
of the requirements for the degree of

Doctor of Philosophy

in

Biochemistry and Molecular Biology

by

Jie Zhu

March 2017

Dissertation Committee:
Dr. Ian Wheeldon, Chairperson
Dr. Xin Ge
Dr. Russ Hille

The Dissertation of Jie Zhu is approved:

_____

_____

_____

Committee Chairperson

University of California, Riverside

ACKNOWLEDGEMENTS

First and foremost, I would like to thank my advisor, Dr. Ian Wheeldon, for giving me the opportunity to finish my PhD thesis in his lab, for his continual support, encouraging discussion and his confidence in me.

The Wheeldon group has been a source of friendships, great advice and collaboration, which contributed to all my working time on campus. I am especially grateful for working together with Cory Schwartz and Jyun-liang Lin. I really appreciated their enthusiasm and amazing ability for the research. Other group members that I have had the pleasure to work with are grad students, Ann-Kathrin Lobs, Louis Lancaster, Jordan Hall, and Brandon Simmons-Rawls; postdocs Yingning Gao; and undergraduate Miranda Diaz.

I would also like to thank Dr. Xin Ge and Dr. Russ Hille for their constant support, research advice, and friendship. And also, thank Dr. Seán O'Leary for reviewing my thesis and being here for my defense.

I am thankful to the publisher of the journal *Microbial Cell Factories* for the permission to reprint the contents of Chapter 2. The text of Chapter 3 and Chapter 4, in part, are reprints of materials as they appear in *Biotechnology Journal* (2016) and *ACS Synthetic Biology* (2017, under review).

Last, I would like to thank my parents for all their love and support during these five years far away from them. Without you, it is impossible for me to stand here and present my work.

ABSTRACT OF THE DISSERTATION

Understanding and Engineering Alcohol-O-acetyl/acyltransferase in Yeast

by

Jie Zhu

Doctor of Philosophy, Graduate Program in Biochemistry and Molecular Biology
University of California, Riverside, March 2017
Dr. Ian Wheeldon, Chairperson

Production of renewable, non-toxic and environmental-friendly biofuels and chemicals has been the focus of metabolic engineering. To achieve high yield production by microbial cell factories, it is necessary to identify highly active biocatalysts and engineer efficient biosynthetic pathways. Alcohol-O-actyl/acyltransferase (AATase) is responsible for synthesis of fatty acid ethyl esters (FAEEs) by condensing acetyl/acyl-CoAs and ethanol in yeast and plants. This work demonstrated that *S. cerevisiae* is a suitable host for FAEE production, because AATase has higher specific enzymatic activity compared to that in *E. coli*. To enable the rapid profiling of AATase activities, a spectrophotometric-based coupled enzyme assay was developed for high throughput screening of AATase enzymatic activity. With this assay, a library of AATases was characterized for the substrate specificity towards acyl-CoAs and Atf-Sl from tomato was discovered with high activity towards various alcohols. Enzyme co-localization and substrate channeling are strategies to improve enzyme cascade reaction rate and yield. A protein-based scaffold based on oleosin-cohesin-dockerin was developed for co-

localizing multienzyme pathways on the surface of intracellular lipid droplets (LDs). The upstream enzyme in yeast ester biosynthesis was recruited to the native localization LDs of the terminal reaction step, AATase.

Fluorescent microscopy studies show that most of the endogenous AATases in *S. cerevisiae* are localized to LDs. To understand the localization mechanism and trafficking pathway of AATase, structure-function analysis and protein-protein interaction studies were performed for Eht1 and its paralogue Eeb1, which arose from genome duplication. N- and C-terminal regions of Eht1 are necessary for initially targeting to the ER membrane and subsequent sorting to LDs. Eht1 is a peripheral membrane protein on ER with both termini exposed to cytosol. The translocation from ER to LDs of Eht1 is related to translocons on the ER. Immunoprecipitation and MS analysis have identified possible physical protein interactions of Eht1 to assist in the trafficking from the ER to LDs. Combined, this work not only engineers AATase in *S. cerevisiae* by investigating highly active AATase and spatially organizing multienzyme pathways, but also understand the mechanism of AATase ER-dependent LDs targeting.

Table of Contents

LIST OF FIGURES

LIST OF TABLES

Chapter 1. Introduction

1.1 Background

Renewable fatty acid-derived chemicals have been an effort for metabolic engineering in last decades. In this thesis, we are interested in producing fatty acid esters. Volatile short and medium chain fatty acid ethyl esters (FAEEs) have distinctive odors and flavors to be widely used in food, beverage, cosmetic and pharmaceutical fields. Long chain wax ester is an attractive biodiesel substitute due to the high energy density and low environment toxicity. Compared to traditional extraction and chemical synthesis of esters, microbial cell factories have been increasingly attractive as an alternative approach for production of various fatty acid esters. All living organisms have endogenous pathways to produce fatty acids and the biosynthesis and regulation have been comprehensively studied and understood in both prokaryotes (2,3) and eukaryotes (4), which open the possibility to utilize microbial cell factories for ester production. Engineered strains can be cultured in industrial-scale bioreactors to convert biomass-derived carbohydrates to desired products through designed microorganism metabolic pathways (Figure 1.1).

1.1.1 Microbial cell factories for biofuel production

Two most common strains used in industrial fermentation are *Escherichia coli* and *Saccharomyces cerevisiae*. *E. coli*, a prokaryote, has been engineered for biodiesel production, including alcohols (1-3) and fatty acid esters (4,5). *S. cerevisiae*, a model yeast, has also been successfully engineered to effectively produce biodiesel (6,7). In our

studies, we are interested in producing FAEEs, which have lower negative environmental effect and slightly higher stability against oxidation compared to fatty acid methyl esters (FAMEs) (8).

E. coli and *S. cerevisiae* both have advantages and disadvantages and have been used as microbial cell factories with designed pathways for FAEEs production (Figure 1.2). The benefits of using *E. coli* include its fast growth rate and ability to be easily genetically modified. However *E. coli* as a host has drawbacks. For example, the product of fatty acids is catalyzed by fatty acyl-acyl carrier protein (ACP) (9), which is linked by enzyme and needs to be hydrolyzed by a thioesterase to free fatty acids. Fatty acid is subsequently converted to fatty acyl-CoA to substrates of alcohol acetyl/acyltransferases (AATases). In addition, *E. coli* is susceptible to phage attacks during industrial fermentation, which can limit production at scale.

Yeast system is more direct and efficient to produce FAEEs, since its fatty acids biosynthetic pathway is much shorter and simpler compared to *E. coli*. The product of *S. cerevisiae* fatty acid synthase is in the form of fatty acyl-CoA (10), the right substrate for AATases. Also, yeast is a robust industrial organism because of its ability to grow at low pH is not susceptible to phage contamination. But, there are some bottlenecks of producing FAEEs in yeast, like the limited supply of fatty acid biosynthesis precursor and cofactors, the tight regulation of fatty acid metabolism, and product toxicity (11).

1.1.2 Biocatalysts to synthesize FAEE

Esterification of organic acid with alcohol is a well-developed process for industrial production. This reaction relies on high temperature and acidic condition to overcome the thermodynamically favored hydrolysis of esters under ambient temperature (12). Ongoing trends in process improvements, such as cost reduction, increasing quality and safety requirements, and increasing environmental conscientiousness and regulation of industrial chemical production have increased the interest in the biocatalysis research. Enzymatic catalysis can address many of the above mentioned concerns as it works under milder conditions and with appreciable selectivity (13).

In nature, there are several classes of biocatalysts responsible for the ester synthesis, such as carboxylesterase (carboxyl ester hydrolase), alcohol dehydrogenase (Adh; EC 1.1.1.1) and alcohol-O-acetyl/acyltransferase (AATase; EC 2.3.1.84) (Figure 1.3). Non-specific esterase (EC 3.1.1.1) and lipase (EC 3.1.1.3), belonging to carboxylesterase, are differentiated on the basis of their substrate specificity (14). A common problem for transesterification reaction catalyzed by hydrolase is the low product yield since the concentration of water in aqueous solution is high. In addition, most of the esters have poor solubility in water, and therefore reactions must be carried out in diluted aqueous solution, which further reduces their value (15). Another pathway for ester synthesis proceeds via hemiacetal dehydrogenation (HADH) reaction, catalyzed by Adh. Its physiological role is not well understood yet, and a possible role could be to remove the toxic aldehydes formed under low reductant (NADH) condition (16). The other

distinctive class of enzyme is AATase, which catalyze the condensation of alcohols and acetyl- or acyl-CoA to synthesize ester (17).

During yeast fermentation and fruit ripening short chain linear and branched alcohols are converted to corresponding acetate esters. AATase genes from yeast and fungi have been cloned and sequenced, and the differences between them are considerable with respect to activity and substrate specificity (16). AATase broad specificity towards extensive substrates (18) enable it to play significant roles in metabolic engineering and industrial fermentations to produce esters, especially short and medium chain fatty acid esters. Another property of interest is the intracellular localization of AATases (Table 1.1). Most of them are membrane associated, such as cell membrane, lipid droplets (LDs) and endoplasmic reticulum (ER).

1.1.3 AATases of *S. cerevisiae*

FAEEs are secondary metabolites *in S. cerevisiae*, their natural physiological role is not well understood and the details about the metabolic pathway of FAEE biosynthesis are not well elucidated. Short and medium chain length (C2-C12) FAEEs contribute to the flavor of fruits and industrial fermented beverages; for example ethyl hexanoate smells like apple, ethyl octanoate like citrus and ethyl decanoate like floral aromas. In *S. cerevisiae*, short and medium chain FAEEs are synthesized by AATases, Atf1p/Atf2p and Eht1p/Eeb1p. Atf1p is responsible for majority of short chain acetate esters, while Atf2p palys a minor role. Deletion of ATF1 gene caused a reduction of 60 to 90% compared to the level in wild-type cells. Single deletion of ATF2 result in only 10 to 35%

decreases in the formation of most esters. Overexpression of ATF1 caused greater increases in ester formation than overexpression of ATF2. Double knockout strain of ATF1 and ATF2 eliminated isoamyl acetate synthesis, but still produced the same concentrations of medium-chain fatty acid ethyl esters as the wild-type cells (19). This indicates that other enzymes, such as Eht1p and Eeb1p instead of Atf1p or Atf2p, are involved in synthesis of these esters in yeast under fermentation condition (20).

1.1.4 Physiological role of short and medium-chain FAEEs biosynthesis

Previous studies suggest that AATases might play important roles in cellular lipid metabolism and detoxification processes. AATases are involved in the esterification and detoxification of endogenous produced fatty acids, which are toxic compounds for yeast similarly to that observed for exogenously added fatty acids. Upon release from the fatty acid synthase complex, fatty acids rapidly dissociate and thus are unable to cross cellular membranes. Esterification allows diffusion of the fatty acid residues and could thus serve as a strategy to remove toxic substrates, AATases localization on the lipid droplets further supports this hypothesis by condensing the ethanol and fatty acids derived acyl-CoAs. Atf1p and Atf2p found to be associated with ER, and subsequently localized to LDs in *S. cerevisiae* (21).

1.1.5 Lipid droplets of yeast

The ability to synthesize neutral lipids and store them as cytoplasmic LDs is a property of eukaryotes (22-24) and even of some prokaryotes (25). LDs of yeast are

composed of a hydrophobic core of neutral lipids, nearly equal amounts of steryl ester (STE) and triacylglyceride (TAG), that is surrounded by a phospholipid monolayer (26) (Figure 1.4). This unique structure provides separation of aqueous and organic phases in the cell, requiring proteins to have specific features for targeting and localizing to LDs.

There is a distinctive set of proteins decorating LDs. However, it is not well understood how proteins target LDs and how this localization is regulated. Most of these proteins are required for lipid metabolism (27), while some lipolytic enzymes are also found to be associated with LDs (28). This suggests that LDs is not only a storage organelle in yeast, but also involved in lipid metabolism. LDs might also contribute to intracellular signaling, protein storage and degradation, and the exchange of lipids between organelles (29-33). LDs dynamically interact with other cellular organelles (34), including ER (35), endosomes (36), peroxisomes (37), and the plasma membrane (38) (Figure 1.5).

The mechanisms of how neutral lipids accumulate and form LDs are currently under study, and several models have been proposed. These models share a common hypothesis that LDs are derived from the ER, where most of the enzymes involved in the neutral lipids formation localize. The canonical model, called the ER-budding model, proposes that neutral lipids form a lens of oil in the ER bilayer and subsequently buds from the membrane, taking with them phospholipids from the ER cytosolic leaflet (Figure 1.6). Alternative models have also been posited, like the Bicelle model and the vesicular-budding model (39). There is substantial evidence to support the canonical model; however, it has not yet been directly observed.

Due to the unique monolayer structure of LDs, proteins that associate with LDs likely have critic structure proteins. The study of LD protein composition of LDs is commonly facilitated by well-established cell fraction methods via sucrose-gradient ultracentrifugation, as well as advanced proteomic technologies and mass spectrometry. Hundreds of coating proteins have been identified and some of them have been further verified by biochemical, microscopic, and functional assays. Among attempts for LD proteome studies of different cell types and organisms, several functional groups of proteins are present consistently and reproducibly, including lipid synthetic enzymes, membrane trafficking proteins, signaling proteins and proteins involved in protein degradation (26,31,40). In addition, some proteins are found in the hydrophobic core of LDs, such as perilipin family proteins (41,42). However, the mechanism of proteins localization to LDs remains to be determined.

Based on the localization origin, proteins targeting to LDs can be sorted in two different classes. Class I proteins can access LDs from the ER either during LD formation or after formation via ER-LD contact sites with an internal hydrophobic hairpin motif or N-terminal hydrophobic sequences. Class II can access to LDs surface from cytosol and bind through amphipathic helices or multiple amphipathic and hydrophobic helices (43). Some proteins that clearly target LDs have been difficult to classify. For example, in yeast, two alcohol acetyl/acyltransferases (AATases), Atf1 and Atf2, localize to the ER and subsequently are sorted to LDs. Segments of the N- and C-terminal amphipathic helices are required for both ER and LDs association (21). The targeting mechanism of AATases is unknown, as is whether AATases target via Class I or Class II pathway.

LD proteomes are adjusted to match metabolic requirements depending on nutrient availability and cell proliferation. In principle, the proteins are removed via relocalization or degradation when LDs shrink during. Class I proteins are thought to degrade either after relocalization of the protein to ER through ER-associated degradation (ERAD) (44) or are directly degraded at the LDs. Removal of Class II proteins may be related to the surface dependent displacement to relieve the surface pressure of LD surface monolayer, or chaperone-mediated autophagy (45,46). Again, the removal of proteins from LDs is poorly understood and remains to be elucidated.

1.2 Dissertation Organization

The general goal of this thesis is to understand and engineer AATases for short and medium chain FAEEs production. To achieve this goal we asked the following questions and developed new engineering technologies. For fundamental study, we want to understand the protein targeting and trafficking mechanism for LD-localized AATase. For industrial application and engineering, we want to answer this question first, which microbial cell factories is a better choice to engineer for FAEE production? Additionally, we want to develop a rapid and high throughput screening method for AATase activity. With the suitable microbial cell factory and highly active AATase, can we develop some biosynthetic strategies to improve FAEE production rate and yield?

In Chapter 1, background of this thesis is presented. At first, the importance of the renewable production of chemicals and fuels in microbial cell factories is addressed. To produce and medium chain FAEEs biologically, we seek to engineer new strains of *S.*

cerevisiae. Even though there are different enzymes that can synthesize esters in nature, AATase was selected for its high activity, broad substrate specificity and native expression in *S. cerevisiae*. Beyond engineering AATase, biochemical studies could help to understand the native physiological role of FAEE synthesis and LDs formation mechanism in *S. cerevisiae*.

In Chapter 2, we use two common microbial cell factories, *E. coli* and *S. cerevisiae*, to produce the short chain FAEE, ethyl acetate by overexpressing various AATases from yeast and fruit tomato. All studied AATases formed intracellular aggregates with low enzymatic activity when expressed in *E. coli*, and any membrane association observed in *S. cerevisiae* was lost in *E. coli*. The expression level of Atf1 and Atf (from *Solanum lycopersicum*) in *E. coli* was up to 100-fold higher than in *S. cerevisiae*. Fermentation and whole cell lysate activity assays demonstrated that the aggregates in *E. coli* were active, but with highly reduced specific activity compared to the activity in *S. cerevisiae*. Activity was partially recovered with lower expression levels, coinciding with smaller aggregate size. These results provide important information on the biochemistry of AATases under homologous and heterologous expression; furthermore, we make the decision to utilize *S. cerevisiae* as the microbial host to produce short and medium chain FAEEs.

There have been previous successes in engineering ester biosynthesis in microbial cell factories; however, protein engineering and enzyme screening have been limited due to a lack of suitable assays for high throughput screening. Traditional headspace gas chromatography (GC) analysis of volatile short chain esters or thin layer chromatography

(TLC) and GC-MS analysis of long chain esters are time consuming and having low throughput. In Chapter 3, we developed a coupled-enzyme assay to quantify ester production spectrophotometrically. Importantly, the assay is suitable for whole cell lysate reactions in 96-well plate. The assay was used to screen a library of AATases for short and medium chain FAEEs synthesis, including AATases from *Saccharomyces* yeast, and two AATases from fruits. In addition, the substrate specificity of Atf1-S.l was characterized towards short and medium chain acyl-CoAs and various alcohols. This coupled enzyme assay will accelerate the protein engineering and new enzyme discovery of AATase, further to improve the production rate of FAEEs in *S. cerevisiae*.

In Chapter 4, the concept of substrate channeling concept via enzyme co-localization strategy was explored with the goal of improving ester production and yield. Substrate channeling is the transfer of a pathway intermediate to transfer from one active site to another without diffusing to the bulk environment (47-49). We engineered an enzyme co-localization protein scaffold to assemble the ethyl ester biosynthesis pathway on intracellular LDs. The rate of ethyl acetate production was increased ~ 2-fold by re-organizing pathway enzymes, controlling architecture of co-localization, and optimizing protein expression levels. This is a possible strategy for engineering synthetic metabolic pathways with controlled intracellular localization.

In Chapter 5, we reveal that the medium chain fatty acid ester synthase, Eht1 is membrane-associated protein, and is localized to ER and LDs. However, it has no clear transmembrane domains and there is no evidence of amphipathic helices or other known LD targeting domains. Structure-function analysis suggests that both N- and C-termini

are important for its membrane association. Fluorescent microscopy analysis suggests that ER translocons may be related to the translocation process of Eht1. Furthermore, we conducted immunoprecipitation experiments and identified associated proteins by mass spectrometry to understand how the interaction between Eht1 and other proteins contribute to the trafficking. In addition, we explored the genetic interactions between the MS-identified proteins and Eht1 with the knockout library. These fundamental studies of Eht1 have also enabled the control trafficking of a close homolog, Eeb1. We demonstrate that control enzyme localization can enhance expression and function.

In the final chapter we summarize the main conclusions of each of previous chapters and discuss possible extensions of this thesis. Our work on microbial host selection, high throughput assay development, and pathway co-localization with protein scaffold contributes to the improvement of FAEEs production rate and yield. This work also raises new questions and investigates novel ways to better understand protein localization on the unique organelle, LDs. Finally, we discuss potential application of the high throughput assay and pathway co-localization on LDs, and highlight future work that will expand on the studies presented here.

1.3 References

1. Atsumi, S., Hanai, T., and Liao, J. C. (2008) Non-fermentative pathways for synthesis of branched-chain higher alcohols as biofuels. *Nature* **451**, 86-U13

2. Desai, S. H., Rabinovitch-Deere, C. A., Tashiro, Y., and Atsumi, S. (2014) Isobutanol production from cellobiose in Escherichia coli. *Applied microbiology and biotechnology* **98**, 3727-3736

3. Hanai, T., Atsumi, S., and Liao, J. C. (2007) Engineered synthetic pathway for isopropanol production in Escherichia coli. *Applied and environmental microbiology* **73**, 7814-7818

4. Steen, E. J., Kang, Y., Bokinsky, G., Hu, Z., Schirmer, A., McClure, A., Del Cardayre, S. B., and Keasling, J. D. (2010) Microbial production of fatty-acid-derived fuels and chemicals from plant biomass. *Nature* **463**, 559-562

5. Kalscheuer, R., Stolting, T., and Steinbuchel, A. (2006) Microdiesel: Escherichia coli engineered for fuel production. *Microbiology* **152**, 2529-2536

6. Runguphan, W., and Keasling, J. D. (2014) Metabolic engineering of Saccharomyces cerevisiae for production of fatty acid-derived biofuels and chemicals. *Metabolic engineering* **21**, 103-113

7. Steen, E. J., Chan, R., Prasad, N., Myers, S., Petzold, C. J., Redding, A., Ouellet, M., and Keasling, J. D. (2008) Metabolic engineering of Saccharomyces cerevisiae for the production of n-butanol. *Microbial cell factories* **7**

8. Yusoff, M. F. M., Xu, X. B., and Guo, Z. (2014) Comparison of Fatty Acid Methyl and Ethyl Esters as Biodiesel Base Stock: a Review on Processing and Production Requirements. *J Am Oil Chem Soc* **91**, 525-531

9. Magnuson, K., Jackowski, S., Rock, C. O., and Cronan, J. E. (1993) Regulation of Fatty-Acid Biosynthesis in Escherichia-Coli. *Microbiol Rev* **57**, 522-542

10. Tehlivets, O., Scheuringer, K., and Kohlwein, S. D. (2007) Fatty acid synthesis and elongation in yeast. *Bba-Mol Cell Biol L* **1771**, 255-270

11. Sheng, J. Y., and Feng, X. Y. (2015) Metabolic engineering of yeast to produce fatty acid-derived biofuels: bottlenecks and solutions. *Front Microbiol* **6**

12. Liu, Y. J., Lotero, E., and Goodwin, J. G. (2006) Effect of water on sulfuric acid catalyzed esterification. *J Mol Catal a-Chem* **245**, 132-140

13. Wohlgemuth, R. (2010) Biocatalysis - key to sustainable industrial chemistry. *Curr Opin Biotech* **21**, 713-724

14. Chahinian, H., and Sarda, L. (2009) Distinction between esterases and lipases: comparative biochemical properties of sequence-related carboxylesterases. *Protein Pept Lett* **16**, 1149-1161

15. Cambou, B., and Klibanov, A. M. (1984) Preparative Production of Optically-Active Esters and Alcohols Using Esterase-Catalyzed Stereospecific Trans-Esterification in Organic Media. *Journal of the American Chemical Society* **106**, 2687-2692

16. Park, Y. C., Shaffer, C. E., and Bennett, G. N. (2009) Microbial formation of esters. *Appl Microbiol Biotechnol* **85**, 13-25

17. Nordstrom, K. (1966) Enzyme Kinetic Model for Formation of Esters from Alcohols by Yeast. *Archives of Biochemistry and Biophysics* **115**, 488-+

18. Fujii, T., Nagasawa, N., Iwamatsu, A., Bogaki, T., Tamai, Y., and Hamachi, M. (1994) Molecular cloning, sequence analysis, and expression of the yeast alcohol acetyltransferase gene. *Appl Environ Microbiol* **60**, 2786-2792

19. Verstrepen, K. J., Van Laere, S. D., Vanderhaegen, B. M., Derdelinckx, G., Dufour, J. P., Pretorius, I. S., Winderickx, J., Thevelein, J. M., and Delvaux, F. R. (2003) Expression levels of the yeast alcohol acetyltransferase genes ATF1, Lg-ATF1, and ATF2 control the formation of a broad range of volatile esters. *Appl Environ Microbiol* **69**, 5228-5237

20. Saerens, S. M., Verstrepen, K. J., Van Laere, S. D., Voet, A. R., Van Dijck, P., Delvaux, F. R., and Thevelein, J. M. (2006) The Saccharomyces cerevisiae EHT1 and EEB1 genes encode novel enzymes with medium-chain fatty acid ethyl ester synthesis and hydrolysis capacity. *J Biol Chem* **281**, 4446-4456

21. Lin, J. L., and Wheeldon, I. (2014) Dual N- and C-Terminal Helices Are Required for Endoplasmic Reticulum and Lipid Droplet Association of Alcohol Acetyltransferases in Saccharomyces cerevisiae. *Plos One* **9**

22. Christiansen, K., and Jensen, P. K. (1972) Membrane-Bound Lipid Particles from Beef Heart - Chemical Composition and Structure. *Biochimica Et Biophysica Acta* **260**, 449-+

23. Clausen, M. K., Christiansen, K., Jensen, P. K., and Behnke, O. (1974) Isolation of Lipid Particles from Bakers-Yeast. *Febs Letters* **43**, 176-179

24. Gemmrich, A. R. (1981) Ultrastructural and Enzymatic Studies on the Development of Microbodies in Germinating Spores of the Fern Anemia-Phyllitidis. *Z Pflanzenphysiol* **102**, 69-80

25. Alvarez, H. M., and Steinbuchel, A. (2002) Triacylglycerols in prokaryotic microorganisms. *Appl Microbiol Biotechnol* **60**, 367-376

26. Grillitsch, K., Connerth, M., Kofeler, H., Arrey, T. N., Rietschel, B., Wagner, B., Karas, M., and Daum, G. (2011) Lipid particles/droplets of the yeast Saccharomyces cerevisiae revisited: lipidome meets proteome. *Biochim Biophys Acta* **1811**, 1165-1176

27. Czabany, T., Athenstaedt, K., and Daum, G. (2007) Synthesis, storage and degradation of neutral lipids in yeast. *Biochim Biophys Acta* **1771**, 299-309

28. Athenstaedt, K., and Daum, G. (2005) Tgl4p and Tgl5p, two triacylglycerol lipases of the yeast Saccharomyces cerevisiae are localized to lipid particles. *J Biol Chem* **280**, 37301-37309

29. Walther, T. C., and Farese, R. V. (2012) Lipid Droplets and Cellular Lipid Metabolism. *Annu Rev Biochem* **81**, 687-714

30. Toulmay, A., and Prinz, W. A. (2011) Lipid transfer and signaling at organelle contact sites: the tip of the iceberg. *Curr Opin Cell Biol* **23**, 458-463

31. Cermelli, S., Guo, Y., Gross, S. P., and Welte, M. A. (2006) The lipid-droplet proteome reveals that droplets are a protein-storage depot. *Curr Biol* **16**, 1783-1795

32. Meadows, J. W., Pitzer, B., Brockman, D. E., and Myatt, L. (2004) Adipophilin and signal transduction from lipid droplets in human fetal membranes. *J Soc Gynecol Invest* **11**, 77a-77a

33. Ren, J. H., Lin, C. P. C., Pathak, M. C., Temple, B. R. S., Nile, A. H., Mousley, C. J., Duncan, M. C., Eckert, D. M., Leiker, T. J., Ivanova, P. T., Myers, D. S., Murphy, R. C., Brown, H. A., Verdaasdonk, J., Bloom, K. S., Ortlund, E. A., Neiman, A. M., and Bankaitis, V. A. (2014) A phosphatidylinositol transfer protein integrates phosphoinositide signaling with lipid droplet metabolism to regulate a developmental program of nutrient stress-induced membrane biogenesis. *Molecular Biology of the Cell* **25**, 712-727

34. Gao, Q., and Goodman, J. M. (2015) The lipid droplet-a well-connected organelle. *Front Cell Dev Biol* **3**, 49

35. Jacquier, N., Choudhary, V., Mari, M., Toulmay, A., Reggiori, F., and Schneiter, R. (2011) Lipid droplets are functionally connected to the endoplasmic reticulum in Saccharomyces cerevisiae. *J Cell Sci* **124**, 2424-2437

36. Liu, P., Bartz, R., Zehmer, J. K., Ying, Y. S., Zhu, M., Serrero, G., and Anderson, R. G. (2007) Rab-regulated interaction of early endosomes with lipid droplets. *Biochim Biophys Acta* **1773**, 784-793

37. Binns, D., Januszewski, T., Chen, Y., Hill, J., Markin, V. S., Zhao, Y. M., Gilpin, C., Chapman, K. D., Anderson, R. G. W., and Goodman, J. M. (2006) An intimate collaboration between peroxisomes and lipid bodies. *J Cell Biol* **173**, 719-731

38. Goodman, J. M. (2008) The gregarious lipid droplet. *Journal of Biological Chemistry* **283**, 28005-28009

39. Guo, Y., Cordes, K. R., Farese, R. V., and Walther, T. C. (2009) Lipid droplets at a glance. *J Cell Sci* **122**, 749-752

40. Schmidt, C., Ploier, B., Koch, B., and Daum, G. (2013) Analysis of yeast lipid droplet proteome and lipidome. *Methods Cell Biol* **116**, 15-37

41. Robenek, H., Robenek, M. J., and Troyer, D. (2005) PAT family proteins pervade lipid droplet cores. *Journal of Lipid Research* **46**, 1331-1338

42. Tauchi-Sato, K., Ozeki, S., Houjou, T., Taguchi, R., and Fujimoto, T. (2002) The surface of lipid droplets is a phospholipid monolayer with a unique fatty acid composition. *Journal of Biological Chemistry* **277**, 44507-44512

43. Kory, N., Farese, R. V., Jr., and Walther, T. C. (2016) Targeting Fat: Mechanisms of Protein Localization to Lipid Droplets. *Trends Cell Biol* **26**, 535-546

44. Ruggiano, A., Mora, G., Buxo, L., and Carvalho, P. (2016) Spatial control of lipid droplet proteins by the ERAD ubiquitin ligase Doa10. *EMBO J* **35**, 1644-1655

45. Kaushik, S., and Cuervo, A. M. (2015) Degradation of lipid droplet-associated proteins by chaperone-mediated autophagy facilitates lipolysis. *Nat Cell Biol* **17**, 759-770

46. Ohsaki, Y., Cheng, J., Fujita, A., Tokumoto, T., and Fujimoto, T. (2006) Cytoplasmic lipid droplets are sites of convergence of proteasomal and autophagic degradation of apolipoprotein B. *Mol Biol Cell* **17**, 2674-2683

47. Anderson, K. S. (1999) Fundamental mechanisms of substrate channeling. *Method Enzymol* **308**, 111-145

48. Miles, E. W., Rhee, S., and Davies, D. R. (1999) The molecular basis of substrate channeling. *Journal of Biological Chemistry* **274**, 12193-12196

49. Spivey, H. O., and Ovadi, J. (1999) Substrate channeling. *Methods* **19**, 306-321

1.4 Figures and Tables

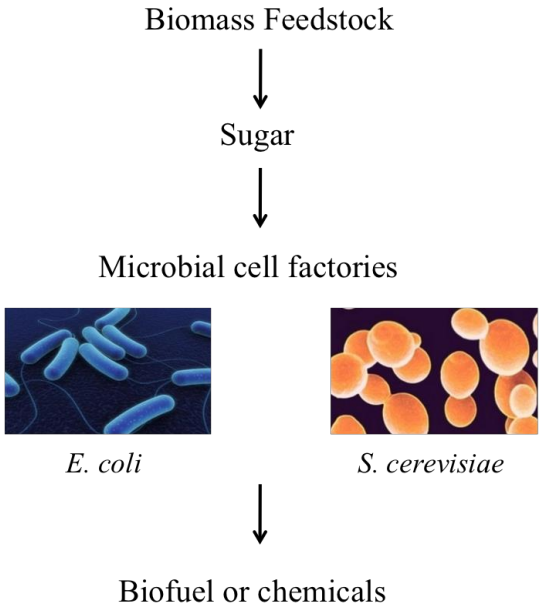

Figure 1.1. Production of renewable biofuels or chemicals by microbial cell factories from biomass feedstock. *E. coli* or *S. cerevisiae* are feed with five- or six- carbon backbone sugars from pretreated biomass and convert to desirable product via designed metabolic and synthetic biological pathways.

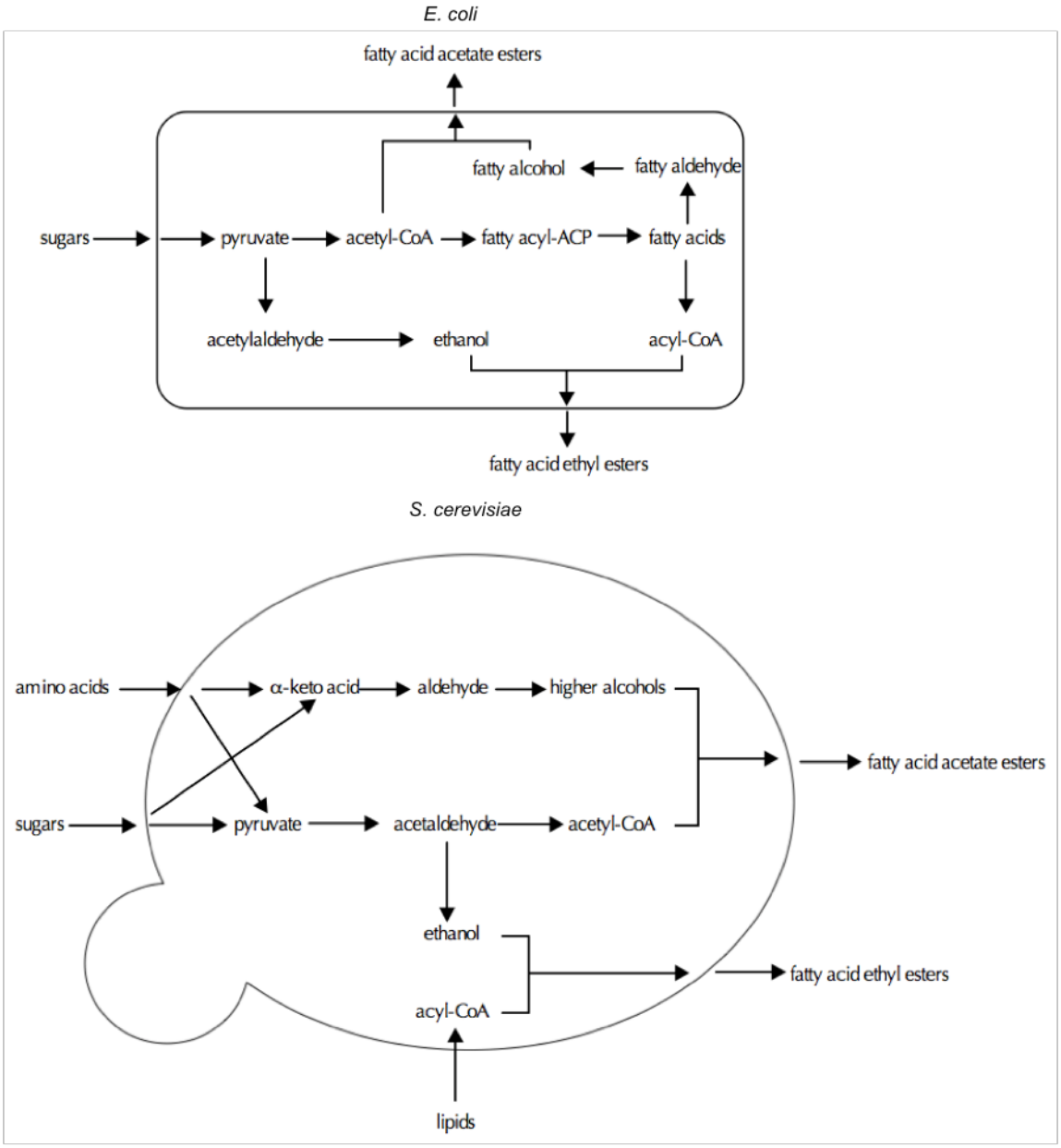

Figure 1.2. Biosynthetic pathways of fatty acid esters production in *E. coli* and *S. cerevisiae* under fermentation condition.

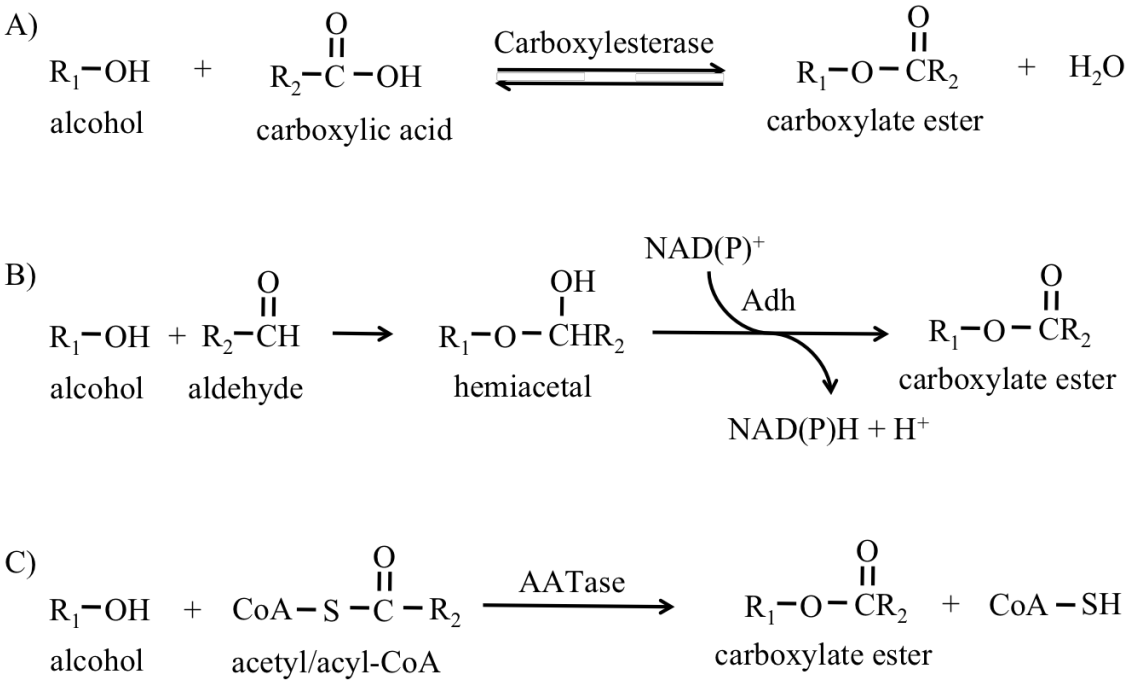

Figure 1.3. Biocatalysts to synthesize FAEEs. A) Carboxylesterase catalyzes the reaction of alcohol and carboxylic acid to produce carboxylic ester and water. B) Alcohol dehydrogenase catalyzes the production of carboxylate ester via hemiacetal dehydrogenation. C) Alcohol-O-acetyl/acyltransferase catalyzes the condensation of alcohol and acetyl/acyl-CoA to synthesize esters.

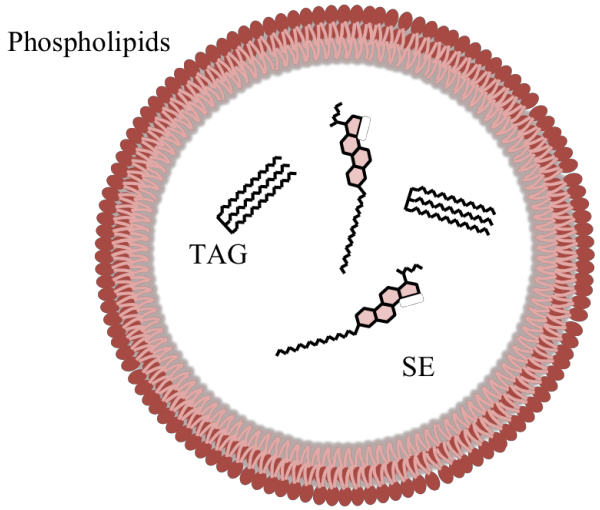

Figure 1.4. Lipid droplet structure. LD is composed of a neutral lipids core, containing triacylglyceride (TAG) and steryl esters (SE), surrounded by a phospholipid monolayer.

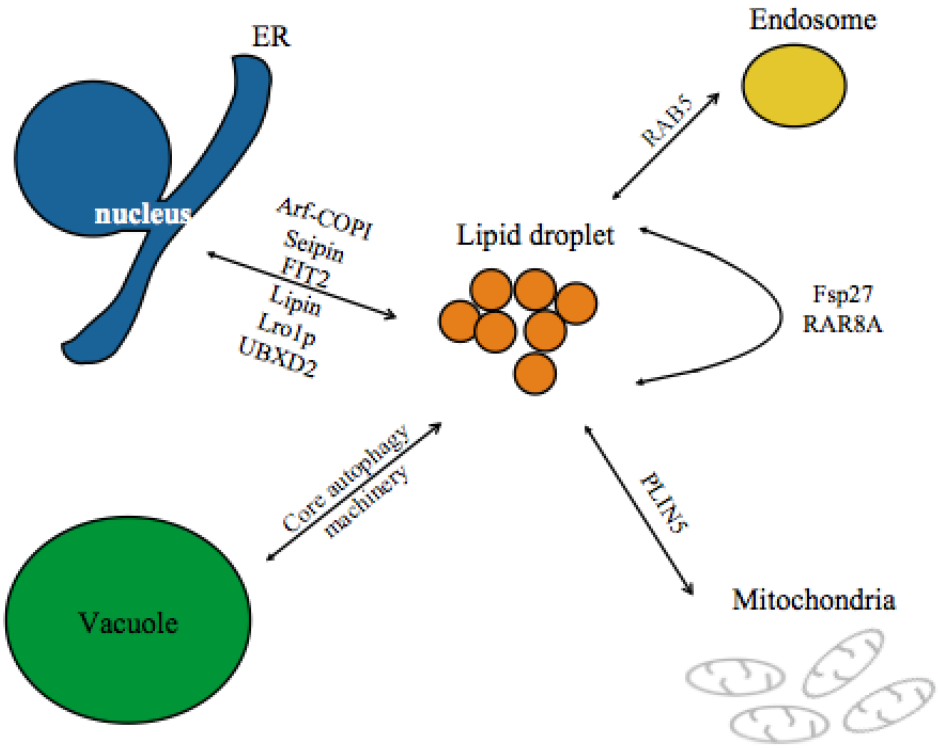

Figure 1.5. Crosstalk between lipid droplet and organelles.

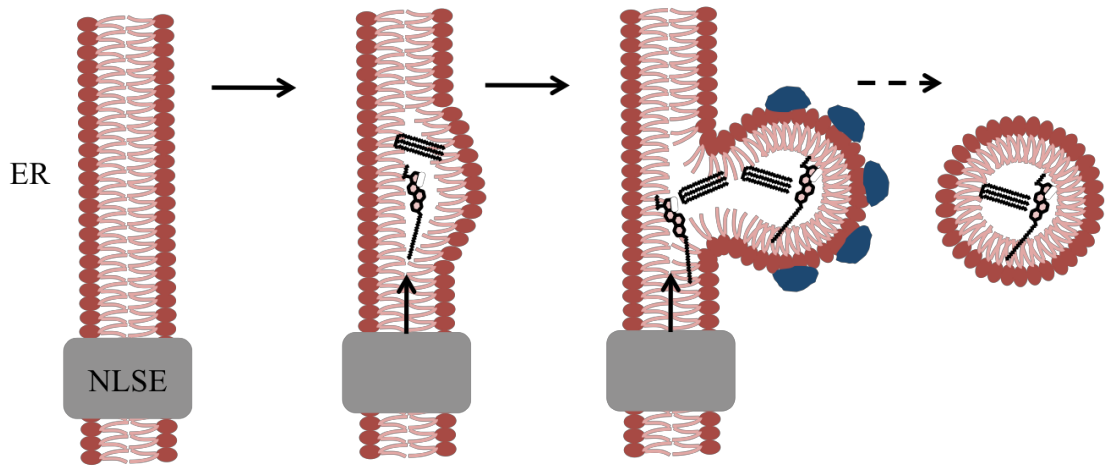

Figure 1.6. Proposed ER-budding mechanisms to form LDs. Neutral lipids are synthesized by neutral lipid-synthesizing enzymes (NLSE) localized on ER membrane and bluge from the outer leaflet of the ER membrane. The nascent droplet may be coated by proteins that facilitate the budding process (39).

Table 1.1. Intracellular localizations of AATases. ER: endoplasmic reticulum; LD: lipid droplet; Mem.: cell membrane.

Enzyme	Species	Localization
WS/DGAT	*A. balylyi*	LD/Mem.
WS2	*M. hydrocarbonoclasticus*	n. d.
Atf1	*P. opacus*	Mem.
WS	*P. arcticulus*	n. d.
Eht1	*S. cerevisiae*	LD/Mem.
Eeb1	*S. cerevisiae*	n. d.
Atf1	*S. cerevisiae*	LD/ER
Atf2	*S. cerevisiae*	LD/ER
lg-Atf1	*S. pastorianus*	LD
Atf	*K. lactis*	cytosol

Chapter 2. Microbial Host Selection Affects Intracellular Localization and Activity of Alcohol-O-acetyltransferase

2.1 Abstract

Background: A key pathway for ester biosynthesis in yeast is the condensation of an alcohol with acetyl-CoA by alcohol-O-acetyltransferase (AATase). This pathway is also prevalent in fruit, producing short and medium chain volatile esters during ripening. In this work, a series of six AATases from *Saccharomyces* and non-*Saccharomyces* yeasts as well as tomato fruit were evaluated with respect to their activity, intracellular localization, and expression in *Saccharomyces cerevisiae* and *Escherichia coli* cell hosts. The series of AATases includes Atf1 and Atf2 from *S. cerevisiae*, as well as AATases from *S. pastorianus*, *Kluyveromyces lactis*, *Pichia anomala*, and *Solanum lycopersicum* (tomato).

Results: When expressed in *S. cerevisiae,* Atf1, Atf2, and an AATase from *S. pastorianus* localized to lipid droplets, while AATases from non-*Saccharomyces* yeasts and tomato fruit did not localize to intracellular membranes and were localized to the cytoplasm. All AATases studied here formed intracellular aggregates when expressed in *E. coli*, and western blot analysis revealed that expression levels in *E. coli* were upwards of 100-fold higher than in *S. cerevisiae*. Fermentation and whole cell lysate activity assays of the two most active AATases, Atf1 from *S. cerevisiae* and an AATase from tomato fruit, demonstrated that the aggregates were enzymatically activity, but with highly reduced specific activity in comparison to activity in *S. cerevisiae*. Activity was partially recovered at lower expression levels, coinciding with smaller intracellular aggregates. *In vivo* and *in vitro* activity assays

from heterologously expressed Atf1 from *S. cerevisiae*, which localizes to lipid droplets under homologous expression, demonstrates that its activity is not membrane dependent.

Conclusions: The results of these studies provide important information on the biochemistry of AATases under homologous and heterologous expression with two common microbial hosts for biochemical processes, *S. cerevisiae* and *E. coli*. All studied AATases formed aggregates with low enzymatic activity when expressed in *E. coli* and any membrane localization observed in *S. cerevisiae* was lost in *E. coli*. In addition, AATases that were found to localize to lipid droplet membranes in *S. cerevisiae* were found to not be membrane dependent with respect to activity.

2.2 Introduction

During yeast fermentation and fruit ripening short chain linear and branched alcohols are converted to their corresponding acetate esters by alcohol-O-acetyltransferase (AATase; E.C. 2.3.1.84; Figure 2.1). These volatile esters produce sweet and fruity fragrances: phenyl ethyl acetate smells of flowers, isoamyl acetate (isopentyl acetate) smells of bananas, and ethyl acetate smells of sweet pears. In plants, these and other esters function as attractors to pollinating species and as a defense mechanism, attracting predators to animals feeding on their leaves and fruit (1,2). The function of microbial ester biosynthesis is not as well understood. AATase activity in *Saccharomcyes cerevisiae* is repressed by oxygen and unsaturated fatty acids (3-5) and it has been suggested that this activity functions as a means of CoA recycling with the co-production of organic acids (6,7), possibly as a response to stress conditions (8).

While there is uncertainty in the biological function of AATase activity in yeast, there are clear roles in metabolic engineering and industrial fermentations. The ester products have value as natural food additives, as aroma and flavor compounds in fermented beverages, and as industrial solvents (7,9). The effects of AATase activity on aroma and flavor profiles in wine, beer, and sake fermentations are well understood (5,10-12). The most well-studied AATases, Atf1 and Atf2 from *S. cerevisiae*, have been used to engineer whole cell *E. coli* catalysts for the conversion of ethanol and isoamyl alcohol to ethyl and isoamyl acetate (13-15) and for the biosynthesis of C4 to C11 volatile esters in *E. coli* (16). An AATase from strawberry fruit (*Fragaria* species) has also been heterologously expressed in *E. coli* for the biosynthesis of butyl acetate and a range of butyrate esters (15,17). Titers from these processes range from 0.04 – 0.23 g/L (13,15,17) to upwards of 17.5 g/L (16) and are, in part, limited by low AATase activity. In addition, the hydrophobic nature of these enzymes and varied intracellular localization of orthologs in their native hosts present complicating factors for heterologous expression in engineered hosts (8,18,19).

We have previously shown that Atf1 and -2 from *S. cerevisiae* localize to lipid droplets (LDs) via N- and C-terminal amphipathic helices (19). The AATase ortholog from *S. pastorianus* also localizes to LDs by a similar mechanism, while AATases from non-*Saccharomyces* yeasts and fruit species, including *Cucumis melo* (melon), and *Solanum lycopersicum* (tomato) that do not have the conserved terminal helices from *S. cerevisiae* and do not localize to LDs. Early biochemical studies of Atf1 and -2 suggest that enzyme activity is membrane dependent. Purification in the presence of non-ionic detergents (e.g., hepthyl thioglucoside, octyl thioglucoside, and Triton-X100) resulted in measurable enzyme activity, while purification in the absence of

such detergents resulted in inactive samples (6,20-22). Due in part to this apparent membrane dependency as well as the hydrophobic nature of the AATase family, the standard activity assay has evolved to include Triton-X100 above the critical micelle concentration (23).

The apparent membrane dependency of Atf1 and -2 activity is interesting in the context of heterologous expression in *E. coli* or other microbial hosts for ester biosynthesis. Reported activities of homologously expressed Atf1 and -2 are moderate, ranging from 0.01 to 10 nmol min^{-1} per mg of protein of whole cell lysate (18,21,22,24), while the activity of orthologs from *Pichia anomla* and *Klyuveromyces lactis* are low (< 1 nmol min^{-1} per mg of protein) (25). Reported activities of strawberry AATases range from 8 – 75 nmol min^{-1} mg of enzyme (26,27). The activities of Atf1 and -2 were measured in whole cell lysates that contain native LDs to which the enzymes can associate or in the presence of suitable membrane substitutes during purification. The successful metabolic engineering of *E. coli* to produce esters via an AATase pathway indicates that Atf1 and -2 maintain some activity in heterologous environments. In the absence of LDs Atf1 and -2 may associate with the plasma membrane, but the intracellular localization of Atf1 and -2 and other AATases heterologously expressed in *E. coli* and the effects of this localization on activity are not known.

In this work, a series of six AATases from *Saccharomyces* and non-*Saccharomyces* yeasts as well as tomato fruit (*S. lycopersicum*) were overexpressed in *S. cerevisiae* and *E. coli* and compared in terms of their intracellular localization, enzymatic activity, and expression level. The studies revealed that some AATases localize to LDs in *S. cerevisiae* and all studied AATases form enzymatically active

aggregates in *E. coli*. Aggregate formation resulted in significantly reduced activities in comparison to activities measured in *S. cerevisiae*. The most active AATases, Atf1 from *S. cerevisiae* and Atf from *S. lycopersicum*, were used to demonstrate an expression strategy to partially recover the lost activity; reduced expression resulted in smaller aggregate size and higher specific activity.

2.3 Material and Methods

Strains, plasmids, and culture conditions

Strains and plasmids used in this work are shown in Table 2.1. Primers used to amplify genes are listed in Table 2.2. *E. Coli* strains were grown in LB medium containing 30 μg/mL kanamycin. *S.cerevisiae* strains were prepared as previously described (19), and were grown in synthetic minimal (SD) medium containing 0.67% yeast nitrogen base (Becton-Dickinson), amino acid supplements (Sunrise), and 2% glucose. Expression in *E. coli* was induced by adding IPTG at OD_{600} of 0.4.

Preparation of whole cell lysate

Cells were harvested by centrifugation at 3,500 rpm for 5 min at 4 °C and washed twice with 100 mM potassium phosphate buffer (pH 7.4) containing 2 mM magnesium chloride. Equal volumes of wet cell pellets and 425-600 μm acid-washed glass beads (Sigma-Aldrich, G8772) were added to a 15 mL tube and resuspended in 1 mL ice-cold lysis buffer (100mM potassium phosphate buffer, 2mM magnesium chloride, 2mM DTT, and protease inhibitor). The cells were disrupted by vortexing 10 times for 30 s. After each vortexing the suspension was kept on ice for 30 s. The beads were removed by centrifugation at 500g for 5 min at 4 °C, and the supernatant

was decanted to a cold 2 mL tube. The protein concentrations of whole cell lysates were determined by Thermo Scientific Pierce 660 nm Protein Assay.

Enzyme activity assays

AATase activity was measured using ethanol and acetyl-CoA as substrates. A reaction mixture contains 100 mM potassium phosphate (pH 7.4), 500 mM ethanol and 0.5 mM acetyl-CoA and 100 μg lysate was used. After incubated at 30 °C for 0.5 hours, the reaction was stopped by the addition 60 μmol H_2SO_4. 100 μg of 1-pentanol was added as an internal standard and 1 g NaCl was added to reduce the solubility of ethyl acetate. The concentration of ethyl acetate produced was measured by headspace gas chromatography. To determine the activity of soluble and insoluble cell fractions, whole cell lysates were centrifuged at 15,000 rpm for 20 min at 4 °C. The supernant was isolated and taken as the soluble fraction. The pellet was washed twice with lysis buffer before re-suspending in lysis buffer. The activity of the re-suspended pellet and soluble fraction were measured as described above.

Fermentations

E. coli strains were grown in Terrific Broth containing 2% glucose and 30 μg/mL kanamycin with IPTG induction at OD_{600} of 0.4. Cells were cultured anaerobically in 125-mL screwed cap flask at 30 °C for 24 hours on a rotary shaker. The shake flask headspace was purged with nitrogen prior to incubation.

Ethyl acetate detection

Produced ethyl acetate was quantified by a headspace gas chromatography with a flame ionization detector (Agilent Technologies 7890A GC with CTC-PAL headspace mode injector). The separation of volatile compounds was carried out by Rtx®-1 column (30 m, 0.32 mmID, 5 μm film thickness; RESTEK) with helium as

carrier gas. GC oven temperature was initially at 75 °C for 7 min and increased with a gradient of 30 °C/min until 175 °C, followed by a gradient of 50 °C/min until 275 °C. The injector and detector were held at 275 °C. 1 mL headspace gas was injected to the GC and 1-pentanol was used as internal standard.

Fluorescent microscopy and image analysis

Cells were observed as described in (19). Briefly, an Olympus BX51 microscope (UPlanFL 100X 1.30 oil-immersion objective lense, mercury lamp) with Q-Imaging Retiga Exi CCD camera was used to capture images. CellSens Dimension 1.7 software (Olympus) was used to process images. Image J software was used to measure protein aggregate size. Quantitative values of aggregates size and number are from a minimum of 100 cells.

Western blot analysis and quantification of protein expression

Western blots were performed using standard procedure. Protein extracts were loaded on Any kD™ Mini-PROTEAN® TGX™ Gel (Bio-Rad) and run at 150 V for 1 hour. Samples were electrophoretically transferred to a PVDF membrane at 25 V overnight. Membranes were blocked with 5% non-fat milk in TBST buffer for 1 hour at room temperature and incubated with GFP Rabbit Serum Polyclonal Antibody (Life Technologies) diluted to 1: 20000 in TBST buffer with 1% non-fat milk. Goat Anti-Rabbit IgG-HRP (Life Technologies) diluted to 1: 10000 was added as secondary antibody and incubated at room temperature for 0.5 hours. After washing with TBST, HRP substrate (Bio-Rad) was used for signal detection. Image-J software was used to quantify band intensity.

2.4 Results

The genes include encoded AATases from *Saccharomyces* yeasts (Atf1-S.c, Atf2-S.c, and Atf1-S.p), and the non-*Saccharomyces* yeasts *P. anomala* (Atf-P.a), and *K. lactis* (Atf-K.l), as well as tomato fruit, *S. lycopersicum* (Atf-S.l). Preliminary activity screening from *S. cerevisiae* whole cell lysates with overexpressed AATases revealed that Atf1-S.c has the highest activity towards C2 to C5 alcohols with acetyl-CoA (Table S2.1). As such, initial experiments focused on determining the intracellular localization and the enzymatic activity of Atf1-S.c towards ethyl acetate when overexpressed in *S. cerevisiae* and *E. coli*. Importantly, *E. coli* BL-21 without chloramphinicol acetyltransferase (CAT) activity was used, as CAT has been shown to exhibit AATase activity toward ethyl acetate synthesis (Figure S2.1 and (16)).

In *S. cerevisiae* Atf1-S.c is known to localize to ER in early exponential phase and sort to LDs as cells progress in to stationary phase (19). Atf1-S.c with a C-terminally fused GFP reporter co-localized with a fluorescently tagged LD marker, Erg6-DsRed, indicating LD localization in *S. cerevisiae* (Figure 2.2A, left). An overexpressed GFP control localized to the cytosol and fluorescent imaging did not indicate LD localization (Figure 2.2A, right). When overexpressed in *E. coli*, fluorescence microscopy revealed that GFP is cytosolically expressed and did not form visible aggregates or puncate structures (Figure 2.2B, right). In contrast, Atf1-S.c. formed aggregates when overexpressed in *E. coli* (Figure 2.2B, left). Nine percent of observed *E. coli* cells expressing Atf1-S.c. had one aggregate, 75% had two aggregates, and 16% had three aggregates, while no cells were observed with zero aggregates or four or more aggregates (Figure 2.2B, bottom). No *E. coli* cells expressing Atf1-S.c were observed to have an expression pattern similar to the GFP

control, which showed fluorescence throughout the cell. Western blot analysis of protein expression in *S. cerevisiae* and *E. coli* showed that Atf1-S.c with a C-terminally fused GFP reporter expressed upwards of 100-fold more in *E. coli* than in *S. cerevisiae* (Figure 2.2C). Whole cell lysate activity assays of Atf1-S.c expressed in *S. cerevisiae* reached 58±8 nmol min^{-1} mg^{-1} of protein. Despite the difference in expression levels, *E. coli* whole cell lysate activity assays where limited to 11.6±0.1 nmol min^{-1} mg^{-1} of protein (Figure 2.2D).

Similar intracellular localization results were observed with other studied AATases (Figure 2.3A, B). Atf2-S.c and Atf-S.p localized to LD in *S. cerevisiae* and formed aggregates when overexpressed in *E. coli*. Fluorescent microscopy imaging revealed that Atf-K.l with C-terminally fused GFP was soluble in *S. cerevisiae,* but formed aggregates in *E. coli*. Punctate structures were observed with Atf-P.a in *S. cerevisiae* and, similar to the other yeast AATases, formed aggregates in *E. coli*. Finally, Atf-S.l from tomato fruit appeared to localize homogenously throughout the cytosol of *S. cerevisiae*, but formed aggregates in *E. coli*. In each case, the majority of *E. coli* cells contained one or two aggregates of a given AATase with less than 8% of cells containing three aggregates (Figure 2.3B, bottom). All observed *E. coli* cells contained at least one aggregate and no cells were observed to contain more than three aggregates.

Whole cell lysate assays revealed that all AATases exhibited measurable activity when expressed in *S. cerevisiae* and *E. coli* (Figure 2.3C). Atf2-S.c activity in *S. cerevisiae* lysate was 1.2±0.6 nmol min^{-1} mg^{-1}, lower than the 3.1±0.9 nmol min^{-1} mg^{-1} observed in *E. coli* lysate. Atf-S.p had activities of 0.3±0.3 and 0.4±0.1 nmol min^{-1} mg^{-1} in *S. cerevisiae* and *E. coli*, respectively. The activities of Atf-K.l and Atf-P.a

reached 0.3±0.2 and 0.4±0.3 nmol min^{-1} mg^{-1} in *S.cerevisiae*, but only reached 0.02±0.02 and 0.001±0.001 nmol min^{-1} mg^{-1} in *E. coli*, respectively. Atf-S.l activity in *E. coli* lysate was limited at 0.5±0.2 nmol min^{-1} mg^{-1}; however, in *S. cerevisiae* lysate Atf-S.l exhibited activity of 21±3 nmol min^{-1} mg^{-1}, second only to the activity of Atf1-S.c. Western blot analysis revealed that in all cases AATase expression in *E. coli* was at least 100-fold greater than expression in *S. cerevisiae* (Figure 2.3D). In this context, normalization of activity to *S. cerevisiae* expression levels revealed that AATase activity in *E. coli* whole cell lysates for all AATases studied here is less than or equal to 0.08 nmol min^{-1} mg^{-1} of protein.

The ethyl acetate activities of Atf1-S.c and Atf-S.l when expressed in *S. cerevisiae* were significantly greater than the activities of all other studied orthologs. As such, subsequent experiments focused on these two enzymes. To determine if the AATase aggregates formed in *E. coli* were insoluble and active, we measured the activity of soluble and insoluble protein fractions after fractionation by centrifugation. Figure 4A shows that soluble lysate fractions maintained high activity for both Atf1-S.c and Atf-S.l in both hosts (Aft1-S.c: 45±18 and 10±3 nmol min^{-1} in *S. cerevisiae* and *E. coli*, respectively; Atf-S.l: 14±4 and 2.2±0.6 nmol min^{-1} in *S. cerevisiae* and *E. coli*, respectively). Atf1-S.c showed higher activity in the insoluble fractions of both *S. cerevisiae* and *E. coli* (50±17 and 42±6 nmol min^{-1}, respectively). In contrast, the insoluble fractions containing overexpressed Atf-S.l showed measurable, but minimal activity (0.25±0.12 and 1.3±0.6 nmol min^{-1} mg^{-1} in *S. cerevisiae* and *E. coli*, respectively). The comparison of activity from *S. cerevisiae* and *E. coli* lysates is not complete without a similar comparison of expression levels in each host (Figure 2.4B). Western blots of *S. cerevisiae* lysates showed that Atf1-S.c separated equally

between the soluble and insoluble fractions, but Atf-S.l separated strongly to the insoluble fraction. When expressed in *E. coli*, both Atf1-S.c and Atf-S.l were largely insoluble. A 100-fold dilution of the insoluble fraction of *E. coli* overexpressing Atf1-S.c and Atf-S.l resulted in western blot bands of near equal intensity to the soluble fractions with no dilution.

To further investigate the relationship between AATase overexpression in *E. coli* and enzymatic activity we modulated expression levels using a standard inducible T7 promoter system. Analysis of fluorescence microscopy images of *E. coli* expressing Atf1-S.c with C-terminal GFP tag revealed that intracellular aggregate size increased from 0.11±0.05 μm^2 when induced with 1 μM IPTG to 0.19±0.08 μm^2 with 10 μM IPTG (Figure 2.5A and S2.2). Aggregate size further increased to 0.44±0.20 μm^2 with 100 μM IPTG. Coincident with increased induction and aggregate size were Atf1-S.c. expression levels (Figure 2.5B and S2.3). Induction with 10 and 100 μM IPTG resulted in 13.5±5.1 and 28.5±5.1 fold increases in protein expression over levels observed with 1 μM IPTG induction. Similar aggregate size and protein expression levels were observed with Atf-S.l. Under low induction conditions aggregates of Atf-S.l with a C-terminal GFP tag were found to be 0.11±0.04 μm^2. Aggregate size increased to 0.20±0.07 and 0.41±0.15 μm^2 when induced with 10 and 100 μM IPTG, respectively. Quantification of western blots showed that protein expression increased by 7.8±1.6 and 16.5±6.6 fold with increased induction levels of 10 and 100 μM IPTG, respectively (Figure 2.5C).

The result of reduced expression level and aggregate size was an increase in specific AATase activity during fermentation. Figures 2.5D shows Atf1-S.c activity in terms ethyl acetate produced during a 24-hour fermentation normalized to the

activity at the lowest protein expression level (i.e., induction with 1 μM IPTG). For Atf1-S.c the amount of ethyl acetate produced in 24-hour of fermentation increased from 1.35±0.10 to 4.78±0.28 and 6.74±0.24 mg/L with induction from 1 to 10 and 100 μM IPTG, respectively, while the amounts of ethanol produce under the same conditions were 0.87±0.07, 0.89±0.04, and 0.94±0.01 g/L, respectively. It is important to note that culture density measured by OD_{600} was unchanged with varied induction levels when expressing Atf1-S.c and a small but statistically significant reduction in OD_{600} was observed between the lowest and highest induction levels when expressing Atf-S.l (OD_{600} of 3.64±0.44 and 2.48±0.36, respectively; Figure S2.4). As shown in Figure 2.5B, Atf1-S.c expression increased by upwards of 28-fold under the same conditions, considerably more than the fold increase in ethyl acetate production, indicating that increasing enzyme expression did not result in a proportional increase in ester synthesis. Normalization to the lowest protein expression level provided an estimate of the reduction in specific AATase activity of Atf1-S.c at higher expression levels, specifically a 72.6±13.1% reduction with 10 μM IPTG and an 84.2±2.7% reduction with 100 μM IPTG (Figure 2.5D). Importantly, the increase in ethyl acetate production with increased expression of Atf1-S.c suggested that AATase activity is rate limiting for the conversion of ethanol to ethyl acetate and that the observed loss in activity is due to the enzyme and not an upstream pathway bottleneck. The low conversions of ethanol to ethyl acetate are also supportive of Atf1-S.c activity as rate limiting.

During 24 hours of *E. coli* fermentation with low expression of Atf-S.l, 0.30±0.09 mg/L of ethyl acetate and 0.95±0.20 g/L of ethanol were produced; there was no statistically significant different in the production of either compound with increased

induction (Figure S2.5). The low levels of ethyl acetate production in comparison to fermentation with Atf1-S.c expressing *E. coli* were expected due to lower activity in comparison to Atf1-S.c; however, varying expression levels of Atf-S.l produced a similar trend in normalized specific activity to that observed with Atf1-S.c. At higher expression levels specific activity was reduced by 85.6±2% and 90.3±4% with inductions of 10 and 100 μM IPTG, respectively. To confirm the effects of varying expression on activity, whole cell lysate assays and corresponding western blots were performed. For both Atf1-S.c and Atf-S.l the relative protein levels in whole cell lysates increased with increased induction (Figure 2.6A,B). Similar to the fermentation studies, the increased protein levels did not result in a proportional increase in ethyl acetate synthesis and normalized specific activity decreased significantly with induction levels of 10 and 100 μM IPTG. For Atf1-S.c the highest protein levels resulted in less of a reduction in activity then with intermediate protein levels (residual activities of 12.4±2.0% and 43.3±6.9% for 10 and 100 μM IPTG, respectively). For Atf-S.l increased protein levels due to induction with 10 and 100 μM IPTG measured specific activities were less than 5% of the specific activity from 1 μM IPTG induction.

2.5 Discussion

A major challenge in engineering metabolic pathways, including ester biosynthesis, is pathway optimization including the alleviation of kinetics bottlenecks and balancing the kinetic capacity of pathway steps. One approach to maximizing flux is pathway engineering to alter the expression levels of each step (28,29). Enzyme engineering to improve the kinetics of key steps is also critical (30). The

difficulty of these approaches is compounded when native intracellular localization, activity, and expression of key enzymes are affected by heterologous expression. Flux analysis and pathway modeling are also negatively affected because experimentally determined kinetic parameters used in modeling do not accurately translate to those exhibited *in vivo*. The AATases studied here are prime examples of these problems as heterologous expression in *E. coli* resulted in losses in specific activity and in some cases a loss of intracellular localization.

Homologous expression of Atf1-S.c in *S. cerevisiae* revealed high activity in whole cell lysates and native localization to LDs. Heterologous expression in *E. coli* was approximately 100-fold higher than in *S. cerevisiae*, but whole cell lysate assays revealed significantly reduced specific activity and *in vivo* fluorescence imaging revealed a loss of membrane localization (Figure 2.2). These results were consistent with Atf2-S.c from *S. cerevisiae* and Atf-S.p from *S. pastorianus*. Enzymes localized to LD in *S. cerevisiae,* but membrane localization was not observed in *E. coli* (Figure 2.2A, B). Despite high expression in *E. coli*, specific activities of Atf2-S.c and Atf-S.p in *E. coli* cell lysates were significantly less that observed in *S. cerevisiae* lysates. AATases from *K. lactis*, *S. lycopersicum*, and *P. anomala* did not localized to LD or other membranes when expressed in *S. cerevisiae* and did not localized to membranes in *E. coli*. Again, expression in *E. coli* was high and specific activities measured in whole cell lysates were significantly reduced in comparison with activities measure in *S. cerevisiae* lysates.

A contributing factor to the loss of activity was AATase aggregation in *E. coli*. Fluorescence imaging of *E. coli* cells revealed that in all cases expressed AATase formed one or more cytosolic aggregates (Figure 2.2B, 2.3B). Importantly, the

aggregates were functional. We expected that loss of tertiary structure in inclusion bodies would destroy protein function, but in all cases C-terminally fused GFP maintained fluorescence and whole cell lysates exhibited AATase activity suggesting that AATases expressed in *E. coli* were not misfolded (31). Moreover, analysis of fractionated *E. coli* lysates containing Atf1-S.c or Atf-S.1 demonstrated measurable activity in both the soluble and insoluble fractions (Figure 2.4). Common to the AATase family are short stretches of hydrophobic amino acids that are a possible source of protein aggregation (8,18). Specific to AATases from *S. cerevisiae* and *S. pastorianus,* the N- and C-terminal amphipathic helices that function as ER and LD membrane anchors may also be a source of aggregation (19). Regardless of mechanism(s), the results of heterologous expression in *E. coli* were clear, the formation of AATase active aggregates. In this context, the loss of activity was most likely due to a combination of diffusion limitations and blocked active sites. The results demonstrating increased specific activity at reduced expression levels supports these conclusions (Figure 2.5 and 2.6). Reduced expression of Atf1-S.c and Atf-S.l in *E. coli* produced smaller aggregates and increased measures of specific activity in both whole cell lysate assays and under fermentation conditions. Reduction in aggregate size increases the ratio of surface to interior proteins thus minimizing blocked active sites. It is also possible that activity in aggregates was due to the disruption of active protein conformation, an effect that is also likely decreased with aggregate size. An alternative explanation is that AATase solubility was increased at lower induction levels, an effect that has previously been demonstrated with single chain antibodies expressed in an *E. coli* host (32).

Biochemical studies of Atf1 from *S. cerevisiae* (Atf1-S.c) have suggested that activity is membrane-dependent (6,20-22). The studies presented here confirm that Atf1-S.c, Atf2-S.c and Atf-S.p localize to LDs in *S. cerevisiae*, but do not localize to membranes in *E. coli*. The loss of membrane localization did not eliminate activity towards ethyl acetate suggesting that these AATases are not strictly membrane dependent with respect to activity (Figures 2.2 and 2.3). Published purification protocols for Atf1-S.c use surfactants or non-ionic detergents and in their absence activity is significantly reduced. In our hands, nickel-affinity chromatography purification of Atf1-S.c resulted in AATase active samples (Figure S2.6), thus supporting the claim that membrane localization is not necessary for enzymatic activity. This lack of strict membrane dependency provides an explanation as to why metabolic engineering of *E. coli* to synthesize short chain volatile esters has been successful, and our analysis of AATase expression and activity in *S. cerevisiae* and *E. coli* hosts provides important information for future metabolic engineering of ester biosynthesis.

2.6 Conclusions

Ester biosynthesis is a promising new target for metabolic engineering. The market price of ethyl and butyl acetates are upwards of $1500 per tonne (http://www.icis.com/), and the total market value for flavor and fragrance compounds is greater than $16 billions (http://www.ialconsultants.com/). The high volatility of shorter chain esters such as ethyl acetate is also attractive from a separation perspective, as high volatility facilitates separation from fermentation broths (33). The results presented here demonstrate that microbial host selection is

critical to ethyl acetate biosynthesis through AATase activity. Heterologous AATase expression in *E. coli* resulted in significantly decreased specific activity in comparison to activity measure in *S. cerevisiae*. All studied AATases formed aggregates when expressed in *E. coli* and any membrane localization in *S. cerevisiae* was lost in *E. coli*. One solution to minimizing the loss of activity is reduced expression levels in *E. coli*, which resulted in smaller aggregate size and increased specific activity in comparison to high overexpression. The effects of host selection on AATase expression and activity described here are interesting in that they provide evidence that the AATases studied here are not strictly membrane dependent with respect to activity and are important when considering metabolic engineering strategies for ester biosynthesis.

2.7 Acknowledgements

This work was supported NSF CBET-1403264 and by Bourns College of Engineering and the University of California, Riverside start-up fund.

2.8 References

1. D'Auria, J. C., Pichersky, E., Schaub, A., Hansel, A., and Gershenzon, J. (2007) Characterization of a BAHD acyltransferase responsible for producing the green leaf volatile (Z)-3-hexen-1-yl acetate in Arabidopsis thaliana. *Plant J* **49**, 194-207

2. Beekwilder, J., Alvarez-Huerta, M., Neef, E., Verstappen, F. W. A., Bouwmeester, H. J., and Aharoni, A. (2004) Functional characterization of enzymes forming volatile esters from strawberry and banana. *Plant Physiol* **135**, 1865-1878

3. Fujiwara, D., Kobayashi, O., Yoshimoto, H., Harashima, S., and Tamai, Y. (1999) Molecular mechanism of the multiple regulation of the Saccharomyces cerevisiae ATF1 gene encoding alcohol acetyltransferase. *Yeast* **15**, 1183-1197

4. Fujii, T., Kobayashi, O., Yoshimoto, H., Furukawa, S., and Tamai, Y. (1997) Effect of aeration and unsaturated fatty acids on expression of the Saccharomyces cerevisiae alcohol acetyltransferase gene. *Appl. Environ. Microbiol.* **63**, 910-915

5. Saerens, S. M. G., Delvaux, F., Verstrepen, K. J., Van Dijck, P., Thevelein, J. M., and Delvaux, F. R. (2008) Parameters affecting ethyl ester production by Saccharomyces cerevisiae during fermentation. *Appl. Environ. Microbiol.* **74**, 454-461

6. Malcorps, P., and Dufour, J. P. (1992) Short-Chain and Medium-Chain Aliphatic-Ester Synthesis in Saccharomyces-Cerevisiae. *European Journal of Biochemistry* **210**, 1015-1022

7. Saerens, S. M. G., Delvaux, F. R., Verstrepen, K. J., and Thevelein, J. M. (2010) Production and biological function of volatile esters in Saccharomyces cerevisiae. *Microb Biotechnol* **3**, 165-177

8. Mason, A. B., and Dufour, J. P. (2000) Alcohol acetyltransferases and the significance of ester synthesis in yeast. *Yeast* **16**, 1287-1298

9. Park, Y. C., Shaffer, C. E. H., and Bennett, G. N. (2009) Microbial formation of esters. *Appl Microbiol Biot* **85**, 13-25

10. Lilly, M., Lambrechts, M. G., and Pretorius, I. S. (2000) Effect of increased yeast alcohol acetyltransferase activity on flavor profiles of wine and distillates. *Appl. Environ. Microbiol.* **66**, 744-753

11. Lilly, M., Bauer, F. F., Lambrechts, M. G., Swiegers, J. H., Cozzolino, D., and Pretorius, I. S. (2006) The effect of increased yeast alcohol

acetyltransferase and esterase activity on the flavour profiles of wine and distillates. *Yeast* **23**, 641-659

12. Saerens, S. M. G., Duong, C. T., and Nevoigt, E. (2010) Genetic improvement of brewer's yeast: current state, perspectives and limits. *Appl Microbiol Biot* **86**, 1195-1212

13. Horton, C. E., Huang, K. X., Bennett, G. N., and Rudolph, F. B. (2003) Heterologous expression of the Saccharomyces cerevisiae alcohol acetyltransferase genes in Clostridium acetobutylicum and Escherichia coli for the production of isoamyl acetate. *J Ind Microbiol Biot* **30**, 427-432

14. Vadali, R. V., Horton, C. E., Rudolph, F. B., Bennett, G. N., and San, K. Y. (2004) Production of isoamyl acetate in ackA-pta and/or ldh mutants of Escherichia coli with overexpression of yeast ATF2. *Appl Microbiol Biot* **63**, 698-704

15. Horton, C. E., and Bennett, G. N. (2006) Ester production in E-coli and C-acetobutylicum. *Enzyme Microb Tech* **38**, 937-943

16. Rodriguez, G. M., Tashiro, Y., and Atsumi, S. (2014) Expanding ester biosynthesis in Escherichia coli. *Nat Chem Biol* **10**, 259-265

17. Layton, D. S., and Trinh, C. T. (2014) Engineering modular ester fermentative pathways in Escherichia coli. *Metab. Eng.* **26**, 77-88

18. Verstrepen, K. J., Van Laere, S. D. M., Vercammen, J., Derdelinckx, G., Dufour, J. P., Pretorius, I. S., Winderickx, J., Thevelein, J. M., and Delvaux, F. R. (2004) The Saccharomyces cerevisiae alcohol acetyl transferase Atf1p is localized in lipid particles. *Yeast* **21**, 367-376

19. Lin, J. L., and Wheeldon, I. (2014) Dual N- and C-Terminal Helices Are Required for Endoplasmic Reticulum and Lipid Droplet Association of Alcohol Acetyltransferases in Saccharomyces cerevisiae. *PLoS One* **9**, e104141

20. Minetoki, T., Bogaki, T., Iwamatsu, A., Fujii, T., and Hamachi, M. (1993) The Purification, Properties and Internal Peptide Sequences of Alcohol Acetyltransferase Isolated from Saccharomyces-Cerevisiae Kyokai No 7. *Biosci Biotech Bioch* **57**, 2094-2098

21. Fujii, T., Nagasawa, N., Iwamatsu, A., Bogaki, T., Tamai, W., and Hamachi, M. (1994) Molecular-Cloning, Sequence-Analysis, and Expression of the Yeast Alcohol Acetyltransferase Gene. *Appl. Environ. Microbiol.* **60**, 2786-2792

22. Nagasawa, N., Bogaki, T., Iwamatsu, A., Hamachi, M., and Kumagai, C. (1998) Cloning and nucleotide sequence of the alcohol acetyltransferase

II gene (ATF2) from Saccharomyces cerevisiae Kyokai No. 7. *Biosci Biotech Bioch* **62**, 1852-1857

23. Tiller, G. E., Mueller, T. J., Dockter, M. E., and Struve, W. G. (1984) Hydrogenation of Triton X-100 Eliminates Its Fluorescence and Ultraviolet-Light Absorption While Preserving Its Detergent Properties. *Anal Biochem* **141**, 262-266

24. Plata, C., Millan, C., Mauricio, J. C., and Ortega, J. M. (2003) Formation of ethyl acetate and isoamyl acetate by various species of wine yeasts. *Food Microbiol* **20**, 217-224

25. Van Laere, S. D. M., Saerens, S. M. G., Verstrepen, K. J., Van Dijck, P., Thevelein, J. M., and Delvaux, F. R. (2008) Flavour formation in fungi: characterisation of KlAtf, the Kluyveromyces lactis orthologue of the Saccharomyces cerevisiae alcohol acetyltransferases Atf1 and Atf2. *Appl Microbiol Biot* **78**, 783-792

26. Cumplido-Laso, G., Medina-Puche, L., Moyano, E., Hoffmann, T., Sinz, Q., Ring, L., Studart-Wittkowski, C., Caballero, J. L., Schwab, W., Munoz-Blanco, J., and Blanco-Portales, R. (2012) The fruit ripening-related gene FaAAT2 encodes an acyl transferase involved in strawberry aroma biogenesis. *J Exp Bot* **63**, 4275-4290

27. Aharoni, A., Keizer, L. C. P., Bouwmeester, H. J., Sun, Z. K., Alvarez-Huerta, M., Verhoeven, H. A., Blaas, J., van Houwelingen, A. M. M. L., De Vos, R. C. H., van der Voet, H., Jansen, R. C., Guis, M., Mol, J., Davis, R. W., Schena, M., van Tunen, A. J., and O'Connell, A. P. (2000) Identification of the SAAT gene involved in strawberry flavor biogenesis by use of DNA microarrays. *Plant Cell* **12**, 647-661

28. Lee, M. E., Aswani, A., Han, A. S., Tomlin, C. J., and Dueber, J. E. (2013) Expression-level optimization of a multi-enzyme pathway in the absence of a high-throughput assay. *Nucleic Acids Research* **41**, 10668-10678

29. Cox, R. S., Surette, M. G., and Elowitz, M. B. (2007) Programming gene expression with combinatorial promoters. *Molecular Systems Biology* **3**

30. Banta, S., Swanson, B. A., Wu, S., Jarnagin, A., and Anderson, S. (2002) Optimizing an artificial metabolic pathway: Engineering the cofactor\ specificity of Corynebacterium 2,5-diketo-D-gluconic acid reductase for\ use in vitamin C biosynthesis. *Biochemistry*\ **41**, 6226\-6236\

31. Waldo, G. S., Standish, B. M., Berendzen, J., and Terwilliger, T. C. (1999) Rapid protein-folding assay using green fluorescent protein. *Nature Biotechnology* **17**, 691-695

32. Sawyer, J. R., Schlom, J., and Kashmiri, S. V. S. (1994) The Effects of Induction Conditions on Production of a Soluble Antitumor Sfv in Escherichia-Coli. *Protein Eng* **7**, 1401-1406

33. Xue, C., Zhao, J. B., Lu, C. C., Yang, S. T., Bai, F. W., and Tang, I. C. (2012) High-titer n-butanol production by clostridium acetobutylicum JB200 in fed-batch fermentation with intermittent gas stripping. *Biotechnology and Bioengineering* **109**, 2746-2756

2.9 Figures and Tables

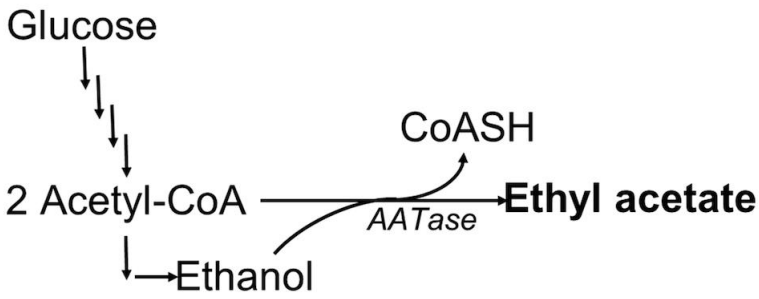

Figure 2.1. Schematic of AATase pathway for ester biosynthesis.

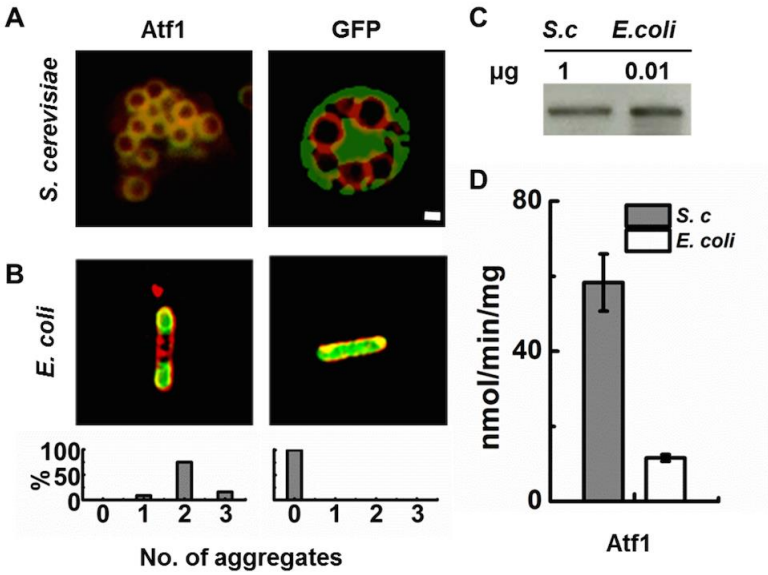

Figure 2.2. Expression, intracellular localization, and activity of Atf1 from *S. cerevisiae* (Atf1-S.c). A) Fluorescence microscopy images of *S. cerevisiae* co-expressing Atf1-GFP, GFP, and the LD marker Erg6-DsRed. Fluorescence from Erg6-DsRed is shown in red and fluorescence from Atf1-GFP is shown in green. Overlapping Erg6-DsRed and Atf1-GFP signals, indicating co-localization, are shown in yellow. GFP controls show cytosolic localization. Scale bar (1 µm) applies to A) and B). B) Fluorescent microscopy images of *E. Coli* expressing Atf1-GFP and GFP. CellMask™ Orange plasma membrane staining is shown in red and fluorescence from Atf1-GFP and GFP is shown in green. Graphs below the fluorescence images indicate the number of aggregates observed in *E. coli* cells. A minimum of 100 cells were counted from three independent experiments. C) Western blot analysis of Atf1-GFP expression in *S. cerevisiae* (S.c) and *E. Coli*. D) *In vitro* ethyl acetate production from total cell lysates of Atf1-GFP expressed in *S. cerevisiae* and *E. Coli*. Error bars represent standard deviation (n=3).

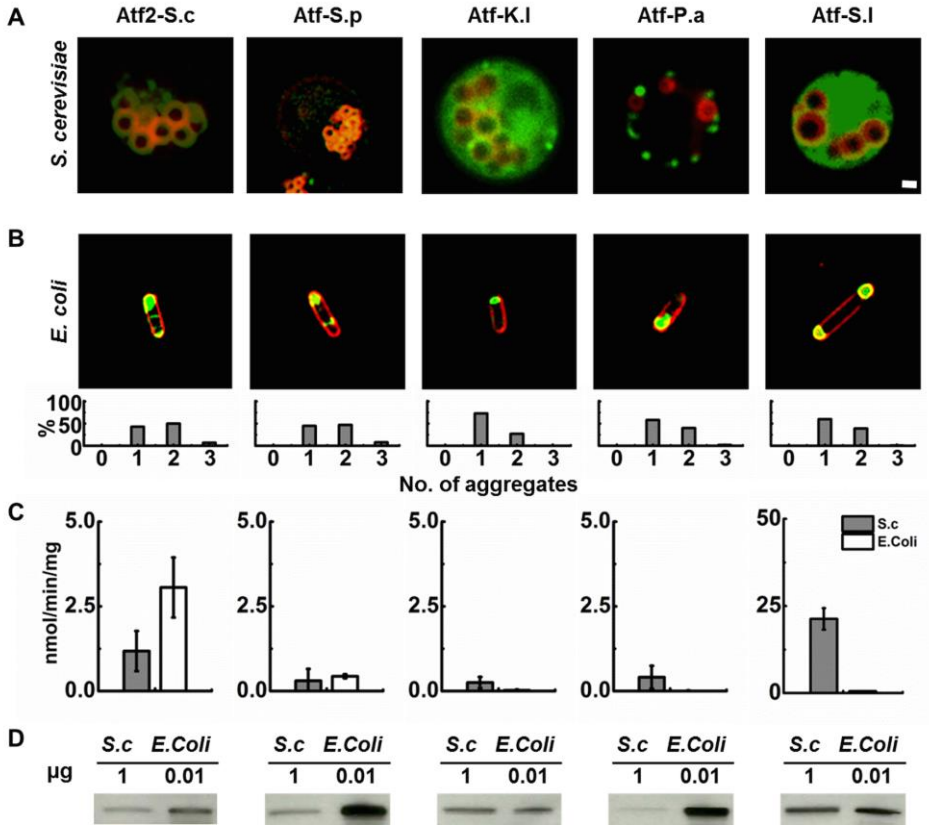

Figure 2.3. Expression, intracellular localization, and activity of AATases. A) Fluorescence microscopy images of *S. cerevisiae* co-expressing AATase-GFP and the LD marker Erg6-DsRed. Expressed AATases include Atf2 from *S. cerevisiae* (Atf2-S.c), and AATases from *S. pastorianus* (Atf-S.p), *K. lactis* (Atf-K.l), *P. anomala* (Atf-P.a), and *S. lycopersicum* (Atf-S.l). Fluorescence from Erg6-DsRed is shown in red and fluorescence from AATase-GFP is shown in green. Overlapping Erg6-DsRed and GFP signals, indicating co-localization, are shown in yellow. Scale bar (1 µm) applies to A) and B). B) Fluorescent microscopy images of *E. Coli* expressing AATases. CellMask™ Orange plasma membrane staining is shown in red and fluorescence from AATase-GFP is shown in green. Graphs below the fluorescence images indicate the number of aggregates observed in *E. coli* cells. A minimum of 100 cells were counted from three independent experiments. C) *In vitro* ethyl acetate production from total cell lysates of AATase-GFP expressed in *S. cerevisiae* (S.c) and *E. Coli*. Error bars represent standard deviation (n=3). D) Western blot analysis of AATase-GFP expression in *S. cerevisiae* and *E. Coli*.

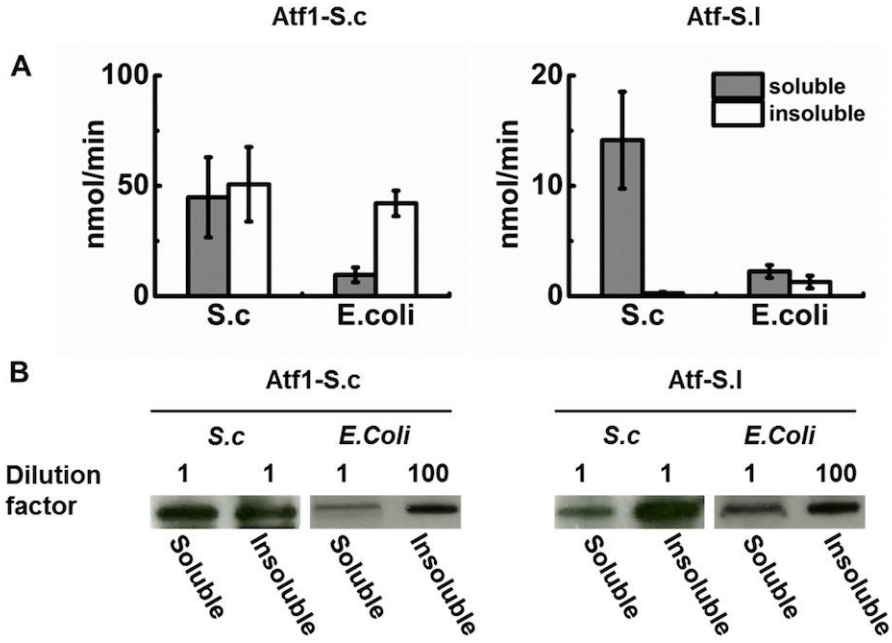

Figure 2.4. Atf1-S.c and Atf-S.l activity in soluble and insoluble cell fractions. A) Comparison of AATase activity in soluble and insoluble fractions from *S. cerevisiae* (S.c) and *E. coli*, Atf1-S.c (left) and Atf-S.l (right). Error bars represent standard deviation (n=3). B) Western blot analysis of soluble and insoluble fractions of Atf1-S.c and Atf-S.l from *S. cerevisiae* and *E. coli* expression.

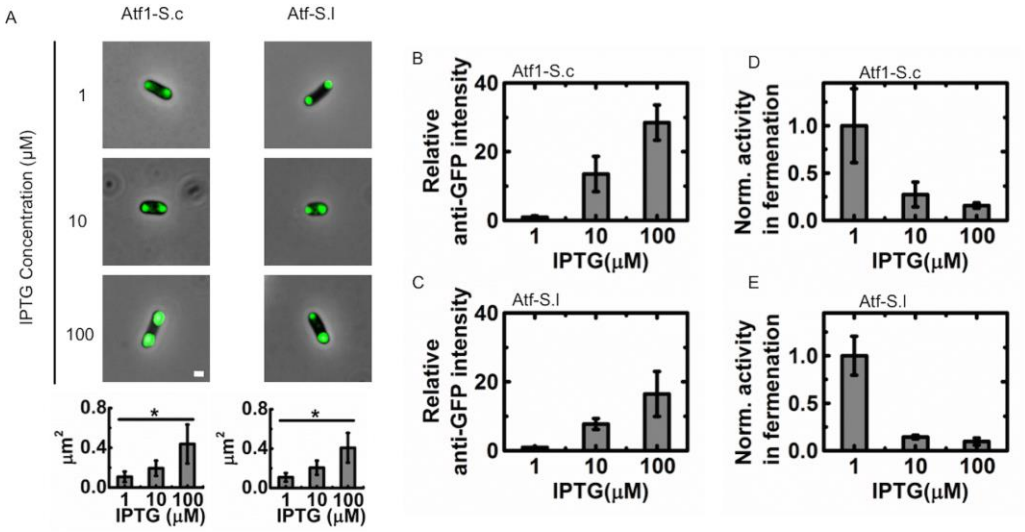

Figure 2.5. Reduced AATase expression decreases aggregates size in *E. coli* fermentations. A) Fluorescence microscopy images and aggregate size measurement of Atf1-S.c and Atf-S.l in *E. coli*. Scale bar is 1 μm. Error bars represent standard deviation (n=100), * $p<0.05$. B, C) Relative expression levels of Atf1-S.c (B) and Atf-S.l (C) in *E. coli* as judged by western blot analysis. Expression levels are normalized to the intensity of anti-GFP signal from *E. coli* induced with 1 μM IPTG. D, E) Normalized AATase activity from Atf1-S.c (D) and Atf-S.l (E) during 24 hour *E. coli* fermentations at 30 °C. Activities are normalized to the lowest expression level, IPTG induction of 1 mM. Error bars represent standard deviation (n=3).

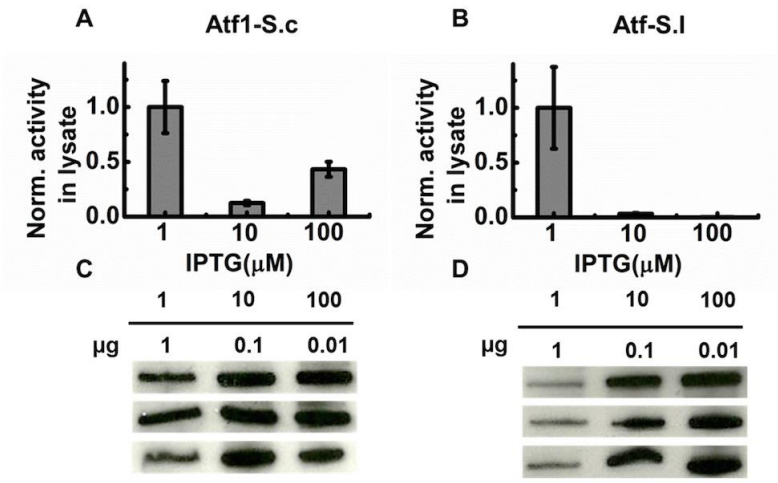

Figure 2.6. **Reduced AATase expression increases specific activity in whole cell lysate assays.** A, B) Atf1-S.c (A) and Atf-S.l (B) activity in *E. coli* whole cell lysates normalized to the expression level from induction with 1 mM IPTG. Error bars represent standard deviation (n=3). C, D) Western blot analysis of Atf1-S.c (C) and Atf-S.l expression levels in *E. coli* with inductions of 1, 10, and 100 mM IPTG.

Table 2.1. Strains and plasmids used in Chapter 2.

Name	Description	Source
Strains		
E. coli BL21(DE3)	F– ompT gal dcm lon hsdSB(rB- mB-) λ(DE3 [lacI lacUV5-T7 gene 1 ind1 sam7 nin5])	New England Biolabs
E. coli BL21(DE3)-RIL plus	F– ompT hsdS(rB– mB–) dcm+ Tetr gal λ(DE3) endA Hte [argU ileY leuW Camr]	Agilent Technologies
S. cerevisiae BY4742	MATα his3Δ1 leu2Δ0 lys2Δ0 ura3Δ0	GE Healthcare
Plasmids		
pGFP	pET-28b(+) derivative with gfp insertion	this study
pATF1G	pET-28b(+) derivative with atf1(S.c)-gfp insertion	this study
pATF2G	pET-28b(+) derivative with atf2(S.c)-gfp insertion	this study
pSPG	pET-28b(+) derivative with atf(S.p)-gfp insertion	this study
pKLG	pET-28b(+) derivative with atf(K.l)-gfp insertion	this study
pPAG	pET-28b(+) derivative with atf(P.a)-gfp insertion	this study
pSLG	pET-28b(+) derivative with atf(S.l)-gfp insertion	this study
pYPGK	pRS426 derivative; PGK1p-PGK1t	Lin, Wheeldon (2014)
pYATF1G	pYPGK derivative with atf1(S.c)-gfp insertion	Lin, Wheeldon (2014)
pYATF2G	pYPGK derivative with atf2(S.c)-gfp insertion	Lin, Wheeldon (2014)
pYSPG	pYPGK derivative with atf(S.p)-gfp insertion	Lin, Wheeldon (2014)
pYKLG	pYPGK derivative with atf(K.l)-gfp insertion	Lin, Wheeldon (2014)
pYPAG	pYPGK derivative with atf(P.a)-gfp insertion	Lin, Wheeldon (2014)
pYSLG	pYPGK derivative with atf(S.l)-gfp insertion	Lin, Wheeldon (2014)

Table 2.2 Primers used in Chapter 2.

Primers		
gfp	5'GCTCTAGAAATAATTTTGTTTAACTTTAAGAAGGAG ATATACCATGGCTAGCATGACTGGTG3'	this study
	5'CCGCTCGAGTTATTTGTATAGTTCATCCATGCCATG3'	this study
atf1-S.c-gfp	5'GCTCTAGAAATAATTTTGTTTAACTTTAAGAAGGAG ATATACCATGAATGAAATCGATGAGAAAAATCAG3'	this study
	5'CCGCTCGAGTTATTTGTATAGTTCATCCATGCCATG3'	this study
atf2-S.c-gfp	5'GCTCTAGAAATAATTTTGTTTAACTTTAAGAAGGAG ATATACCATGGAAGATATAGAAGGATACGAACCACA TATCACTC3'	this study
	5'ACGCGTCGACTTATTTGTATAGTTCATCCATGCCAT G3'	this study
atf-S.p-gfp	5'GCTCTAGAAATAATTTTGTTTAACTTTAAGAAGGAG ATATACCATGGAAACAGAAGAAAGCCAATTTAGCAG TATAAC3'	this study
	5'CCGCTCGAGTTATTTGTATAGTTCATCCATGCCATG3'	this study
atf-K.l-gfp	5'GCTCTAGAAATAATTTTGTTTAACTTTAAGAAGGAG ATATACCATGGGTTCGGTGTGTTTATCATCAAAAAAG TTAG3'	this study
	5'CCGCTCGAGTTATTTGTATAGTTCATCCATGCCATG3'	this study
atf-P.a-gfp	5'GCTCTAGAAATAATTTTGTTTAACTTTAAGAAGGAG ATATACCATGGTTGTTAAATTCAAAAGCAAAATCAAT AACAAAGG3'	this study
	5'CCGCTCGAGTTATTTGTATAGTTCATCCATGCCATG3'	this study
atf-S.l-gfp	5'GCTCTAGAAATAATTTTGTTTAACTTTAAGAAGGAG ATATACCATGGCTAATATTTTGCCAATTTC3'	this study
	5'CCGCTCGAGTTATTTGTATAGTTCATCCATGCCATG3'	this study

2.10 Supporting Information

Table S2.1. AATases activity towards different alcohols and acetyl-CoA. Data shown is mean (n=3). Not detected (n.d.).

Alcohol	Alcohol Acetyltransferase Activity (µmol/(min•mg))						
	ATF1 (sc)	ATF2 (sc)	ATF1 (sl)	ATF1 (cm)	ATF1 (sp)	ATF1 (pa)	ATF1 (kl)
Methanol	0.0311	n.d.	0.0007	n.d.	n.d.	n.d.	n.d.
Ethanol	0.8795	0.0245	0.2406	n.d.	n.d.	n.d.	0.0040
Propanol	0.0522	0.0049	0.0104	0.0005	0.0006	0.0003	0.0004
Isopropanol	0.0130	n.d.	n.d.	n.d.	n.d.	n.d.	n.d.
Butanol	0.0143	0.0011	n.d.	n.d.	n.d.	n.d.	n.d.
Isobutanol	0.0067	0.0105	0.0003	n.d.	0.0008	n.d.	n.d.
Pentanol	0.0030	0.0012	0.0011	n.d.	n.d.	0.0006	0.0023
Isopentanol	0.0041	0.0012	0.0004	0.0121	n.d.	n.d.	0.0016

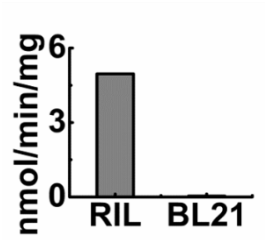

Figure S2.1. Background ethyl acetate synthesis from *E. coli* strains BL21(DE3)-RIP plus and BL21(DE3). The RIL strain expresses chloramphinicol acetyltransferase, which exhibits AATase activity towards ethanol and acetyl-CoA.

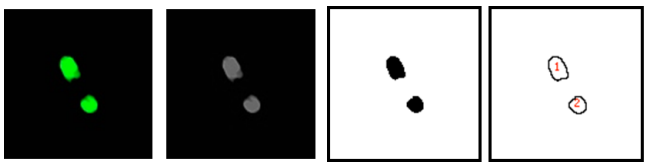

No	Area
1	944849.116
2	607700.312

Figure S2.2. Image J analysis of protein aggregate size in *E. coli*.

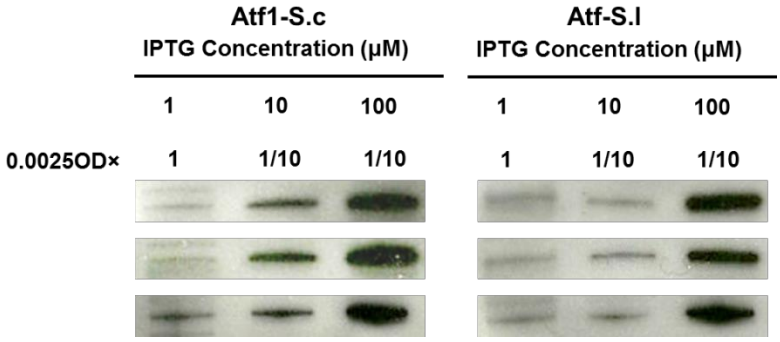

Figure S2.3. Western blots of Atf1-S.c and Atf-S.l expressed in *E. coli* with increasing IPTG concentration.

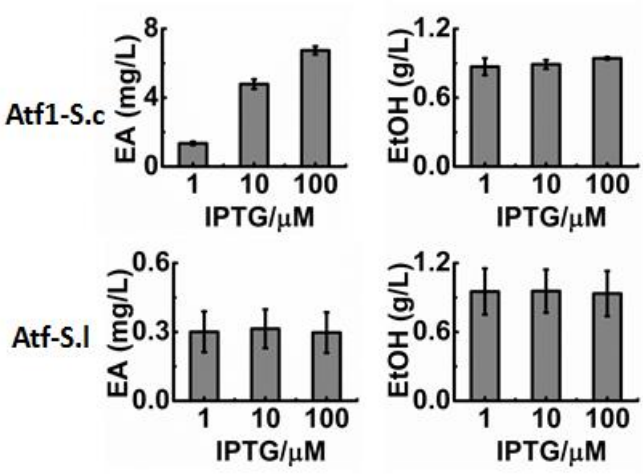

Figure S2.4. Ethyl acetate (EA) and ethanol (EtOH) production of E. coli harboring plasmids pET28-Atf1-S.c and pET28-Atf-S.l induced with different IPTG concentration under fermentation condition.

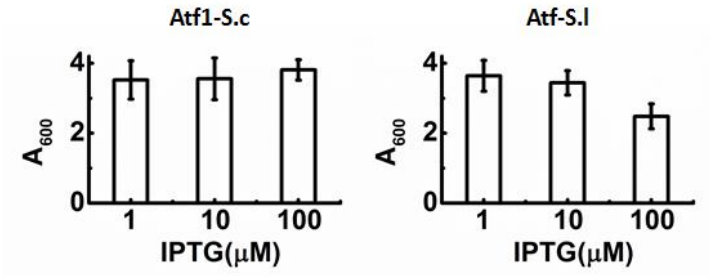

Figure S2.5. A600 values of E. coli harboring plasmids pET28-Atf1-S.c and pET28-Atf-S.l induced with different IPTG concentration under fermentation condition.

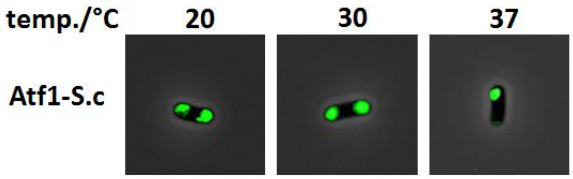

Figure S2.6. Fluorescent microscopy imaging of E. coli expressing Atf1-S.c at culture temperatures (temp.) of 20, 30, and 37 °C.

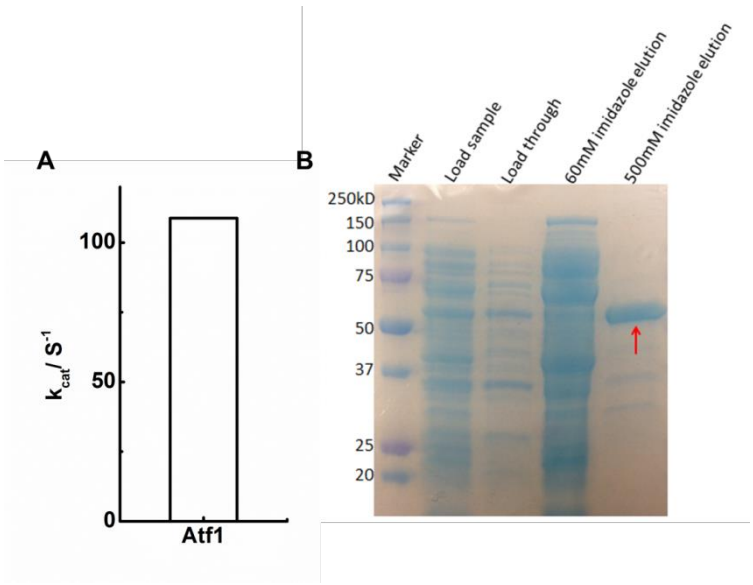

Figure S2.7. A) Specific activity of purified Atf1-S.c with C-terminal his tag. B) SDS-PAGE gel of purified Atf1-S.c. The red arrow points to Atf1.

Chapter 3. Rapid Ester Biosynthesis Screening Reveals a High Activity Alcohol-O-acyltransferase from Tomato Fruit

3.1 Abstract

Alcohol-O-acetyl/acyltransferase (AATase) is the last-step enzyme to condense the alcohols and acetyl- or acyl-CoAs to synthesize a broad spectrum of fatty acid esters in yeast. There is no suitable assay for high throughput screening to protein engineer AATase. Here, we have developed a spectrophotometric assay to quantify AATase activity in real time from whole cell lysate. This coupled enzyme assay has been demonstrated to be robust by measuring enzyme activity with a range of whole cell lysate concentrations. It is also feasible for high throughput screening on 96-well plates via Z'-factor analysis. This assay was used to screen a library of AATases for fatty acid ethyl esters synthesis, including AATases from *Saccharomyces* yeast (Atf1, Atf2, Eht1, and Eeb1), an AATase from melon (*C. melo*; Atf-C.m), and an AATase from tomato fruit (*S. lycopersicum*; Atf1-S.l). An uncharacterized Atf1-S.l was identified to be active towards short and medium chain acyl-CoAs and different alcohols. This coupled enzyme assay will help accelerate AATase protein engineering and the discovery of new AATase enzymes.

3.2 Introduction

Recently, it has been a focus of metabolic engineering to produce short- or medium-chain fatty acid esters. Volatile short- or medium-chain esters have distinct odors and flavors that are valuable as natural food additives (e.g., isoamyl acetate and phenyl ethyl acetate) and industrial solvents (e.g., ethyl acetate). They have been produced in native yeast strains (1,2) and engineered *E. coli* (3-6). The pathways to produce these compounds share a common terminal reaction by condensing an alcohol and acetyl- or acyl-CoAs by alchohol-O-acetyl/acyltransferase (AATase, E.C. 2.3.1.84 and 2.3.1.75, respectively). Some of AATases from yeast and fruit species have been identified to be active towards short and medium chain esters during fermentation and fruit ripening (7-13). Orthologs to these AATases, called wax ester synthases, can produce waxy esters with long chain acyl-CoAs and fatty alcohols (14,15).

There have been successes in engineering biosynthesis of esters in microbial cell factories; however, protein engineering and enzyme screening have been limited. Rational design is challenging because of lacking known crystal structures of AATases and high similarity templates results in low confidence homology models (16,17). Directed evolution and enzyme screening are limited by a lack of suitable high throughput assays. Part of the challenge is that many AATases are membrane associated, localizing to the endoplasmic reticulum (ER) and lipid droplets (18-20). Loss of localization during heterologous expression in *E. coli* results in aggregation and low enzymatic activity (21). Purification is also challenging requiring non-ionic detergents or protein solubility tags to maintain activity (16,22,23). Therefore, headspace gas chromatography (GC) analysis of whole cell lysate reactions is the

most common activity assay for volatile esters (21), while thin layer chromatography and GC-MS are applied for measuring long chain esters (24). These assay are not ideal and effective for identifying high activity enzymes or protein engineering to alter substrate specificity and improve turnover.

Here, we developed a coupled enzyme assay to quantify ester production spectrophotometrically. It is developed for whole cell lysate reactions of AATase activity and it enables high throughput screening of AATase libraries and directed evolution. The yeast *S. cerevisiae* was used as the host to allow for native localization of homologous enzymes and membrane association of heterologous enzymes. A library of six AATases, two homologs from *S. cerevisiae*, Atf1 and Atf2, with specificity towards acetate esters; Eht1 and Eeb1 from *S.cerevisiae* with specificity towards medium chain ethyl esters; a medium chain acetate ester specific AATase from *Cucumis melo* (melon); and an uncharacterized AATase from *Solanum lycopersicum* (tomato fruit), was screened to validate and apply this assay.

3.3 Material and Methods

Strains, plasmids, enzymes, and cell culture

The strains and plasmids used in this work are shown in Table 3.1. The plasmid pRS426-pPGK1 containing a phosphoglycerate kinase I (PGK) expression cassette was used for enzyme overexpression in *S. cerevisiae* (18). Six AATase genes, including *ATF1*, *ATF2*, *EHT1*, and *EEB1* from *S. cerevisiae*, an AATase from *S. lycopersicum* (*Atf-s.l*), and an AATase from *C. melo* (*Atf-c.m*), with encoded C-terminal myc tags were cloned into the SacII and NotI sites of pRS426-pPGK1. Genes from *S. cerevisiae* were amplified by PCR from genomic DNA, whereas genes

from *S. lycopericum* and *C. melo* were created by gene assembly as previously described (18). Primers used to amplify genes are provided in Table S3.1. Molecular cloning was accomplished in *E. coli* cells, while *S. cerevisiae* was used for overexpression. Cells harvesting expression plasmids were grown in synthetic minimal (SD) medium containing 0.67% yeast nitrogen base (Becton-Dickinson), amino acid supplement without uracil, and 2% glucose.

Preparation of whole cell lysate

Yeast cells harboring expression plasmids were cultured to early stationary phase in 50 ml SD media without uracil in 250 ml baffled flasks. Cells were harvested by centrifugation at 3,500 rpm for 5 min at 4 °C and washed twice with 100 mM potassium phosphate buffer (pH 7.4) containing 2 mM magnesium chloride. Equal volumes of wet cell pellets and 425-600 μm diameter acid-washed glass beads (Sigma-Aldrich) were added to a 15 mL tube and resuspended in 1 mL ice-cold lysis buffer (100mM potassium phosphate buffer, 2mM magnesium chloride, 2mM DTT, and protease inhibitor cocktail (Roche), pH7.4). Cells were disrupted by vortexing 10 times for 30 s. After each vortexing the suspension was kept on ice for 30 s. The beads were removed by centrifugation at 500g for 5 min at 4 °C and the supernatant was transferred to a pre-cooled 1.5 mL tube. Whole cell lysate protein concentrations were determined by a commercially available assay (Pierce 660 nm Protein Assay, Thermo Fisher).

AATase activity assay and screening

Alcohol-O-acetyl/acyltransferase activity was determined by monitoring NADH production from a coupled reaction with α-ketoglutarate dehydrogenase (α-KGDH). The reaction was performed at room temperature in 100 mM potassium phosphate

buffer, pH 7.4. The assay solution contained final concentrations of 2 mM α-ketoglutarate (α-KG), 10 mM cystein, 2 mM NAD^+, 10 mM $MgCl_2$, and 0.03 U α-KGDH (Sigma-Aldrich). Whole cell lysate samples, pyrazole (15 mM final concentration), and alcohol (20 mM final concentration) were added to the assay solution. It has previously been reported that the order of substrate addition affects long chain AATase activity (25). The coupled enzyme reaction was initiated by adding 0.5 mM acetyl/acyl-CoA to the reaction solution. The assay was monitored by measuring the absorbance of NADH at 340 nm (ε_{340} = 6.22 $mM^{-1}cm^{-1}$) for 4 minutes. Screening experiments were performed in 96-well microtiter plates with a final volume of 100 μL and the rate of NADH production was monitored with a BioTek Synergy H4 hybrid multi-mode microplate reader.

The library of six AATases (Atf1, Atf2, Eht1, Eeb1, Atf-C.m, and Atf-S.l) was screened for ethyl ester synthesis with acetyl-, butyryl-, hexanoyl, octanoyl, decanoyl, and lauroyl-CoA. Atf-S.l was also screened for acetate ester synthesis with methanol, ethanol, 1-propanol, 1-butanol, 2-butanol, isobutanol, 1-pentanol, and 3-methyl-1-butanol.

Western blot analysis

Whole cell lysates were prepared from cells grown to early stationary phase and 1 μg total protein was used for western blot analysis. Mouse anti-myc (Invitrogen), mouse anti-GAPDH (Thermo Fisher Scientific), goat anti-mouse IgG-HRP (Thermo Fisher Scientific) and chemiluminescent HRP substrate (Immobilon Western, Millipore) were used for protein analysis and signal detection.

3.4 Results and Discussion

The strains, plasmids, and AATase genes used in this study are listed in Table 3.1. The genes encode AATases from *Saccharomyces* yeast (Atf1, Atf2, Eht1, and Eeb1), an AATase from melon (*C. melo*; Atf-C.m), and an AATase from tomato fruit (*S. lycopersicum*; Atf1-S.l). Each gene was overexpressed in *S. cerevisiae* from a 2μ plasmid under the constitutive PGK promoter.

Alcohol and acetyl- or acyl-CoA are condensed to produce corresponding esters through AATases activity. Free CoA-SH is generated by breaking of the thioester bond of acetyl- or acyl-CoA and is quantified through a coupled α-KGDH reaction with NAD^+ as co-factor (Figure 1). With CoA-SH, α-KG, cystein, and NAD^+, α-KGDH produces succinyl-CoA, CO_2 and reduced co-factor, NADH, which can be followed by absorbance at 340 nm. The free thiol group of CoA-SH can also be quantified by Ellman's reagent (15,25) and an α-KGDH-based assay has previously been used to quantity acetyltransferase activity (26,27); however, these assays require purified enzyme samples to minimize background and non-specific activity. Whole cell lysates from cells harboring empty vectors showed rapid NAD^+ reduction in presences of ethanol and acetyl-CoA and α-KGDH and its substrates (α-KG, cystein, and NAD^+). In *S. cerevisiae*, there are up to seven native NAD^+-dependent alcohol dehydrogenases (ADHs) contributing to the high NADH background (28). Pyrazole, an inhibitor of ADH, was added to the reaction to suppress the background with concentration as 15 mM (Figure S3.1). The feasibility of this coupled enzyme assay was tested with different whole cell lysate concentrations. The measured activities of Atf1 and Eht1 increased linearly with whole cell lysate concentrations from 0.25 to 1.0 μg (Figure S3.2), thus providing evidence of a robust assay. The assay also

proved to be suitable for high throughput screening through Z'-factor analysis (Z' values greater than 0.5 are acceptable) (29). Atf1 was used as the positive control for short chain ethyl ester synthesis and Eht1 for medium chain ethyl ester synthesis. In both cases, Z' factors are greater than 0.5 (Figure S3.3), indicating that the coupled enzyme assay was suitable for high throughput screening.

A library of AATase including Atf1, Atf2, Eth1, and Eeb1 from *S. cerevisiae*, Atf-C.m from melon, and Atf-S.l from tomato fruit was tested to validate that this assay is suitable for rapid and high throughput screening of whole cell lysates. This library was screened for fatty acid ethyl esters synthsis with corresponding acyl-CoA substrates, ranging from C2 to C12. Eht1 and Eeb1 have been well studied with substrate specificity to be used as internal standard to validate the assay. Eht1 and Eeb1 are found to be active towards butyryl-, hexanoyl-, and octanoyl-CoA (C4, C6, and C8 acyl chain lengths, respectively) with the highest activity towards octanoyl-CoA (9,26). Furthermore, the screen was used to generate new data for the acyl-CoA specificity of Atf1, Atf2, Atf-C.m. and Atf-S.l, as well as the alcohol substrate specificity of Atf-S.l.

In Figure 3.2A, the screening results are showed as heat map of enzymatic activity (it is also provided as numbers in Table S3.2) in terms of nmol of ethyl ester produced per min. Western blot analysis of protein expression level (Figure 3.2B) is accompanied with the screening results. It shows that the expression levels of native *S. cerevisiae* enzymes Atf1, Atf2, Eht1, and Eeb1, were significantly higher than the expression levels of the heterologous AATases from tomato (Atf-S.l) and melon (Atf-C.m). Atf1, Atf2, Eht1, and Eeb1 showed measurable activity towards the set of screened acyl-CoAs. Also, Eht1 exhibited the highest activity towards ethyl ester

synthesis and Atf1 exhibited the highest acetylation activity. Considering the protein expression levels, the normalized activities of Atf-C.m and Atf-S.l are comparable with both Atf1 and Atf2. Also, both of Atf-C.m and Atf-S.l were active with acyl-CoA with acyl length up to C10.

Eht1 and Eeb1 as internal standards have been characterized as medium chain fatty acid ethyl ester synthases with activity towards butyryl-, hexanoyl-, and octanoly-CoA (9). Eht1 is further characterized that it has activity with acyl-CoAs with acyl chain length up to C12 and shows a preference towards octanoly-CoA (26). Our assay results are consistent with the previous studies: Eht1 was active with acyl-CoAs with acyl length between C2 and C12 and the highest activity was observed towards octanoyl-CoA (2.22±0.19 nmol min^{-1}); Eeb1 had highest activity with octanoyl-CoA (1.48±0.14 nmol min^{-1}) and showed broad acyl-CoA specificity. For Eht1 and Eeb1, they are poorly active for acetylation, with relatively low activity towards acetyl-CoA (0.044±0.014 and 0.037±0.004 nmol min^{-1}, respectively).

The screening results showed in Figure 3.2 and Table S3.2 revealed the broad specificity towards acyl-CoA for Atf1. Atf1 exhibited measurable activity towards ethyl esters from acyl-CoA ranging from C2 to C12 acyl chain lengths, and the highest activity is towards acetyl-CoA. This screen was also used to evaluate acyl-CoA specificity for ethyl ester production; the alcohol substrate specificity has been characterized with the highest activity reported for isobutyl alcohol (3) and isopentyl alcohol (4,22,30).

Atf1 is known to localize to lipid droplets in *S. cervisiae* (18) and shows specificity towards sterol acetylation (31,32). It has been used to produce ethyl, butyl, isobutyl, and isoamyl acetates by whole cell catalysis and fermentation (4,21,30). Atf2 showed

similar substrate specificity as Atf1 with preference to octanoly-CoA. It can produce 0.23±0.03 nmol min^{-1} of ethyl octanote, 10-fold higher than the rate of ethyl acetate synthesis (0.020±0.002 nmol min^{-1}), which suggests that Atf2 may have biological function beyond acetylation of sterols.

Atf-C.m has been characterized in cell-free extracts from ripe melon fruit and it exhibited acetylation activity towards several alcohols, including 1-butanol, 1-hexanol, isopentyl alcohol, and phenylethyl alcohol (33). Recombinant expression of AATases from melon have also been studied and showed broad alcohol substrate specificity with acetyl-CoA (17). The screening of Atf-C.m from this work confirmed acetylation activity with ethanol as a co-substrate. It also exhibited activity towards longer chain acyl-CoAs with the highest activity toeards decanoyl-CoA (1.46±0.15 nmol min^{-1}). Atf-C.m may have higher specific activity than the native *S. cerevisiae* enzymes after normalized with the relative low expression level. This result suggests that Atf-C.m could be a useful enzyme for metabolic engineering of medium chain esters including butyrates if its expression level could be further improved (5).

Atf-S.l corresponds to an AATase gene from *S. lycopersicum*, which was previously identified with the NCBI protein data bank under the accession number NP_001234496.1 (34). This gene encodes for an enzyme with 442 amino acids, which has the putative AATase active site, H-X-X-X-D, beginning at residue 221 (18). Our group has demonstrated that Atf-S.l is dispersed in the cytosol (18) and has activity towards ethyl acetate synthesis (21). AATase activity has also been identified in the tomato fruit extracts (35), but the activity and substrate specificity has not been studied. The screening results conducted in this work showed that it is active towards acyl-CoAs with acyl chain length up to C10 and the highest activity is with hexanoyl-

CoA (0.326±0.042 nmol min^{-1}). Similar to Atf-C.m, the expression level of Atf-S.l is relatively lower than the native *S. cerevisiae* enzymes, which suggests that it may have the highest specific activity in this screened library.

The substrate specificities for alcohols of Atf1, Atf2, Eht1, Eeb1, and Atf-C.m have previously been characterized, but a similar characterization of Atf-S.l has not been accomplished yet. Therefore, this coupled enzyme assay was applied to screen the acetate ester synthesis activity of Atf-S.l with different primary and secondary alcohols with carbon chain lengths up to C5 (Figure 3.3). The screen showed no activity for methanol and the secondary alcohol, 2-butanol. Ethanol, 1-propanol, and 1-butanol were acceptable substrates with activities of 0.11±0.04, 0.12±0.04, and 0.13±0.04 nmol min^{-1}. Atf-S.l showed higher activity with 0.29±0.03 and 0.15±0.02 nmol min^{-1}, respectively. It exhibited the highest activity (0.55±0.05 nmol min^{-1}) towards 1-pentanol to synthesize pentyl acetate.

3.5 Conclusions

AATase discovery and protein engineering has been limited because of lacking a suitable high throughput screening method. Typically, the activity towards short and medium chain volatile ester is measured by headspace GC, while the longer chain ester synthesis activity is by GC-MS. In this work, we developed a spectrophotometer based coupled enzyme assay which could be used for high throughput screening of ester synthesis activity by AATases. The produced CoA-SH by AATase is converted to succinyl-CoA by α-KGDH with other saturated substrates. The rate of reducing NAD^+ to NADH was measured by following the absorbance at 340nm, which enables the spectrophotometric measurement of AATase activity. Pyrazole is added to

suppress the whole cell lysate background from ADHs. The assay developed in this work was used to rapidly screen a library of six AATases with acyl-CoAs ranging from C2 to C12 and ethanol as co-substrate. AATase from tomato fruit, Atf-S.l of this library, was further characterized for its substrate specificity. It was found to be highly active towards ethyl ester synthesis with acyl-CoAs up to decanoyl-CoA and be specific to 1-pentanol as a co-substrate. This high throughput assay was used to screen short and medium chain ethyl ester synthesis as well as short and medium chain acetate ester synthesis. We anticipate that it is also suitable for discovering long chain ester synthase and protein engineering.

3.6 Acknowledgements

This work was supported NSF CBET-1403264 and by Bourns College of Engineering and the University of California, Riverside start-up fund.

3.7 References

1. Loser, C., Urit, T., Stukert, A., and Bley, T. (2013) Formation of ethyl acetate from whey by Kluyveromyces marxianus on a pilot scale. *J Biotechnol* **163**, 17-23

2. Urit, T., Manthey, R., Bley, T., and Loser, C. (2013) Formation of ethyl acetate by Kluyveromyces marxianus on whey: Influence of aeration and inhibition of yeast growth by ethyl acetate. *Eng Life Sci* **13**, 247-260

3. Rodriguez, G. M., Tashiro, Y., and Atsumi, S. (2014) Expanding ester biosynthesis in Escherichia coli. *Nat Chem Biol* **10**, 259-265

4. Tai, Y. S., Xiong, M. Y., and Zhang, K. C. (2015) Engineered biosynthesis of medium-chain esters in Escherichia coli. *Metab. Eng.* **27**, 20-28

5. Layton, D. S., and Trinh, C. T. (2014) Engineering modular ester fermentative pathways in Escherichia coli. *Metab. Eng.* **26**, 77-88

6. Vadali, R. V., Bennett, G. N., and San, K. Y. (2004) Applicability of CoA/acetyl-CoA manipulation system to enhance isoamyl acetate production in Escherichia coli. *Metab. Eng.* **6**, 294-299

7. Fujii, T., Nagasawa, N., Iwamatsu, A., Bogaki, T., Tamai, W., and Hamachi, M. (1994) Molecular-Cloning, Sequence-Analysis, and Expression of the Yeast Alcohol Acetyltransferase Gene. *Appl. Environ. Microbiol.* **60**, 2786-2792

8. Nagasawa, N., Bogaki, T., Iwamatsu, A., Hamachi, M., and Kumagai, C. (1998) Cloning and nucleotide sequence of the alcohol acetyltransferase II gene (ATF2) from Saccharomyces cerevisiae Kyokai No. 7. *Biosci Biotech Bioch* **62**, 1852-1857

9. Saerens, S. M. G., Verstrepen, K. J., Van Laere, S. D. M., Voet, A. R. D., Van Dijck, P., Delvaux, F. R., and Thevelein, J. M. (2006) The Saccharomyces cerevisiae EHT1 and EEB1 genes encode novel enzymes with medium-chain fatty acid ethyl ester synthesis and hydrolysis capacity. *J Biol Chem* **281**, 4446-4456

10. Salas, J. J. (2004) Characterization of alcohol acyltransferase from olive fruit. *J. Agric. Food Chem.* **52**, 3155-3158

11. Lucchetta, L., Manriquez, D., El-Sharkawy, I., Flores, F. B., Sanchez-Bel, P., Zouine, M., Ginies, C., Bouzayen, M., Rombaldi, C., Pech, J. C., and Latche, A. (2007) Biochemical and catalytic properties of three recombinant alcohol acyltransferases of melon. Sulfur-containing ester formation, regulatory role of CoA-SH in activity, and sequence elements conferring substrate preference. *J. Agric. Food Chem.* **55**, 5213-5220

12. Cumplido-Laso, G., Medina-Puche, L., Moyano, E., Hoffmann, T., Sinz, Q., Ring, L., Studart-Wittkowski, C., Caballero, J. L., Schwab, W., Munoz-Blanco, J., and Blanco-Portales, R. (2012) The fruit ripening-related gene FaAAT2 encodes an acyl transferase involved in strawberry aroma biogenesis. *J Exp Bot* **63**, 4275-4290

13. Park, Y. C., Shaffer, C. E. H., and Bennett, G. N. (2009) Microbial formation of esters. *Appl Microbiol Biot* **85**, 13-25

14. Kalscheuer, R., and Steinbuchel, A. (2003) A novel bifunctional wax ester synthase/acyl-CoA : diacylglycerol acyltransferase mediates wax ester and triacylglycerol biosynthesis in Acinetobacter calcoaceticus ADP1. *J Biol Chem* **278**, 8075-8082

15. Holtzapple, E., and Schmidt-Dannert, C. (2007) Biosynthesis of isoprenoid wax ester in Marinobacter hydrocarbonoclasticus DSM 8798: Identification and characterization of isoprenoid coenzyme A synthetase and wax ester synthases. *Journal of Bacteriology* **189**, 3804-3812

16. Barney, B. M., Mann, R. L., and Ohlert, J. M. (2013) Identification of a Residue Affecting Fatty Alcohol Selectivity in Wax Ester Synthase. *Appl. Environ. Microbiol.* **79**, 396-399

17. Galaz, S., Morales-Quintana, L., Moya-Leon, M. A., and Herrera, R. (2013) Structural analysis of the alcohol acyltransferase protein family from Cucumismelo shows that enzyme activity depends on an essential solvent channel. *Febs J* **280**, 1344-1357

18. Lin, J. L., and Wheeldon, I. (2014) Dual N- and C-Terminal Helices Are Required for Endoplasmic Reticulum and Lipid Droplet Association of Alcohol Acetyltransferases in Saccharomyces cerevisiae. *PLoS One* **9**, e104141

19. Athenstaedt, K., Zweytick, D., Jandrositz, A., Kohlwein, S. D., and Daum, G. (1999) Identification and characterization of major lipid particle proteins of the yeast Saccharomyces cerevisiae. *Journal of Bacteriology* **181**, 6441-6448

20. Stoveken, T., Kalscheuer, R., Malkus, U., Reichelt, R., and Steinbuchel, A. (2005) The wax ester synthase/acyl coenzyme A : diacylglycerol acyltransferase from Acinetobacter sp strain ADP1: Characterization of a novel type of acyltransferase. *Journal of Bacteriology* **187**, 1369-1376

21. Zhu, J., Lin, J.-L., Palomec, L., and Wheeldon, I. (2015) Microbial host selection affects intracellular localization and activity of alcohol-O-acetyltransferase. *Microbial Cell Factories* **14**, 35

22. Minetoki, T., Bogaki, T., Iwamatsu, A., Fujii, T., and Hamachi, M. (1993) The Purification, Properties and Internal Peptide Sequences of Alcohol

Acetyltransferase Isolated from Saccharomyces-Cerevisiae Kyokai No 7. *Biosci Biotech Bioch* **57**, 2094-2098

23. Malcorps, P., and Dufour, J. P. (1992) Short-Chain and Medium-Chain Aliphatic-Ester Synthesis in Saccharomyces-Cerevisiae. *European Journal of Biochemistry* **210**, 1015-1022

24. Shi, S. B., Valle-Rodriguez, J. O., Khoomrung, S., Siewers, V., and Nielsen, J. (2012) Functional expression and characterization of five wax ester synthases in Saccharomyces cerevisiae and their utility for biodiesel production. *Biotechnology for Biofuels* **5**

25. Barney, B. M., Wahlen, B. D., Garner, E., Wei, J. S., and Seefeldt, L. C. (2012) Differences in Substrate Specificities of Five Bacterial Wax Ester Synthases. *Appl. Environ. Microbiol.* **78**, 5734-5745

26. Knight, M. J., Bull, I. D., and Curnow, P. (2014) The yeast enzyme Ehtl is an octanoyl-CoA:ethanol acyltransferase that also functions as a thioesterase. *Yeast* **31**, 463-474

27. Dunn, B. J., Cane, D. E., and Khosla, C. (2013) Mechanism and Specificity of an Acyltransferase Domain from a Modular Polyketide Synthase. *Biochemistry-Us* **52**, 1839-1841

28. de Smidt, O., du Preez, J., and Albertyn, J. (2008) The alcohol dehydrogenases of Saccharomyces cerevisiae: a comprehensive review. *Fems Yeast Res* **8**, 967 - 978

29. Zhang, J. H., Chung, T. D. Y., and Oldenburg, K. R. (1999) A simple statistical parameter for use in evaluation and validation of\ high throughput screening assays. *J. Biomol. Screen*\ **4**\, 67\-73\

30. Horton, C. E., and Bennett, G. N. (2006) Ester production in E-coli and C-acetobutylicum. *Enzyme Microb Tech* **38**, 937-943

31. Tiwari, R., Koffel, R., and Schneiter, R. (2007) An acetylation/deacetylation cycle controls the export of sterols and steroids from S-cerevisiae. *Embo Journal* **26**, 5109-5119

32. Cauet, G., Degryse, E., Ledoux, C., Spagnoli, R., and Achstetter, T. (1999) Pregnenolone esterification in Saccharomyces cerevisiae - A potential detoxification mechanism. *European Journal of Biochemistry* **261**, 317-324

33. Shalit, M., Katzir, N., Tadmor, Y., Larkov, O., Burger, Y., Shalekhet, F., Lastochkin, E., Ravid, U., Amar, O., Edelstein, M., Karchi, Z., and Lewinsohn, E. (2001) Acetyl-CoA: Alcohol acetyltransferase activity and aroma formation in ripening melon fruits. *J. Agric. Food Chem.* **49**, 794-799

34. Matsuba, Y., Nguyen, T. T. H., Wiegert, K., Falara, V., Gonzales-Vigil, E., Leong, B., Schafer, P., Kudrna, D., Wing, R. A., Bolger, A. M., Usadel, B., Tissier, A., Fernie, A. R., Barry, C. S., and Pichersky, E. (2013) Evolution of a Complex Locus for Terpene Biosynthesis in Solanum. *Plant Cell* **25**, 2022-2036

35. Ueda, Y., Nishimura, K., and Chachin, K. (1997) Alcohol Acetyltransferase in Tomato. *Applied Biological Science* **3**, 25-32

3.8 Figures and Tables

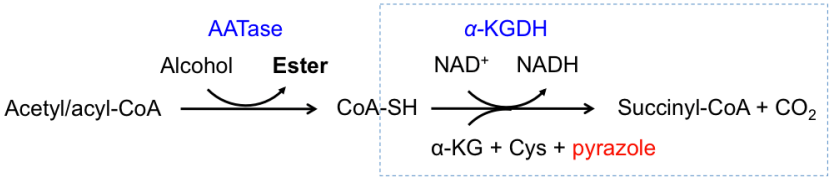

Figure 3.1. A coupled-enzyme reaction for determing alcohol-O-acetyl/acyltransferase (AATase) activity. α-ketoglutarate (α-KG), cystein (Cys), and NAD^+ are substrates required for α-ketoglutarate dehydrogenase (α-KGDH). Pyrazole is a chemical inhibitor of alcohol dehydrogenase (ADH) and is included in the assay to suppress background NAD^+ reduction activity from *S. cerevisiae* whole cell lysate samples. The rate of ester synthesis by AATase was measured the generation of NADH ($\varepsilon_{NADH,340nm}$ = 6.22 $mM^{-1}cm^{-1}$).

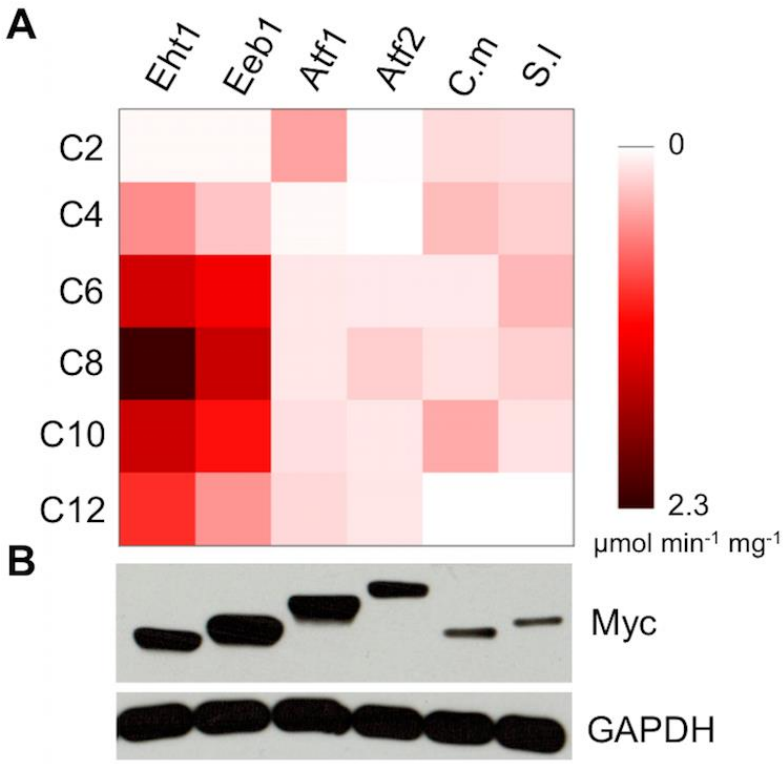

Figure 3.2. AATase library screening. (**A**) Heat map of ethyl ester synthesis rates from Eht1 (*S. cerevisiae*), Eeb1 (*S. cerevisiae*), Atf1 (*S. cerevisiae*), Atf2 (*S. cerevisiae*), Atf-C.m (*C. melo*), and Atf-S.l (*S. lycopersicum*). All assays were performed with the following reaction conditions: 20 mM ethanol, 0.5 mM acetyl/acyl-CoA, 2 mM α-KG, 10 mM cystein, 2 mM NAD^+, 10 mM $MgCl_2$, and 0.03 U α-KGDH. Reactions were buffered with 100 mM phosphate, pH 7.4 and 1 μg of whole cell lysate protein was used in each assay. All reactions were performed in triplicate. (B) Western blot analysis of protein expression. Anti-myc antibody was used to against AATases while anti-GAPDH was used as the loading control.

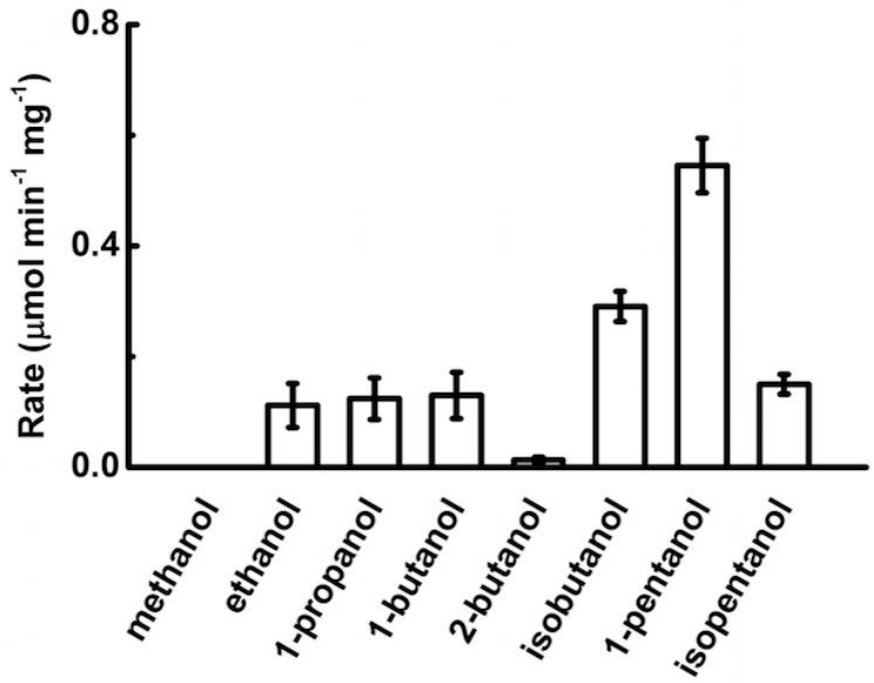

Figure 3.3. Alcohol-O-acyltransferase from tomato fruit (Atf-S.l) has high activity towards 1-pentanol as a co-substrate during acetate ester synthesis. All reactions were performed in triplicate.

Table 3.1. Strains, plasmids, and AATase genes used in Chapter 3.

Name	Description	Source
Strains		
S. cerevisiae (BY4742)	*MATα his3Δ1 leu2Δ0 lys2Δ0 ura3Δ0*	Lin and Wheeldon[1]
E. coli (DH5α)	*F– Φ80lacZΔM15 Δ(lacZYA-argF) U169 recA1 endA1 hsdR17 (rK–, mK+) phoA supE44 λ– thi-1 gyrA96 relA1*	Life technologies
Plasmids		
pRS426		GE Healthcare
pPGK1	Constitutive expression driven by PGK1p-PGK1t	Lin and Wheeldon[1]
pPGK1-Atf1(Sc)-myc	Atf1 from *S. cerevisiae* cloned into SacII and NotI sites of pPGK1	this study
pPGK1-Atf2(Sc)-myc	Atf2 from *S. cerevisiae* cloned into SacII and NotI sites of pPGK1	this study
pPGK1-Atf1(Sl)-myc	Atf1 from *S. lycopersicum* cloned into SacII and NotI sites of pPGK1	this study
pPGK1-Atf1(Cm)-myc	Atf1 from *C. melo* cloned into SacII and NotI sites of pPGK1	this study
pPGK1-Eht1(Sc)-myc	Eht1 from *S. cerevisiae* cloned into SacII and NotI sites of pPGK1	this study
pPGK1-Eeb1(Sc)-myc	Eeb1 from *S. cerevisiae* cloned into SacII and NotI sites of pPGK1	this study
Genes		
Atf1 (Sc)	NCBI accession no.: NP_015022	
Atf2 (Sc)	NCBI accession no.: NP_011693	
Atf1 (Sl)	NCBI accession no.: NP_001234496	
Atf1 (Cm)	NCBI accession no.: BAB78588	
Eht1(Sc)	NCBI accession no.: NP_009736	
Eeb1 (Sc)	NCBI accession no.: NP_015230	

3.9 Supporting Information

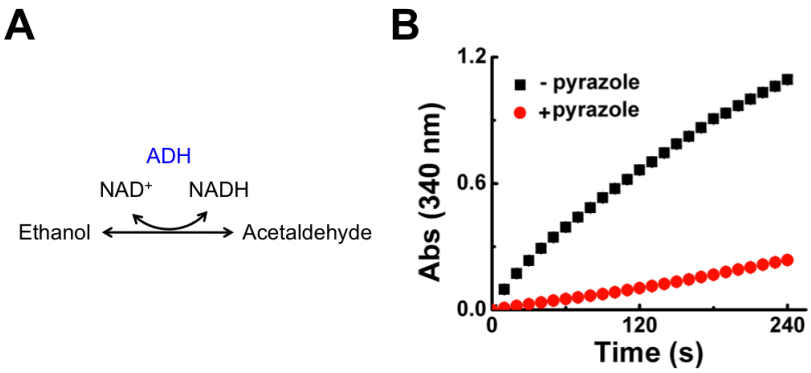

Figure S3.1. Pyrazole reduces NADH background activity in whole cell lysates of *S. cerevisiae*. (**A**) Alcohol dehydrogenase activity (ADH) reduces NAD^+ to NADH in the presence of ethanol. (**B**) The addition of 15 mM pyrazole to whole cell lysate samples suppresses the background activity (Reaction conditions: 20 mM ethanol, 0.5 mM acetyl-CoA, 2 mM α-KG, 10 mM cystein, 2 mM NAD^+, 10 mM $MgCl_2$, and 0.03 U α-KGDH, and 100 mM phosphate, pH 7.4).

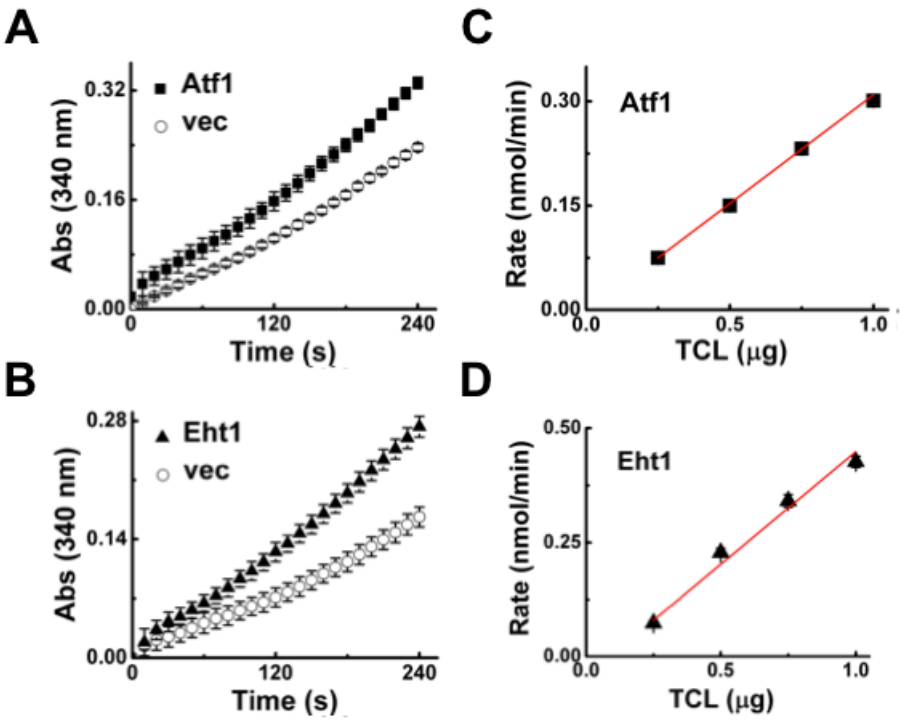

Figure S3.2. Coupled enzyme assay for quantifying short and medium chain ethyl ester biosynthesis. (**A**) Atf1 synthesis of ethyl acetate produced NADH from the coupled α-KGDH reaction at a higher rate than the empty vector control. (**B**) Ester biosynthesis assay of Eht1 with ethanol and butyryl-CoA. (**C,D**) Atf1 and Eht1 ethyl ester synthesis rates measured by the α-KGDH coupled reaction increased linearly with total whole cell lsyate. All assays were performed with the following reaction conditions: 20 mM ethanol, 0.5 mM acetyl/acyl-CoA, 2 mM α-KG, 10 mM cystein, 2 mM NAD^+, 10 mM $MgCl_2$, and 0.03 U α-KGDH, and 100 mM phosphate, pH 7.4. One-μg of whole cell lysate protein was used in the A and B.

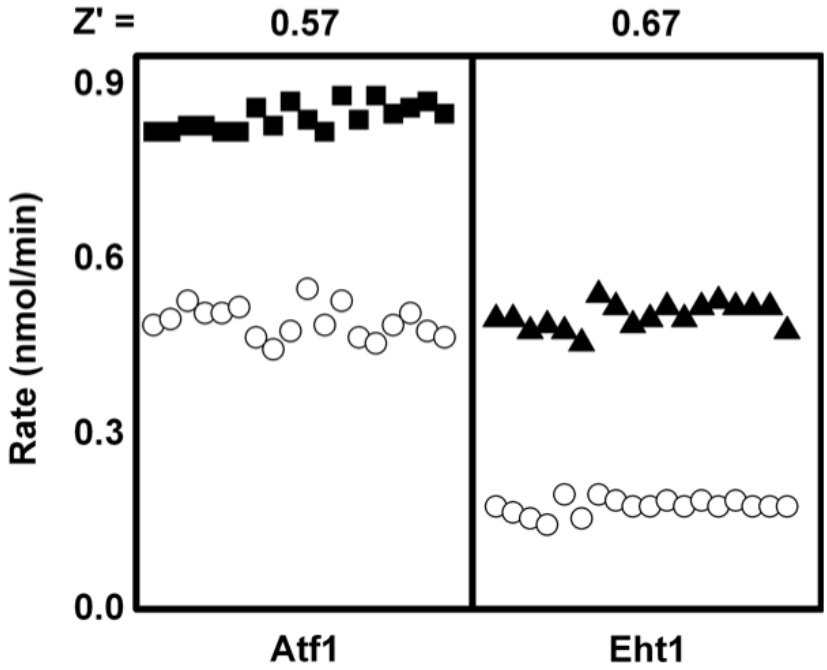

Figure S3.3. Z' factor analysis of the α-KGDH coupled enzyme assay for AATase activity screening. Aft1 synthesis of ethyl acetate from ethanol and acetyl-CoA (solid squares), Eht1 synthesis of ethyl butyrate from ethanol and butyryl-CoA (solid triangles), and empty vector controls (open circles).

Table S3.1 Primers used to amplify genes.

Primers	DNA sequence	
Atf1(Sc)-myc	Forward: CAAACCGCGGATGAATGAAATCGATGAGAAAAAT C Reverse: CAAAGCGGCCGCCTAGAGGTCTTCTTCGGAAATCAACTTCTGTTC AGGGCCTAAAAGGAGAGC	this study
Atf2(Sc)-myc	Forward: CAAACCGCGGATGGAAGATATAGAAGGATACGAAC Reverse: CAAAGCGGCCGCTTAGAGGTCTTCTTCGGAAATCAACTTCTGTTC AAGCGACGCAAATTCGCC	this study
Atf1(Sl)-myc	Forward: CAAACCGCGGATGGCTAATATTTTGCCAATTTCT Reverse: CAAAGCGGCCGCTTAGAGGTCTTCTTCGGAAATCAACTTCTGTTC AATATTAGAAATAATAACTCTGAAAGTCAT	this study
Atf1(Cm)-myc	Forward: CAAACCGCGGATGGAAACTATGCAAACTATTGATTT Reverse: CAAAGCGGCCGCTTAGAGGTCTTCTTCGGAAATCAACTTCTGTTC CAAAGCAGACAAAATAGTTTGCA	this study
Eht1(Sc)-myc	Forward: CAAACCGCGGATGTCAGAAGTTTCCAAATGGC Reverse: GAAAACTAGTCTAGAGGTCTTCTTCGGAAATCAACTTCTGTTC TACGACTAATTCATCAAACTTAGTGAAA	this study
Eeb1(Sc)-myc	Forward: CAAACCGCGGATGTTTCGCTCGGGTTACTAT Reverse: GAAAACTAGTCTAGAGGTCTTCTTCGGAAATCAACTTCTGTTC TAAAACTAACTCATCAAAGCTGCC	this study

Table S3.2. AATase library screening. Reaction rates of ethyl ester synthesis from Eht1 (*S. cerevisiae*), Eeb1 (*S. cerevisiae*), Atf1 (*S. cerevisiae*), Atf2 (*S. cerevisiae*), Atf-C.m (*C. melo*), and Atf-Sl (*S. lycopersicum*). Assays contained 1 mg of whole cell lysate protein.

nmol/min	acetyl-CoA	butyryl-CoA	hexanoyl-CoA	octanoyl-CoA	decanoyl-CoA	lauroyl-CoA
Eht1	0.044±0.014	0.518±0.090	1.415±0.083	2.220±0.186	1.463±0.154	0.933±0.280
Eeb1	0.037±0.004	0.267±0.021	1.248±0.095	1.482±0.144	1.079±0.118	0.478±0.080
Atf1	0.428±0.022	0.039±0.210	0.106±0.021	0.111±0.017	0.144±0.055	0.174±0.032
Atf2	0.020±0.002	N/A	0.102±0.051	0.229±0.031	0.115±0.060	0.119±0.018
C.m	0.161±0.027	0.311±0.086	0.099±0.064	0.140±0.071	0.388±0.043	N/A
S.l	0.156±0.041	0.216±0.106	0.326±0.042	0.222±0.015	0.136±0.039	N/A

Chapter 4. Synthetic Protein Scaffolds for Biosynthetic Pathway Co-Localization on Lipid Droplet Membranes

4.1 Abstract

Eukaryotes, containing organelles as a distinctive feature from prokaryotes, are able to organize metabolic pathways throughout the cell. This organization is often lost when engineering pathways, resulting in flux imbalance and loss of kinetic advantages of substrate channeling. Here, we develop a protein-based scaffold for co-localizing multiple enzymes on the membrane of intracellular lipid droplets (LDs). LD targeting protein oleosin and cohesin-dockerin interaction pairs recruited upstream enzymes for ester biosynthesis in *S. cerevisiae* to the native localization of the terminal reaction enzyme, alcohol-O-acetyltransferase (Atf1). The effect of colocalization and substrate channeling was demonstrated by fluorescence microscopy and Förster Resonance Energy Transfer (FRET) studies. With further optimized scaffolds and pathway expression levels, the production rate of ethyl acetate *in vivo* was increased nearly two-fold. This strategy can be applied for biocatalysts of which activity are membrane-dependent by co-localizing and spatially organizing pathway enzymes on LDs.

4.2 Introduction

A defining feature of eukaryotic biochemistry is the spatial organization of metabolic pathways in and on membrane-bound organelles. This organization provides potentially viable targets for improving the rates of microbial biosynthesis. Key steps in yeast long chain fatty acid synthesis and lipid storage are localized to the endoplasmic reticulum (ER),(1,2) many plant secondary metabolite pathways that produce valuable pharmaceuticals are often organized on vacuole and ER membranes,(3) and the focus of this study, yeast ester biosynthesis, localizes to lipid droplets (LDs).(4,5) The intracellular organization of these and other membrane-bound pathways is catalytically useful. Native multienzyme structures with controlled interenzyme distances and ratios of active sites can concentrate metabolites and drive reactions counter to unfavorable thermodynamics, isolate toxic intermediates from the rest of the cell, and prevent the loss of substrates to alternative pathways.(6,7) When engineering synthetic pathways, the benefits of spatial organization are often lost, as differences in eukaryote physiologies can disrupt localization and translating pathways to the common bacterial host *E. coli* or other prokaryotes results in a loss of native organelles.

Metabolic engineering and synthetic biology use genome engineering and pathway refactoring tools to optimize flux along targeted biosynthetic pathways by disrupting non-essential competing pathways, increasing the activity of native and heterologous enzymes to alleviate kinetic bottlenecks, and modifying transcription to control pathway expression.(8) Enzyme co-localization has emerged as an additional strategy to re-create some of the effects of natural spatial organization and introduce substrate (or metabolite)

channeling in synthetic pathways.(9,10) Molecular scaffolds with domains that selectively bind pathway enzymes can create multienzyme aggregates with high enzyme concentrations, minimal distance between active sites, controlled ratios of enzymes, and optimized spatial organization.(11) Using intracellular scaffolds of protein-protein interaction domains, this strategy has been used to co-localize pathways for mevalonate, glucaric acid, and butyrate biosynthesis in *E. coli,* resulting in 77-, 5-, and 3-fold improvements in product titers, respectively.(12-14) Resveratrol and 1,2 propanediol titers have also been improved (5 and 4.5-fold, respectively) with plasmid-based DNA scaffolds that recruit and co-localize zinc-finger modified multienzyme pathways in *E. coli*.(15) Controlled intracellular assembly of multistep pathways has also been achieved with RNA scaffolds. Modified enzymes that bind to aptamers within the scaffold were used to created two-, three-, and four-step pathways that enhanced product titers and in some cases overall production rates.(16,17) These examples of multienzyme co-localization are evidence that pathway structure can improve metabolite titers, but the scaffolding technologies have been limited to cytosolic organization and are not accessible to membrane-bound pathways. The lack of membrane-based scaffolding technologies is beginning to be addressed with engineered synthetic lipid-containing scaffolds. Lipid/protein particles based on the proteins of lipid-encapsulated bacteriophage ϕ6 have recently been used to assemble a two-step biosynthetic pathway in *E. coli*.(18)

Enhanced product titers from engineered microbes with spatially organized pathways are not necessarily the result of equivalent increases in biosynthetic rates. Analysis of *in*

vivo scaffolded pathways points to a range of effects that can produce higher titers. Co-localization and controlled clustering of enzymes in engineered pathways can benefit microbial growth by limiting the concentrations of toxic pathway intermediates,(12,19) improve the underlying kinetics of bottleneck enzymes,(13) and minimize metabolic burden by enabling low pathway expression-levels.(10,12) Overall reaction rates can also be increased: controlled spatial organization can limit parasitic side reactions, enhancing flux along the desired pathway;(17) molecular scaffolds can increase local substrate concentrations driving higher rates at low substrate concentrations;(20,21) and, enzyme proximity can enhance pre-steady state kinetics.(21) The limits of rate acceleration have recently been modeled, suggesting that with optimized multienzyme cluster size, architecture, and number per cell, up to ~6-fold enhancements in the rate of two-step pathways are possible.(22)

To take advantage of the benefits of spatial organization with membrane-bound pathways we engineered a protein scaffold in yeast to co-localize the ester biosynthesis pathway on the outer membrane surface of intracellular LDs. In yeast fermentations, low concentrations of short and medium chain volatile esters are synthesized through the condensation of an alcohol and acetyl-CoA by alcohol-O-acetyltransferase (AATase; Figure 4.1a). The produced esters (*e.g.*, ethyl and isoamyl acetate, among others) are responsible for the distinctive smells of yeast fermentations and are industrially useful as solvents and flavor and fragrance compounds. The predominant AATase for short chain ester synthesis in *S. cerevisiae* is Atf1, with contributions from Atf2.(23) Atf1 and -2 are membrane-associated proteins that localize to the ER and traffic to LDs during the

stationary phase.(4) Heterologous expression of Atf1 and -2 as well as AATases from other yeasts and fruit results in a loss of membrane localization and the formation of low activity aggregates in the cytosol.(24) Overexpression in *S. cerevisiae* does not disrupt native localization and maintains high Atf activity. Upstream enzymes in the acetyl-CoA branch of yeast ester biosynthesis, aldehyde dehydrogenase (Ald6) and acetyl-CoA synthetase (Acs1), are naturally segregated from Atf1, localizing to the cytosol (Ald6 and Acs1) and mitochondria (Acs1).(25-27) We reasoned that the spatial organization of upstream enzymes around the native intracellular localization of the terminal reaction step, Atf1, would produce high local enzyme concentrations and limit crosstalk with other metabolic pathways, thus increasing pathway flux and the conversion of intracellular acetyl-CoA to ethyl acetate under ethanol producing fermentation conditions.

The re-localization of enzymes from their native targets to LDs requires a localization tag that can be fused to target proteins. Oleosin was identified to localize to yeast LDs under fermentation conditions (Figure S4.1). The oleosin domain formed the basis of a synthetic protein scaffold of cohesin and dockerin protein-protein interaction domains that was able to co-localize native *S. cereisiae* Ald6 and Acs1 with Atf1 on LDs (Figure 4.1b). Fluorescence microscopy and Förster Resonance Energy Transfer (FRET) studies showed that the enzymes are tightly clustered on LDs and *in vitro* kinetic analysis revealed increased rates of ethyl acetate synthesis due to co-localization. To rapidly optimize scaffold and pathway expression and structure, we used a colorimetric assay for ethyl acetate biosynthesis and screened a combinatorial library of scaffolds with a series

of different strength promoters to drive enzyme and scaffold expression. This approach enabled us to re-localize upstream pathway enzymes around the native LD-localization of Atf1 and demonstrate the effects of co-localization on pathway flux and ethyl acetate fermentation titers.

4.3 Methods

Strains and culture conditions

All *E. coil* and *S. cerevisiae* strains used in this work are summarized in Table 4.1. All modified yeast strains were derived from BY4742. *E. coli* DH5α and BL21(DE3) used for molecular cloning and protein expression, respectively. *E. coli* was grown in Luria Broth (LB) (Sigma) medium containing 50 μg mL^{-1} ampicillin (Fisher) for cloning experiment and 50 μg mL^{-1} kanamycin (Fisher) for HA-myc-GFP-$(His)_6$ expression. All *S. cerevisiae* BY4742 strains were grown in synthetic complete medium (SC) containing 0.67% yeast nitrogen base (Bacton-Dickinson), amino acid supplements (Sunrise and Sigma), and 2% glucose (Sigma).

Plasmid and yeast strain construction

The plasmids used in this study are listed in Table 4.2. All heterologous genes were codon optimized for expression in *S. cerevisiae* by IDT codon optimization tool and synthesized by a gene assembly method.(28) DNA sequences of heterologous genes are provided in Table 4.3. Yeast genes, promoters, and terminators were amplified from genomic DNA. The peptide tags used for western blot were incorporated into proteins by including the DNA sequence in the appropriate PCR amplification primers.

Synthetic scaffolds, Ole-C_1-C_2 and its variants, were assembled from oleosin,(29) X82 (C_1),(30) and cohesin (C_2).(31) Enzyme-dockerin and enzyme-fluorescent protein-dockerin fusions were assembled via OE-PCR. The resulting fragments were cloned into either pRS426-P_{PGK1}-T_{PGK1} at SacII and SpeI sites or p413-P_{GPD} at SpeI and XhoI sites. pRS426-P_{PGK1}-*Oleosin-Cohesin* (C_2)-*YFP*-T_{PGK1} was constructed with an insertion of YFP at NotI and SpeI sites and Oleosin-Cohesin (C_2) at SacII and NotI sites. pRS426-P_{PGK1}-*ATF1-DsRed*-T_{PGK1} was constructed with an insertion of *ATF1* at SacII and NotI sites and DsRed at NotI and SpeI sites of pRS426-P_{PGK1}-T_{PGK1}. Plasmids for overexpression of the pathways were assembled in either pRS316 or pRS426 by transforming promoters, genes, and terminators to *S. cerevisiae* through DNA assembler.(32)

The combinatorial library for pathway optimization included synthetic scaffolds with 2- and 3-cohesin (C_2) domains and a second copy of Acs1. Both the scaffold and Acs1 were combined with a series of differed promoters. Oleosin-X82 (C_1)-cohesin (C_2) was extended with 1- or 2-copies of cohesin (C_2) at 3' end by Gibson assembly. Casettes that included the additional copy of Acs1 and the scaffolds were also assembled by Gibson assembly. The resulting genetic components were transformed into *S. cerevisiae* for assembly by the DNA assembler moethod.(32) Pathway vectors constructed by yeast homologous recombination were isolated by Zymoprep™ Yeast Plasmid Miniprep I kit. Isolated plasmids were transformed into *E. coli*, amplified, and sequenced. A second chromosomal copy of *ATF1* was integrated at the *yprcΔ15* locus of chromosome 16 by homologous recombination. The cassette included the *LEU2* marker amplified from

pRS315, P_{TDH3}, *ATF1*, and T_{TEF2}, which were assembled into pRS316. Finally, epitope-tagged GFP was constructed with a forward primer containing HA and myc tags and a reverse primer containing His tag. The resulted fragment was cloned into pET29 between XbaI and XhoI sites.

Fluorescence microscopy and FRET analysis

Cells were imaged using an Olympus BX51 microscope (UPlanFL 100X 1.30 oil-immersion objective lens, mercury lamp) and fluorescence micrographs were captured by a Q-Imaging Retiga Exi CCD camera. Images were processed using CellSens Dimension 1.7 software (Olympus). In all cases, at least three cell populations were analyzed and images representative of the cell populations are shown. FRET analysis was accomplished using confocal laser microscopy (Leica SP5; Bannockburn, IL) on cells that had reached stationary phase by the quantitative acceptor photobleaching method. Pre- and post-bleaching images were captured with CFP excitation at 458 nm and YFP excitation at 514 nm using an argon laser and appropriate emission bands. The acceptor was bleached with high intensity at 514 nm and donor intensity in the region of interest was compared before and after acceptor bleaching. FRET efficiency (E_{FRET}) was calculated on a pixel-by-pixel basis as $E_{FRET} = 1-(D_{pre}/D_{post})$. Positive FRET occurred if acceptor bleaching resulted in increased donor fluorescence.

Preparation of cell lysates

Yeast cells harboring expression plasmids were cultured to early stationary phase in 50 mL SC-Ura in 250 ml baffled flasks. Cells were harvested by centrifugation at 3,500 rpm for 5 min at 4 °C, and washed twice with 100 mM potassium phosphate buffer (pH

7.4) containing 2 mM $MgCl_2$. Equal volumes of wet cell pellets and 425-600 μm diameter acid-washed glass beads (Sigma-Aldrich) were added to a 15 mL tube and resuspended in 1 mL ice-cold lysis buffer (100mM potassium phosphate buffer, 2 mM $MgCl_2$, 2 mM dithiothreitol (DTT), and protease inhibitor cocktail (Roche), pH7.4). Cells were disrupted by vortexing 10 times for 30 s. After each vortexing, the suspension was kept on ice for 30 s. Beads were removed by centrifugation at 500g for 5 min at 4 °C and the supernatant was transferred to a pre-cooled 1.5 mL tube. Cell lysate protein concentrations were determined by a commercially available assay (Pierce 660 nm Protein Assay, Thermo Fisher) and quantified with Nanodrop 2000c.

Enzyme and pathway activity assays

Aldehyde dehydrogenase (Ald6) and acetyl-CoA synthetase (Acs1) activity assays were conducted as previously described.(33) Aldehyde dehydrogenase activity reaction mixtures containing 0.4 mM DTT, 10 mM $MgCl_2$, 0.4 mM $NADP^+$, 15 mM pyrazole, and 100 mM potassium phosaphate buffer (pH 8.0) were used with 1-5 μg cell lysate protein. Reactions were initiated with 0.1 mM acetaldehyde. To determine the activity of acetyl-CoA synthetase, reactions consisting of 10 mM malate, 8 mM ATP, 1 mM NAD^+, 10 mM $MgCl_2$, 3 U malate dehydrogenase (Sigma), 0.4 U citrate synthase (Sigma), and 100 mM potassium phosphate (pH 7.4) were used with 1-5 μg cell lysate protein. Reactions were initiated with 0.2 mM CoA-SH and 10 mM potassium acetate.

To evaluate pathway efficiency from acetyl-CoA synthetase (Acs1) to alcohol acetyltransferase (Atf1), reaction mixtures containing 10 mM $MgCl_2$, 500 mM ethanol, 8 mM ATP, 1 mM CoA, and 100 mM potassium phosphate (pH 7.4) were used with 5 μg

cell lysate protein. Reactions were initiated with 100 mM potassium acetate and were allowed to continue for 5 min. 1 g NaCl was used to stop the reaction and produced ethyl acetate was quantified by headspace gas chromatography (GC). To evaluate pathway efficiency from aldehyde dehydrogenase (Ald6) to acetyl-CoA synthetase (Acs1), reaction mixtures containing 10 mM $MgCl_2$, 0.4 mM DTT, 0.4 mM $NADP^+$, 8 mM ATP, 15 mM pyrazole, 0.5 mM CoA and 100 mM potassium phosphate (pH 7.4) were used with 5 μg cell lysate protein. Reactions were initiated by adding 0.1 mM acetaldehyde and stopped by adding perchloric acid to a final concentration of 1 M. Samples were neutralized with KOH and the resulting solutions were analyzed by the acetyl-CoA Assay Kit (Sigma-Aldrich). All reaction assays were completed with a minimum of three replicates. In all cases the mean and standard deviation are presented.

Protein expression analysis

Western blots were performed using standard procedure. Briefly, 5 μg cell lysate protein were loaded on Any kD™ or 7.5% Mini-PROTEAN® TGX™ Gel (Bio-Rad) and run at 150 V for 30 to 60 min. Samples were electrophoretically transferred overnight to a PVDF membrane at 25 V. Membranes were blocked with 5% non-fat milk in Tris buffer saline with TWEEN-20 (TBST) buffer for 1 h at room temperature, washed, and incubated with primary antibody in TBST with 1% non-fat milk for 1 h. Secondary antibody in TBST with 1% non-fat milk was applied, and incubated at room temperature for 0.5 h. After washing with TBST, Immobilon Western HRP Substrate (Millipore) was used for signal detection and UN-SCAN-IT gel 6.1 software was used to quantify band intensity. The following antibodies were used: rabbit anti-HA (71-5500; Invitrogen),

mouse anti-His (A00186-100; Genescript), rabbit anti-V5 (V8137, Sigma), rabbit anti-myc (C3956; Sigma), mouse anti-GAPDH (MA5-15738; Thermo Fisher Scientific), goat anti-rabbit IgG-HRP (65-6120; Invitrogen), goat anti-mouse IgG-HRP (31430; Thermo Fisher Scientific).

UV-Vis ester detection assay and library screening

A colorimetric assay based on the stoichiometric conversion of esters to a ferric chelate complex was developed for rapid library screening.[44] Briefly, hexane extracted ethyl acetate was first reacted with alkaline hydroxylamine to produce hydroxamic acid and ethanol. The hydroxamic acid product was subsequently reacted with ferric ions to form a ferric chelate complex with strong absorbance at 520 nm. Alkaline hydroxylamine solutions were prepared by combining equal volumes of 2.5% (w/v) solutions hydroxylamine•HCl and sodium hydroxide in 95% ethanol. Ferric perchlorate stock solutions (0.8% v/v) were prepared by combining ferric chloride dissolved in 75% perchloric acid and deionized water. Ferric perchlorate working solutions were prepared from stock solutions by diluting 20 times in absolute ethanol. The colorimetric assay was performed by mixing 150 μL of hexane-extracted ethyl acetate and with 50 μl of alkaline hydroxylamine solution and allowing the reaction to proceed for 10 mins at room temperature. The produced hydroxamic acid was reacted with ferric perchlorate working solutions for 5 min to form ferric chelate complex. Ethyl acetate quantification was accomplished by measuring the absorbance of the ferric chelate complex at 520 nm and comparing to a standardized calibration curve.

Single colonies were cultured overnight at 250 rpm and 30 °C in 2 mL of SC -Ura with 2% glucose in 14 mL culture tubes. Overnight cultures were transferred to 3 mL SC -Ura with 10% glucose in 15 mL conical tubes with a starting OD_{600} of 0.05. Fermentations continued for 24 h at 250 rpm and 30 °C. Post fermentation, 50 μL of culture was withdrawn for OD_{600} measurement and ethyl acetate was extracted with 3 mL hexane. Extraction was conducted with a rotary shaker (MAXQ 2508) for 10 min with vigorous mixing. 1.4 mL of the mixtures was transferred to microcentrifuge tubes and 13,000 rpm was used to separate the hexane and aqueous phases. Ethyl acetate extracted in the top layer was withdrawn and quantified using the developed colorimetric assay in 96-well microplates.

Ethyl acetate fermentations

Single colonies were inoculated into 2 mL SC -Ura and with 2% glucose in 14 mL culture tubes and grown overnight at 250 rpm and 30 °C. Overnight cultures were transferred to 20 mL SC -Ura with 2% glucose in 50 mL conical tubes. The cultures were initiated with OD_{600} of 0.05 cells, and fermented for 24 h at 250 rpm and 30 °C. 1.4 mL fermentation culture was transferred to a microcentrifuge tube, centrifuged at 13,000 rpm, and 1 mL fermented broth was harvested and transferred to a 10 mL glass vial (Fisher) for GC analysis. 1 g NaCl was added to the sample and 50 mg L^{-1} pentanol was used as the internal standard.

Gas chromatography analysis

Ethyl acetate was quantified by a headspace gas chromatography (GC) with a flame ionization detector (FID) (Agilent Technologies 7890A GC with CTC-PAL headspace

mode injector). The separation of volatile compounds was carried out by Rtx®-WAX column (30 m, 0.32 mmID, 5 mm film thickness; RESTEK) with helium as carrier gas. The GC oven temperature was initially held at 30 °C for 7 min and increased with a gradient of 50 °C/min until 200 °C, and the held for 4 min. The FID was held at 250 °C. 1 ml headspace gas was injected to the GC with 10:1 split ratio, and 1-pentanol was used as internal standard.

4.4 Results

Spatial organization of a multi-enzyme pathway co-localized to LDs

Theoretical and experimental analysis of substrate channeling in coupled enzyme reactions suggests that the distance between enzyme anchor points should be less than ~5 nm to produce significant enhancements in catalysis.(34) The flexibility of the cohesion-based protein scaffold prevents accurate calculation of the distance between immobilized Ald6-D_1, Acs1-D_2, and LD-localized Atf1, as such we quantified pathway organization by FRET microscopy (Figure 4.2). Acceptor photobleaching experiments showed that scaffold-bound Ald6-YFP-D_1 and Acs1-CFP-D_2 maintained a FRET efficiency of 13±4%, while a CFP-tagged scaffold and YFP-tagged Atf1 had an efficiency of 15±2% (< 4.5 nm average interenzyme distance).(35,36) Control experiments with cytosolic YFP and CFP tagged scaffold did not produce a positive FRET signal. The interenzyme distances achieved with the LD scaffold are sufficient to produce an effect of metabolic channeling and are comparable to a LD-localized CFP-YFP fusion, which produced a FRET efficiency of 37±4% (< 3 nm average interenzyme distance).

Enzyme co-localization accelerates acetyl-CoA and ethyl acetate biosynthesis rates

The scaffold Ole-C_1-C_2, Acs1-D_2, and Ald6-D_1 were co-expressed from a single copy number expression vector, while *ATF1* was integrated in the genome at the *yprcΔ15* locus on Chr XVI, a previously characterized high expression integration site.(37) P_{TEF1}, P_{TDH2}, P_{TDH3}, and P_{ADH1} constitutive promoters were used to transcribe *ACS1-D_2, ALD6-D_1*, *ATF1*, and *OLE-C_1-C_2*, respectively. Preliminary experiments testing the effect of episomal pathway expression showed reduced Atf1 expression when Ole-C_1-C_2 was co-expressed (Figure S4.2). Variable enzyme expression levels in the presence and absence of the scaffold would complicate analysis of the co-localization effect, thus *ATF1* was integrated in the genome resulting in normalized pathway expression levels.

To demonstrate the effects of pathway co-localization we first evaluated acetyl-CoA and ethyl acetate biosynthesis from two-step pathways (Ald6/Acs1 and Acs1/Atf1, respectively). Cell lysates prepared from stationary phase cultures were equilibrated with pathway substrates and cofactors (ATP, CoA-SH, and $NADP^+$ for Ald6/Acs1; ethanol, ATP, and CoA-SH for Acs1/Atf1) and reactions were initiated by the addition of acetaldehyde (Ald6/Acs1) and acetate (Acs1/Atf1). To confirm that LDs remained intact, cell lysates containing Ole-CFP were prepared in parallel and LD morphology was confirmed by fluorescence microscopy (Figure S4.3). *S. cerevisiae* with integrated *ATF1* produced 85±20 nmol $min^{-1}mg^{-1}$of acetyl-CoA from natively expressed Ald6 and Acs1 (Figure 4.3b). The rate of acetyl-CoA synthesis was 93±15 nmol $min^{-1}mg^{-1}$ when Ald6-D_1 and Acs1-D_2 were overexpressed. Co-localization of the pathway enzymes on LDs with the co-expression of the Ole-C_1-C_2 scaffold increased the rate of acetyl-CoA

production to 159±8 nmol $min^{-1}mg^{-1}$, 1.8-fold enhancement over the control strain and unassembled pathway. Similarly, the rate of the last two reaction steps of ethyl acetate biosynthesis, Acs1/Atf1, increased 2.9 and 1.9-fold over the control strain and unassembled pathway, respectively (Figure 4.3c; *ATF1* integrated control, 14±1 nmol $min^{-1}mg^{-1}$; unassembled control, 21±0.4 nmol $min^{-1}mg^{-1}$; and, co-localized pathway, 40±2 nmol $min^{-1}mg^{-1}$). Western blot analysis of the expressed pathway and scaffold revealed that enzyme levels were consistent across the tested strains (Figure S4.4).

A traditional test for substrate channeling is the competition for pathway intermediates by an orthogonal reaction.(6,7) Competing side reactions reduce the overall pathway reaction rate by consuming pathway intermediates that diffuse to the bulk solution. The effect of substrate channeling is protection against competing reactions and an increase in the rate of the co-localized pathway. The cell lysate assays shown in Figure 4.3 inherently create a test for channeling because natively expressed enzymes (*e.g.*, pyruvate dehydrogenase, citrate synthase, and acetyl-CoA synthetase-2, among others) compete for the acetate, CoA-SH, and acetyl-CoA intermediates of the Ald6/Acs1 and Acs1/Atf1 coupled reactions. The rates of the Ald6/Acs1 and Acs1/Atf1 reactions increased when co-localized on the LD-membrane while enzyme levels remained constant in comparison to the unassembled pathways, thus providing evidence of substrate channeling along the structured ethyl acetate biosynthesis pathway.

Optimizing pathway architecture and expression enhances ester biosynthesis

The *in vitro* kinetic analysis of the assembled and un-assembled pathways provided evidence that co-localization of Ald6-D_1, Acs1-D_2, and Atf1 enhanced the rate of ethyl

acetate biosynthesis. To optimize pathway flux, we created a combinatorial library of the pathway by varying scaffold design and promoter strength. Kinetic analysis of Acs1-D_2 and Ald6-D_1 suggested that Acs1 activity was limiting (Figure 4.3). Western blot analysis of the expressed pathway supports this conclusion. Comparison of Ald6-D_1, Acs1-D_2, and Atf1 expression levels relative to a GFP standard revealed low Acs1-D_1 expression (Figure S4.5). In light of these results, our optimization strategy focused on increasing Acs1-D_2 expression and varying the ratio of Acs1-D_2 to Ald6-D_1 on the LD-localization scaffold. A library of 60 pathway variants was created by homologous recombination in *S. cerevisiae* as previously described.(32) The design of the genetic constructs and pathway variants are shown in Figure 4.4a. A second copy of Acs1-D_2 with different strength promoters (P_{PGK1}, P_{CCW12}, P_{HXT7}, and P_{ADH1}) was included to increase expression. LD-localized pathway stoichiometry was varied by expressing scaffolds with one, two, and three copies of C_2 (cohesin from *Clostridium thermocellum* that corresponds to the D_2 dockerin fused to Acs1), while scaffold expression was altered with a second promoter series (P_{RNR1}, P_{PGI1}, P_{RPL18B}, P_{REV1}, and P_{ADH1}). Pathway naming followed the convention of $P_xP_yS_z$ where P_x refers to the promoter of Acs1-D_2, P_y refers to the scaffold promoter, and S_z refers to scaffold design.

The genetic constructs of each library member were transformed into *S. cerevisiae* with the previously integrated copy of Atf1 and five randomly selected colonies of each pathway variant were independently screened (Tables S4.1). Screening was accomplished with a UV-Vis based ester quantification assay (Figure S4.6).(38) Analysis of the screened library supports our hypothesis that Acs1 activity was likely limiting. Colonies

that produced ethyl acetate three or more standard deviations above the library average of 46.6 mg L^{-1} had scaffolds with two or three C_2 domains (Figure 4.4b). This subset included $P_2P_5S_3$, $P_4P_3S_2$, $P_4P_5S_3$, $P_1P_3S_3$, $P_2P_4S_3$, and two colonies of $P_4P_4S_3$. The highest producing colony, $P_2P_5S_3$, expressed Ole-C_1-3C_2 from the strong Adh1 promoter and Acs1-D_2 from a CCW12 promoter, and generated 84.5 mg L^{-1} of ethyl acetate over a 24 hour period. The control pathway, $P_0P_5S_1$ (the construct evaluated *in vitro*; Figure 4.3) produced 33.6 mg L^{-1} of ethyl acetate, two standard deviations below the library average.

To better evaluate the optimized pathway, the high producing $P_2P_5S_3$ construct was isolated, amplified, and re-transformed to the *ATF1* integrated strain of *S. cerevisiae*. Sequencing of the isolated plasmid confirmed that the pathway was assembled as designed and western blot analysis confirmed expression of all parts of the pathways (Figure S4.7). The re-transformed $P_2P_5S_3$ pathway produced 14.8 mg L^{-1} OD^{-1} of ethyl acetate, productivity significantly greater than the control pathways with and without the expression of the scaffold (Figure 4.4c). Expression of an oleosin-only scaffold ($P_2P_5S_{ole}$) that did not bind Ald6-D_1 and Acs1-D_2 produced 8.5±0.8 mg L^{-1} OD^{-1} of ethyl acetate. Similar ethyl acetate productivity was observed in the absence of the scaffold ($P_2P_5S_0$; 8.5±0.9 mg L^{-1} OD^{-1}) and with the un-optimized scaffold ($P_0P_5S_1$; 8.3±0.1 mg L^{-1} OD^{-1}). Importantly, enzyme expression levels remained consistent across the tested pathway variants (Figure S4.7). It is interesting to note that the co-localization effect was significantly enhanced with the optimized scaffold architecture. A comparison of the scaffold-less controls and their corresponding scaffold samples (*i.e.,* $P_2P_5S_0$ *vs.* $P_2P_5S_3$ and $P_0P_5S_0$ *vs.* $P_0P_5S_1$) revealed that the optimized scaffold increased ethyl acetate

productivity by 1.7-fold, while the effect was limited a >5% increase in the un-optimized case. Combined, the library screening results, GC analysis of the optimized and control pathways, along with the results of the *in vitro* analysis of the pathway in the presence and absence of the scaffold support the conclusion that the re-localization of upstream enzymes to the native localization of Atf1 increased the rate of ester biosynthesis.

4.5 Discussion

Enzyme co-localization is proving to be an effective tool for metabolic engineering. By mimicking substrate channeling effects that occur in natural multienzyme complexes and bifunctional enzymes (*e.g.*, malate dehydrogenase-citrate synthase, key steps in the TCA cycle that electrostatically channel pathway intermediates between active sites(39)) engineered intracellular scaffolding can enhance the rates and titers of microbial biosynthesis.(12-17,19,22) In this work, we open this concept to pathway spatial organization on LD membranes by enhancing the productivity and rate of ethyl acetate biosynthesis in *S. cerevisiae*. Re-localizing upstream enzymes that naturally localize to the cytosol (Ald6 and Acs1) and mitochrondria (Acs1) to the outer surface of LDs —the natural localization of the terminal ester biosynthesis step, Atf1— produced a clustered three-step pathway that channels key intermediates. We targeted ester biosynthesis as the LD-localization of Atf1 is necessary for high alcohol acetyltransferase activity,(24) but we anticipate that this and similar technologies may be applicable to other biosynthetic and signaling pathways with essential steps localized to intracellular membranes and compartmentalized in organelles.

FRET microscopy and *in vitro* kinetic analysis of the LD-assembled pathway revealed that the nanometer spacing between co-localized enzymes (Figure 4.2) increased pathway rate (Figure 4.3). When measure *in vitro*, the rates of both the up- and downstream coupled enzyme reactions (Ald6/Acs1 and Acs1/Atf1) increased nearly 2-fold when assembled on LDs. Due to the presence of natively expressed enzymes competing for pathway intermediates (CoA-SH, acetyl-CoA, and acetate), the cell lysate assays are evidence of substrate channeling: pathway rates increased when co-localized in the presence of competing reaction.(6,7) The rate advantage was partially maintained during fermentation once the scaffold was optimized. With optimized scaffold architecture and pathway expression levels the rate of ethyl acetate production on a per cell basis was 1.7-fold above the unassembled control (Figure 4.4), an enhancement comparable to those achieved by cytosolic scaffolding. For example, protein scaffolding of a three-step glucaric acid pathway in *E. coli* increased rate by 5-fold, in part due to pathway co-localization and in part due to activation of the bottleneck enzyme (myo-inostiol oxygenase; MIOX).(13) Cytosolic scaffolding of a threonine pathway in *E. coli* enhanced the production rate by ~50% while improving growth kinetics.(19) With respect to rate enhancement, the example of mevalonate production in *E. coli* stands out.[13] Co-localization of acetoacetyl-CoA thiolase (AtoB), hydroxy-methylglutaryl-CoA synthase (HMGS), and hydroxymethylglutaryl-CoA reductase (HMGR) produced a 77-fold increase in mevalonate titer over a 96-hour period in comparison to an unassembled control. This increase in titer resulted from a combination of effects including improved growth kinetics and improved rate. As a point of comparison, a 50-fold increase in

reaction rate of a typical enzyme catalyzed reaction (E_a ~50 kJ mol^{-1}) requires a temperature input of ~75 °C equivalent to fermentations above 100 °C, suggesting that in this case rate enhancement is only part of the overall co-localization effect. In our ester biosynthesis example, localizing ethyl acetate production to LDs did not affect cell growth (Table S4.1) but by controlling the flux of central metabolites (acetate, acetyl-CoA and CoA-SH) along an artificially structured pathway we were able to increase the rate of production on a per cell basis by ~2-fold.

Yeast fermentation naturally produces small quantities of esters including ethyl acetate as well as isoamyl and phenylethyl acetate.(23) Translating Atf1-based pathways from yeast to *E. coli* has enabled the biosynthesis of a range of short and medium chain volatile esters including isobutyl acetate, isoamyl acetate, and butyrate esters.(40-42) Ethyl acetate has also been produced, but rates and specific productivities have been limited.(24,40) Fermentation for 24-hours with overexpressed Atf1 in *E. coli* produced 1.8 mg $L^{-1}OD^{-1}$.[23] Chromosomal overexpression of *ATF1* in *S. cerevisiae* produced only ~0.2 mg $L^{-1}OD^{-1}$ over the same time period (Figure 4.4c). Optimization of pathway expression levels and localization to LDs in yeast increased productivity to nearly 15 mg $L^{-1}OD^{-1}$.

By using cell localization and protein-protein interactions domains we engineered an enzyme co-localization scaffold that assembles the final three reactions steps of yeast ester biosynthesis on intracellular LDs. Re-organizing pathway enzymes and controlling the architecture of co-localization and optimizing expression level increased the rate of ethyl acetate fermentation. This is a possible strategy for engineering the flux of

metabolites down natural and synthetic metabolic pathways with controlled intracellular localizations and targeting lipid modifying enzymes to the intracellular location of lipid storage, LDs.

4.6 Acknowledgements

This work was supported by the Army Research Office MURI (#W911NF1410263) and NSF CBET-1403264. We thank Harvey Blanch for his comments and discussion.

4.7 References

1. Ivessa, A. S., Schneiter, R., and Kohlwein, S. D. (1997) Yeast acetyl-CoA carboxylase is associated with the cytoplasmic surface of the endoplasmic reticulum. *Eur J Cell Biol* **74**, 399-406

2. Markgraf, D. F., Klemm, R. W., Junker, M., Hannibal-Bach, H. K., Ejsing, C. S., and Rapoport, T. A. (2014) An ER Protein Functionally Couples Neutral Lipid Metabolism on Lipid Droplets to Membrane Lipid Synthesis in the ER. *Cell Rep* **6**, 44-55

3. Ziegler, J., and Facchini, P. J. (2008) Alkaloid biosynthesis: Metabolism and trafficking. *Annual Review of Plant Biology* **59**, 735-769

4. Lin, J. L., and Wheeldon, I. (2014) Dual N- and C-Terminal Helices Are Required for Endoplasmic Reticulum and Lipid Droplet Association of Alcohol Acetyltransferases in Saccharomyces cerevisiae. *PLoS One* **9**, e104141

5. Tiwari, R., Koffel, R., and Schneiter, R. (2007) An acetylation/deacetylation cycle controls the export of sterols and steroids from S-cerevisiae. *Embo Journal* **26**, 5109-5119

6. Spivey, H. O., and Ovadi, J. (1999) Substrate channeling. *Methods* **19**, 306-321

7. Wheeldon, I., Minteer, S. D., Banta, S., Barton, S. C., Atanassov, P., and Sigman, M. (2016) Substrate channelling as an approach to cascade reactions. *Nat Chem* **8**, 299-309

8. Lee, J. W., Na, D., Park, J. M., Lee, J., Choi, S., and Lee, S. Y. (2012) Systems metabolic engineering of microorganisms for natural and non-natural chemicals. *Nat. Chem. Biol.* **8**, 536-546

9. Conrado, R. J., Varner, J. D., and DeLisa, M. P. (2008) Engineering the spatial organization of metabolic enzymes: mimicking nature's synergy. *Current Opinion in Biotechnology* **19**, 492-499

10. Lee, H., DeLoache, W. C., and Dueber, J. E. (2012) Spatial organization of enzymes for metabolic engineering. *Metab. Eng.* **14**, 242-251

11. Lin, J.-L., Palomec, L., and Wheeldon, I. (2014) Design and Analysis of Enhanced Catalysis in Scaffolded Multienzyme Cascade Reactions. *ACS Catalysis*, 505-511

12. Dueber, J. E., Wu, G. C., Malmirchegini, G. R., Moon, T. S., Petzold, C. J., Ullal, A. V., Prather, K. L. J., and Keasling, J. D. (2009) Synthetic protein scaffolds provide modular control over metabolic flux. *Nature Biotechnology* **27**, 753-U107

13. Moon, T. S., Dueber, J. E., Shiue, E., and Prather, K. L. J. (2010) Use of modular, synthetic scaffolds for improved production of glucaric acid in engineered E. coli. *Metab. Eng.* **12**, 298-305

14. Baek, J. M., Mazumdar, S., Lee, S. W., Jung, M. Y., Lim, J. H., Seo, S. W., Jung, G. Y., and Oh, M. K. (2013) Butyrate Production in Engineered Escherichia coli With Synthetic Scaffolds. *Biotechnology and Bioengineering* **110**, 2790-2794

15. Conrado, R. J., Wu, G. C., Boock, J. T., Xu, H., Chen, S. Y., Lebar, T., Turnsek, J., Tomsic, N., Avbelj, M., Gaber, R., Koprivnjak, T., Mori, J., Glavnik, V., Vovk, I., Bencina, M., Hodnik, V., Anderluh, G., Dueber, J. E., Jerala, R., and Delisa, M. P. (2011) DNA-guided assembly of biosynthetic pathways promotes improved catalytic efficiency. *Nucleic Acids Res* **40**, 1879-1889

16. Delebecque, C. J., Lindner, A. B., Silver, P. A., and Aldaye, F. A. (2011) Organization of intracellular reactions with rationally designed RNA assemblies. *Science* **333**, 470-474

17. Sachdeva, G., Garg, A., Godding, D., Way, J. C., and Silver, P. A. (2014) In vivo co-localization of enzymes on RNA scaffolds increases metabolic production in a geometrically dependent manner. *Nucleic Acids Research* **42**, 9493-9503

18. Myhrvold, C., Polka, J. K., and Silver, P. A. (2016) Synthetic Lipid-Containing Scaffolds Enhance Production by Colocalizing Enzymes. *Acs Synth Biol* **5**, 1396-1403

19. Lee, J. H., Jung, S. C., Bui, L. M., Kang, K. H., Song, J. J., and Kim, S. C. (2013) Improved Production of L-Threonine in Escherichia coli by Use of a DNA Scaffold System. *Appl. Environ. Microbiol.* **79**, 774-782

20. Gao, Y., Roberts, C. C., Zhu, J., Lin, J.-L., Chang, C.-e. A., and Wheeldon, I. (2015) Tuning enzyme kinetics through designed intermolecular interactions far from the active site. *ACS Catalysis*

21. Idan, O., and Hess, H. (2013) Origins of Activity Enhancement in Enzyme Cascades on Scaffolds. *ACS Nano*

22. Castellana, M., Wilson, M. Z., Xu, Y. F., Joshi, P., Cristea, I. M., Rabinowitz, J. D., Gitai, Z., and Wingreen, N. S. (2014) Enzyme clustering accelerates processing

of intermediates through metabolic channeling. *Nature Biotechnology* **32**, 1011-+

23. Verstrepen, K. J., Van Laere, S. D. M., Vanderhaegen, B. M. P., Derdelinckx, G., Dufour, J. P., Pretorius, I. S., Winderickx, J., Thevelein, J. M., and Delvaux, F. R. (2003) Expression levels of the yeast alcohol acetyltransferase genes ATF1, Lg-ATF1, and ATF2 control the formation of a broad range of volatile esters. *Appl. Environ. Microbiol.* **69**, 5228-5237

24. Zhu, J., Lin, J.-L., Palomec, L., and Wheeldon, I. (2015) Microbial host selection affects intracellular localization and activity of alcohol-O-acetyltransferase. *Microbial Cell Factories* **14**, 35

25. Meaden, P. G., Dickinson, F. M., Mifsud, A., Tessier, W., Westwater, J., Bussey, H., and Midgley, M. (1997) The ALD6 gene of Saccharomyces cerevisiae encodes a cytosolic, Mg2+-activated acetaldehyde dehydrogenase. *Yeast* **13**, 1319-1327

26. Sickmann, A., Reinders, J., Wagner, Y., Joppich, C., Zahedi, R., Meyer, H. E., Schonfisch, B., Perschil, I., Chacinska, A., Guiard, B., Rehling, P., Pfanner, N., and Meisinger, C. (2003) The proteome of Saccharomyces cerevisiae mitochondria. *Proceedings of the National Academy of Sciences of the United States of America* **100**, 13207-13212

27. Chen, Y., Siewers, V., and Nielsen, J. (2012) Profiling of Cytosolic and Peroxisomal Acetyl-CoA Metabolism in Saccharomyces cerevisiae. *Plos One* **7**

28. Hoover, D. M., and Lubkowski, J. (2002) DNAWorks: an automated method for designing oligonucleotides for PCR-based gene synthesis. *Nucleic Acids Research* **30**

29. Qu, R., and Huang, A. H. C. (1990) Oleosin Kd-18 on the Surface of Oil Bodies in Maize - Genomic and Cdna Sequences and the Deduced Protein-Structure. *J Biol Chem* **265**, 2238-2243

30. Adams, J. J., Gregg, K., Bayer, E. A., Boraston, A. B., and Smith, S. P. (2008) Structural basis of Clostridium perfringens toxin complex formation. *Proceedings of the National Academy of Sciences of the United States of America* **105**, 12194-12199

31. Carvalho, A. L., Dias, F. M. V., Prates, J. A. M., Nagy, T., Gilbert, H. J., Davies, G. J., Ferreira, L. M. A., Roma?o, M. J., and Fontes, C. M. G. A. (2003) Cellulosome assembly revealed by the crystal structure of the cohesin-dockerin complex.

Proceedings of the National Academy of Sciences of the United States of America **100**, 13809-13814

32. Shao, Z. Y., and Zhao, H. M. (2013) Construction and Engineering of Large Biochemical Pathways via DNA Assembler. *Synthetic Biology* **1073**, 85-106

33. Postma, E., Verduyn, C., Scheffers, W. A., and Vandijken, J. P. (1989) Enzymic Analysis of the Crabtree Effect in Glucose-Limited Chemostat Cultures of Saccharomyces-Cerevisiae. *Appl. Environ. Microbiol.* **55**, 468-477

34. Bauler, P., Huber, G., Leyh, T., and McCammon, J. A. (2010) Channeling by Proximity: The Catalytic Advantages of Active Site Colocalization Using Brownian Dynamics. *J Phys Chem Lett* **1**, 1332-1335

35. Piston, D. W., and Kremers, G. J. (2007) Fluorescent protein FRET: the good, the bad and the ugly. *Trends Biochem.Sci.* **32**, 407-414

36. Sahoo, H. (2011) Forster resonance energy transfer - A spectroscopic nanoruler: Principle and applications. *J Photoch Photobio C* **12**, 20-30

37. Flagfeldt, D. B., Siewers, V., Huang, L., and Nielsen, J. (2009) Characterization of chromosomal integration sites for heterologous gene expression in Saccharomyces cerevisiae. *Yeast* **26**, 545-551

38. Löbs, A.-K., Lin, J.-L., Cook, M., and Wheeldon, I. (2016) High throughput, colorimetric screening of microbial ester biosynthesis reveals high ethyl acetate production from Kluyveromyces marxianus on C5, C6, and C12 carbon sources. *Biotechnol. J.* **11**, 1274-1281

39. Wu, F., and Minteer, S. (2015) Krebs Cycle Metabolon: Structural Evidence of Substrate Channeling Revealed by Cross-Linking and Mass Spectrometry. *Angewandte Chemie International Edition* **54**, 1851-1854

40. Rodriguez, G. M., Tashiro, Y., and Atsumi, S. (2014) Expanding ester biosynthesis in Escherichia coli. *Nat Chem Biol* **10**, 259-265

41. Layton, D. S., and Trinh, C. T. (2014) Engineering modular ester fermentative pathways in Escherichia coli. *Metab. Eng.* **26**, 77-88

42. Tai, Y. S., Xiong, M. Y., and Zhang, K. C. (2015) Engineered biosynthesis of medium-chain esters in Escherichia coli. *Metab. Eng.* **27**, 20-28

4.8 Figures and Tables

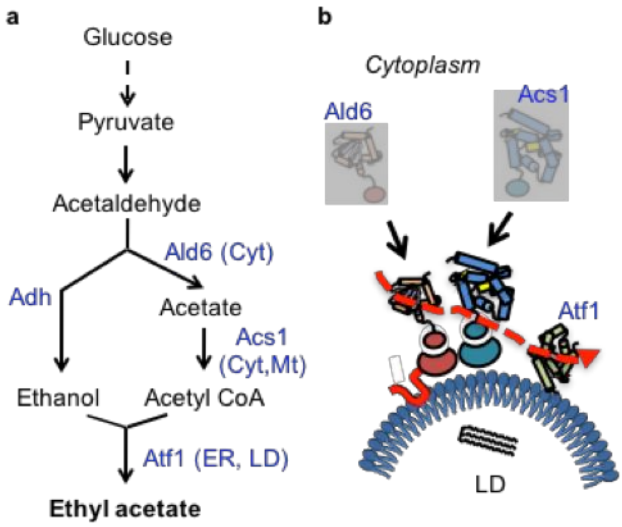

Figure 4.1. Pathway co-localization on intracellular LD membranes in *S. cerevisiae*. (a) Ethyl acetate biosynthesis in *S. cerevisiae* and the subcelluar localization of aldehyde dehydrogenase (Ald6), acetyl-coA synthetase (Acs1), and alcohol-O-acetyltransferase (Atf1). Abbreviations: Cyt, cytosol; Mt, mitochondria; ER, endoplasmic reticulum; and, LD, lipid droplet. (b) A schematic diagram of the scaffolding strategy, co-localizing Ald6 and Acs1 with Atf1 on LDs via a membrane bound protein scaffold.

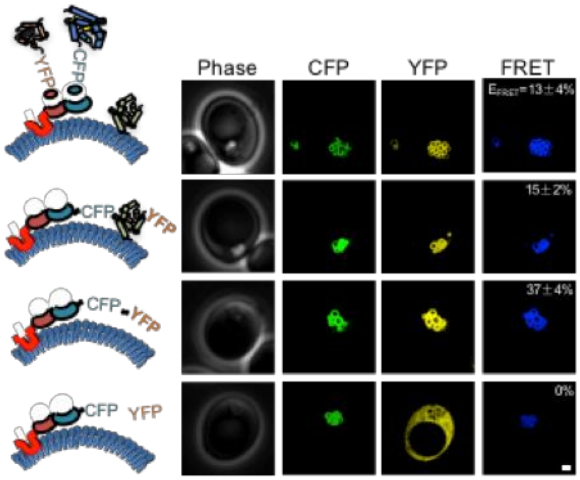

Figure 4.2. FRET microscopy and quantitative analysis of multienzyme co-localization. Stationary phase cells expressing scaffold-bound Ald6-YFP-D_1 and Acs1-CFP-D_2, Ole-C_1-C_2-CFP and Atf1-YFP, Ole-C_1-C_2 with C-terminally fused CFP-YFP, and Ole-C_1-C_2-CFP with cytosolically expressed YFP were imaged and analyzed. Phase contrast micrographs and fluorescence images of the CFP donor, YFP acceptor, and raw FRET signal are shown. CFP signal is shown in green (Ex/Em: 426-450nm/502-538nm), YFP signal is shown in yellow (Ex/Em: 488-512nm532-554nm), and the FRET signal is shown in blue (Ex/Em:426-450nm/532-554nm). FRET efficiency was quantified using the Leica SP5 FRAP (fluorescence recovery after photobleaching) protocol with acceptor fluorescence photobleached to ~10% of its initial value. Presented data represents the mean and standard deviation of five samples. The scale bar represents 1 μm.

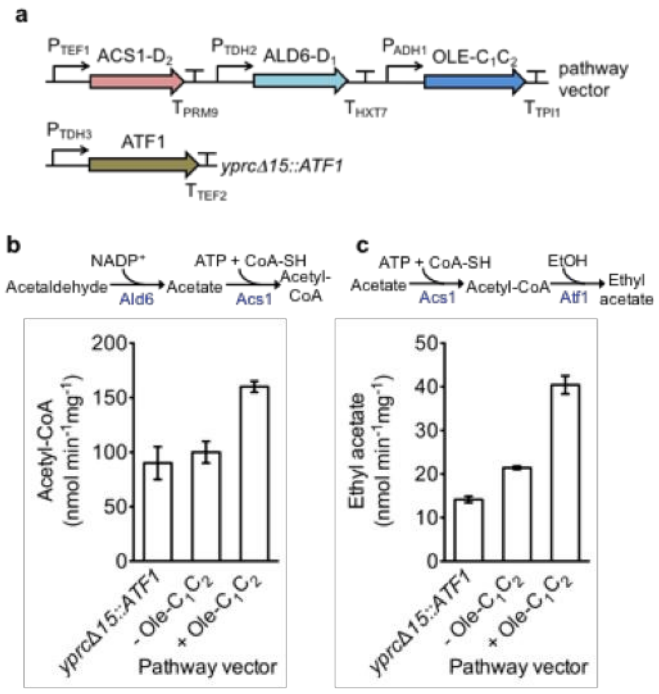

Figure 4.3. *In vitro* evaluation of pathway activity from Ald6 to Acs1 and Acs1 to Atf1. (a) Genetic constructs used to overexpress pathway genes. (b) Catalytic reactions of Ald6 and Acs1, and the overall pathway activity converting acetaldehyde to acetyl-CoA. (c) Catalytic reactions of Acs1 and Atf1, and the overall pathway activity converting acetate to ethyl acetate. The mean and standard deviation are shown (n=3).

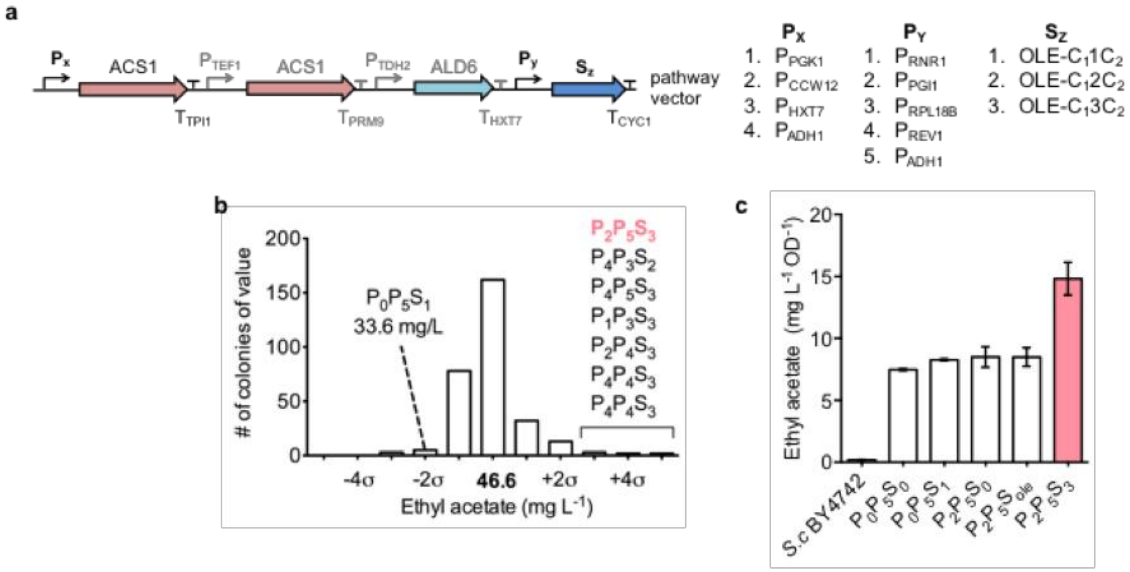

Figure 4.4. Optimizing ester biosynthesis pathway structure. (a) Genetic constructs and nomenclature of the combinatorial library used for pathway expression. (b) Histogram of ethyl acetate titers from the pathway library. The titers were quantified by the colorimetric assay described in the Method section. (c) Specific productivity of ethyl acetate from 24 hr fermentations with strains expressing the pathway without a scaffold ($P_0P_5S_0$), with scaffold ($P_0P_5S_1$), with optimized scaffold ($P_2P_5S_3$), without the optimized scaffold ($P_2P_5S_0$), and with an oleosin-only scaffold ($P_0P_5S_{ole}$). The titers were quantified by GC-FID. The mean and standard deviation are shown (n=3).

Table 4.1. Strains used in Chapter 4.

Strains	Genotype	Source
E. coli DH5α	*F– Φ80lacZΔM15 Δ(lacZYA-argF) U169 recA1 endA1 hsdR17 (rK–, mK+) phoA supE44 λ– thi-1 gyrA96 relA1*	Life technologies
S. cerevisiae BY4742	*MATα his3Δ1 leu2Δ0 lys2Δ0 ura3Δ0*	GE Healthcare
YS419	*MATα his3Δ1 leu2Δ0 lys2Δ0 ura3Δ0 yprcΔ15::LEU2-P_{TDH3}-ATF1-myc-T_{TEF2}*	this study
YS724	*MATα his3Δ1 leu2Δ0 lys2Δ0 ura3Δ0 yprcΔ15::LEU2-P_{PGK1}-YFP-T_{TEF2}*	this study
YS750	*MATα his3Δ1 leu2Δ0 lys2Δ0 ura3Δ0 yprcΔ15::LEU2-P_{PGK1}-ATF1-YFP-T_{TEF2}*	this study

Table 4.2. Plasmids used in Chapter 4.

Plasmid	Description	Source
pIW7	pRS426	GE Healthcare
pIW147	pRS426-P_{PGK1}-*Oleosin (1-186)-CFP*-T_{PGK1}	this study
pIW617	pRS316-Ald6-YFP-Doc (Cp)-Acs1-CFP-Doc (Ct)-Oleosin-Coh (Cp)-Coh (Ct)	this study
pIW618	pRS316-Oleosin-Coh (Cp)-Coh (Ct)-CFP	this study
pIW619	pRS316-Oleosin-Coh (Cp)-Coh (Ct)-CFP-YFP	this study
pIW310	pRS316-P_{TEF1}-*ACS1-HA-Doc (Ct)*-T_{PRM9}-P_{TDH2}-*ALD6-(His)6-Doc (Cp)*-T_{HXT7}-P_{ADH1}-*Oleosin-X82 (Cp)-Coh (Ct)-V5*-T_{TPI1}	this study
pIW313	pRS316-P_{TEF1}-*ACS1-HA-Doc (Ct)*-T_{PRM9}-P_{TDH2}-*ALD6-(His)*$_6$-*Doc (Cp)*-T_{HXT7}	this study
pIW395	pRS316-P_{CCW12}-*ACS1-HA-Doc (Ct)*-T_{TPI1}-P_{TEF1}-*ACS1-HA-Doc (Ct)*-T_{PRM9}-P_{TDH2}-*ALD6-(His)*$_6$-*Doc (Cp)*-T_{HXT7}-P_{ADH1}-*Oleosin-Coh (Cp)-Coh (Ct)-Coh (Ct)-Coh (Ct)*-T_{CYC1}	this study
pIW203	pRS426-P_{PGK1}-*Atf1-myc*-T_{TEF2}	this study
pIW254	pRS426-P_{TEF1}-*Oleosin-X82 (Cp)-Coh (Ct)*-T_{TPI1}-P_{PGK1}-*Atf1-myc*-T_{TEF2}-P_{TPI1}-*ACS1-HA-Doc (Ct)*-T_{CYC1}-P_{TDH2}-*ALD6-(His)*$_6$-*Doc (Cp)*-T_{HXT7}	this study
pIW255	pRS426-P_{PGK1}-*Atf1-myc*-T_{TEF2}-P_{TPI1}-*ACS1-HA-Doc (Ct)*-T_{CYC1}-P_{TDH2}-*ALD6-(His)6-Doc (Cp)*-T_{HXT7}	this study
pIW147	pRS426-P_{PGK1}-*Oleosin (1-186)-CFP*-T_{PGK1}	this study
pIW185	pET29-*HA-myc-GFP-(His)*$_6$	this study
pIW306	pRS316-*LEU2*-P_{TDH3}-*ATF1-myc*-T_{TEF2}	this study
pIW615	pRS316-LEU2-PGK1p-YFP-TEF2t	this study
pIW616	pRS316-LEU2-PGK1p-ATF1-YFP-TEF2t	this study
pIW800	pRS316-P_{CCW12}-*ACS1-HA-Doc (Ct)*-T_{TPI1}-P_{TEF1}-*ACS1-HA-Doc (Ct)*-T_{PRM9}-P_{TDH2}-*ALD6-(His)*$_6$-*Doc (Cp)*-T_{HXT7}	this study
pIW801	pRS316-P_{CCW12}-*ACS1-HA-Doc (Ct)*-T_{TPI1}-P_{TEF1}-*ACS1-HA-Doc (Ct)*-T_{PRM9}-P_{TDH2}-*ALD6-(His)*$_6$-*Doc (Cp)*-T_{HXT7}-P_{ADH1}-*Oleosin*-T_{CYC1}	this study

Table 4.3. DNA sequences of protein parts including oleosin, cohesin, and dockerin used in Chapter 4. Numbers indicated in parentheses are amino acid sequences used from given proteins.

Oleosin (1-186) ACG49220.1
ATGGCTGATA GAGATAGGTC TGGTATTTAT GGGGGTGCTC ACGCGACTTA TGGTCAACAA
CAGCAACAAG GTGGAGGTGG TAGGCCAATG GGTGAACAAG TTAAAGGTAT GTTGCATGAT
AAAGGTCCAA CTGCTTCTCA AGCTTTGACT GTGGCTACTT TGTTTCCATT GGGTGGGCTT
TTGTTGGTTT TGTCTGGTTT GGCCTTGACT GCGTCTGTGG TCGGTTTAGC TGTTGCTACA
CCTGTTTTCT TGATTTTTTC TCCGGTTTTG GTTCCAGCTG CACTATTGAT TGGTACTGCT
GTTATGGGTT TTTTGACTAG TGGTGCTTTG GGTTTGGGCG GTTTGTCTAG TTTGACATGT
TTGGCTAATA CTGCTCGTCA AGCCTTTCAA AGAACTCCAG ATTATGTTGA AGAAGCACAT
AGAAGAATGG CCGAGGCTGC TGCTCATGCT GGGCATAAAA CTGCCCAAGC TGGTCAAGCT
ATTCAAGGTA GAGCTCAAGA AGCTGGGGCA GGGGGTGGTG CAGGTGCGGG TGCTGGTGGC
GGTGGAAGAG CCTCTAGC

Cohesin (*C. thermocellum*) 1OHZ:A
ATGGCCTCTG ATGGGGTGGT TGTGGAAATT GGAAAAGTTA CTGGGAGCGT GGGTACCACT
GTTGAAATCC CGGTCTATTT CAGGGGAGTT CCATCTAAAG GTATCGCAAA CTGTGACTTT
GTCTTTAGAT ACGACCCTAA CGTTCTTGAG ATAATCGGTA TAGATCCAGG CGATATCATT
GTGGATCCTA ATCCTACTAA GAGCTTCGAC ACGGCTATAT ATCCAGATAG AAAAATTATT
GTATTTTTGT TTGCAGAAGA CTCAGGGACT GGGGCATATG CTATCACTAA GGATGGTGTG
TTTGCTAAAA TACGTGCTAC CGTTAAGTCC TCAGCACCTG GTTATATCAC TTTCGACGAA
GTTGGTGGCT TTGCCGACAA TGATCTAGTG GAACAAAAGG TATCATTCAT TGATGGTGGT
GTAAATGTCG GTAATGCAAC ACCGACCAAA GGAGCCACTC CCACTAACAC AGCAACTCCA
ACCAAA

Dockerin (*C. thermocellum*) 1OHZ:B
GGTGGTGGTG GTTCTATGGG TGATGTTAAT GGTGATGGCA CGATAAACTC CACGGATCTT
ACTATGTTAA AAAGATCTGT TTTACGTGCG ATCACATTAA CAGACGATGC TAAGGCAAGG
GCTGATGTAG ATAAAAATGG TTCAATCAAT AGCACAGATG TCTTACTATT ATCCAGATAC
CTTTTGAGAG TGATT

X82 (*C. perfringens*) 2OZN:A
ATGTCCAGCG GACTTGTCCC AAGAGGAAGT CATATGGCCA GTAAATTAAA
AGAAAATGCA GAGGTGACTG GATCTGTCAG TCTAGAAGCT TTGGAAGAAG
TACAAGTTGG AGAAAATCTA GAGGTGGGTG TAGGAATAGA TGAATTGGTC
AACGCGGAAG CATTTGCTTA TGACTTTACT TTGAATTATG ATGAAAATGC
TTTCGAGTAT GTGGAAGCTA TCTCTGATGA TGGTGTGTTC GTTAATGCGA
AAAAGATTGA GGATGGCAAG GTGAGAGTCT TAGTTTCTTC ACTTACTGGT
GAACCCTTAC CTGCTAAGGA GGTACTGGCC AAAGTCGTCT TAAGAGCTGA
AGCCAAAGCA GAAGGATCCA ACCTTTCAGT GACTAATTCT TCCGTCGGTG
ACGGCGAAGG GTTGGTTCAC GAGATCGCTG GGACTGAGAA AACCGTCAAC
ATCATCGAAG GAACATCT

Dockerin (*C. perfringens*) 2OZN:B
GGAGATTTCA ATGGTAATGG AAAAATAGAT ATCGGCGATT TGGCTATGGT TTCTAAGAAT
ATTGGGAGCA CCACAAACAC TTCATTAGAT TTGAATAAGG ACGGGTCTAT TGATGAATAT
GAAATTTCAT TCATAAACCA CCGTATTTTA AATTTAGAA

4.9 Supporting Information

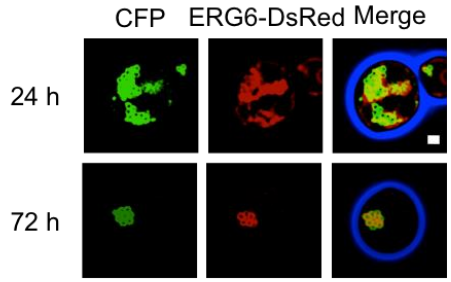

Figure S4.1. Fluorescent images of Oleosin-CFP in *S. cerevisiae* at 24 hours and under fermentation condition 72 hours. Scale bar, 1 μm.

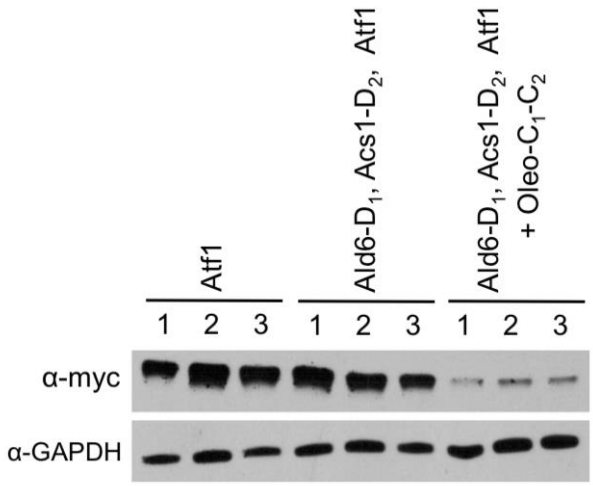

Figure S4.2. Western blot analysis of myc-tagged Atf1 in *S. cerevisiae* strains harboring different pathway expression vectors, including overexpression of Atf1-myc, Ald6-(His)$_6$-D$_1$/Acs1-HA-D$_2$/Aft1-myc, and Ald6-(His)$_6$-D$_1$/Acs1-HA-D$_2$/Atf1-myc/Ole-C$_1$-C$_2$-V5. Genes were overexpressed with high copy number plasmids (pRS426). anti-myc antibody was used to detect Atf1-myc and GAPDH was used as the loading control. Three unique colonies were tested for expression. 5 μg whole cell lysate was used for the analysis. Peptide tags used for western blot analysis for proteins are not shown in the figure.

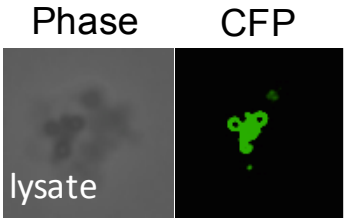

Figure S4.3. Fluorescence microscopy analysis of lipid droplet morphology after mechanical disruption of cell lysis. To monitor the morphology of lipid droplets, cells overexpressing oleosin-CFP was disrupted with glass beads, and the resulted lysate was analyzed for fluorescence.

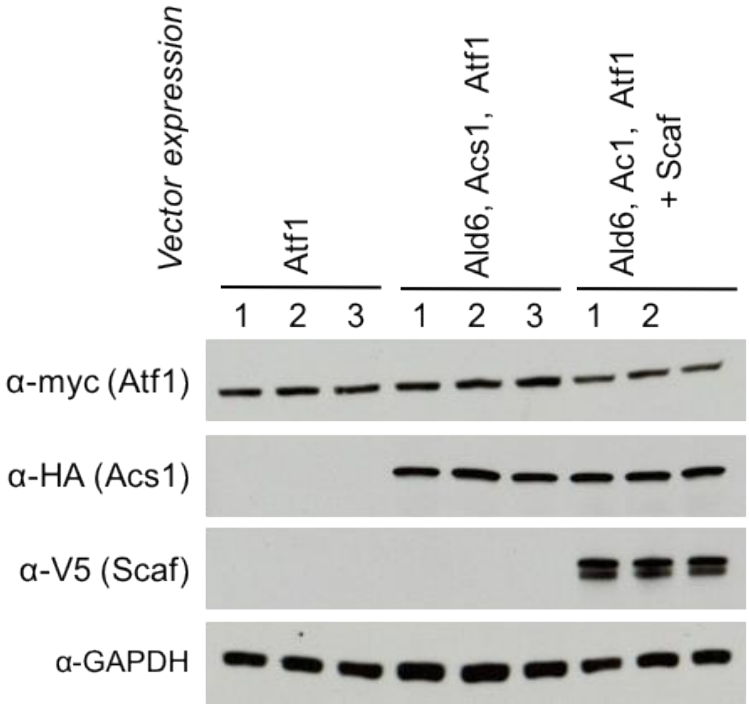

Figure S4.4. Western blot analysis of protein expression levels of Ald6, Acs1, Atf1, and the scaffold. To maintain similar protein level of Atf1 among strains, an additional copy of Atf1-myc was integrated to the genomic locus, yprcΔ15, for overexpression. An empty vector, vectors containing Ald6-$(His)_6$-D_1/Acs1-HA-D_2 and Ald6-$(His)_6$-D_1/Acs1-HA-D_2/Oleo-C_1-C_2-V5 were transformed into the Atf1-myc integrated strain. A low copy number plasmid (pRS316) was used to carry these expression cassettes. Anti-myc, anti-HA, and anti-V5 antibodies were used to against Atf1, Acs1, and Oleo-C_1-C_2, respectively. GAPDH was used as the loading control. Three unique colonies were tested for expression. 5 μg whole cell lysate was used for the analysis. Peptide tags used for western blot analysis for proteins are not shown in the figure.

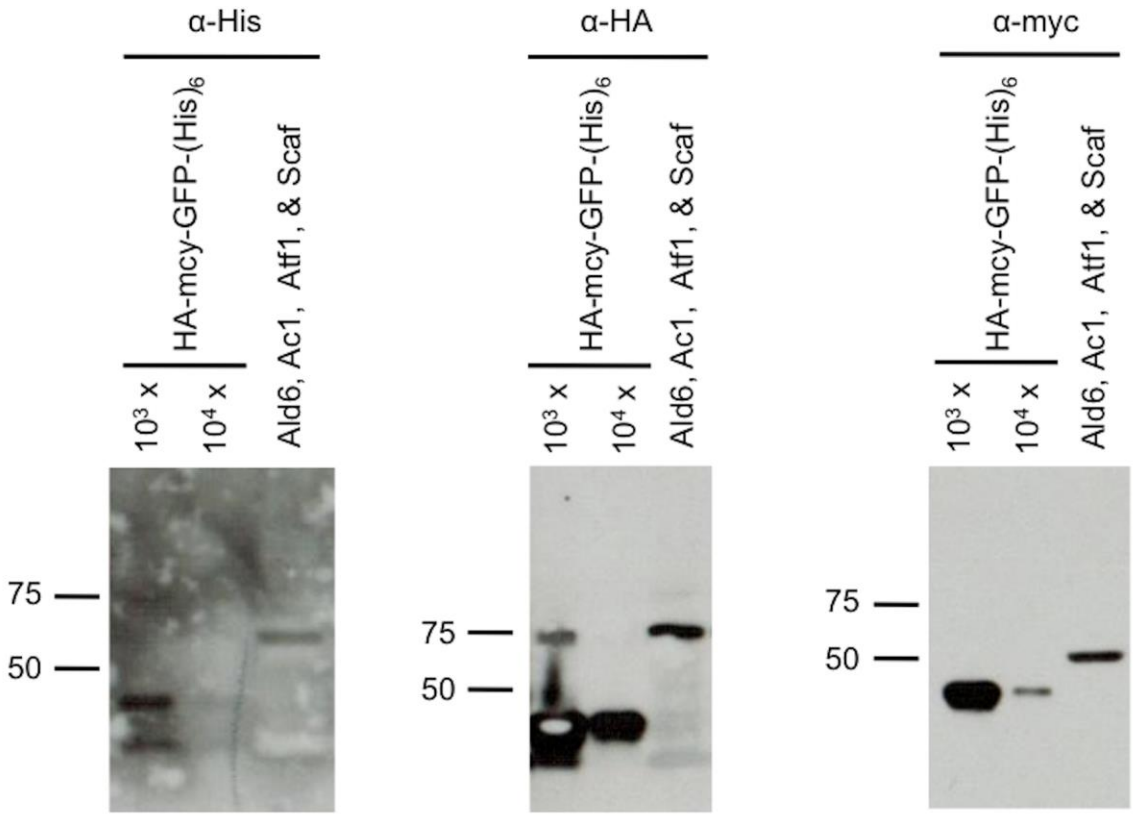

Figure S4.5. Western blot analysis of the relative expression of Ald6, Acs1, and Atf1. Atf1-myc was overexpressed by chromosomal integration of an additional copy while Ald6-(His)7-D_1, Acs1-HA-D_2, and the scaffold Ole-C_1-C_2–V5 were expressed with low copy number plasmids (pRS316). GFP with terminal HA, myc, and His tags was used as the standard (expression in BL21(DE3) harboring pET28-HA-myc-GFP-$(His)_6$). 10 µL of *E. coli* lysate with 10^3- or 10^4-fold dilution was loaded for analysis. anti-$(His)_6$, anti-HA, and anti-myc antibody were used to against Ald6, Acs1, and Atf1, respectively. A comparison of the relative expression levels of each enzyme to the GFP control shows that HA tagged Acs1 has low expression. To simplify the labels, peptide tags and protein parts (cohesin, dockerin, and oleosin) used are not shown in the figure.

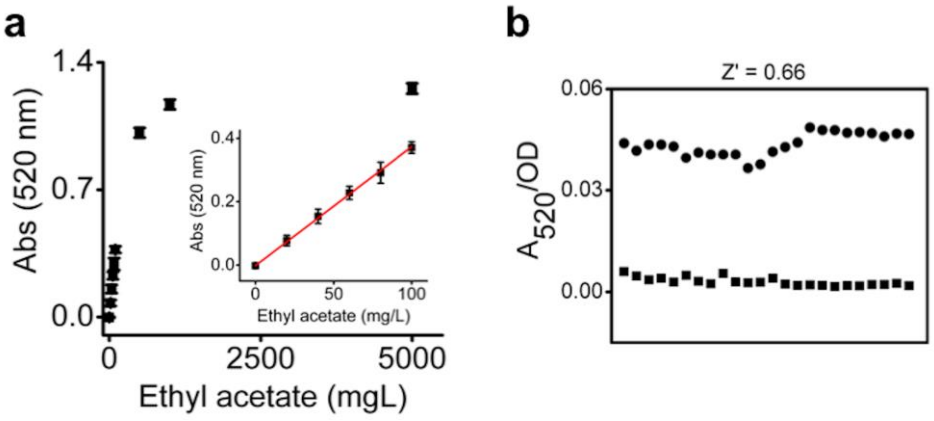

Figure S4.6. A colorimetric assay for ethyl acetate quantification. (a) Demonstration of the assay responding to different ethyl acetate concentrations. 0 to 5000 mg/L ethyl acetate dissolved in ethanol was tested with the assay. A linear relationship between absorbance and ethyl acetate concentration is shown in the inset. Reported data are the mean and standard deviation of three unique samples. (b) Z' factor analysis for the assay. Yeast strains BY4742 *yprcΔ15::*P_{TDH3}*-ATF1-myc-*T_{TEF2} and BY4742 transformed with pRS316 were used as the positive and negative control, respectively. Ethyl acetate extracted with hexane from the fermented cultures was quantified with the assay. Experimental details are provided in Methods.

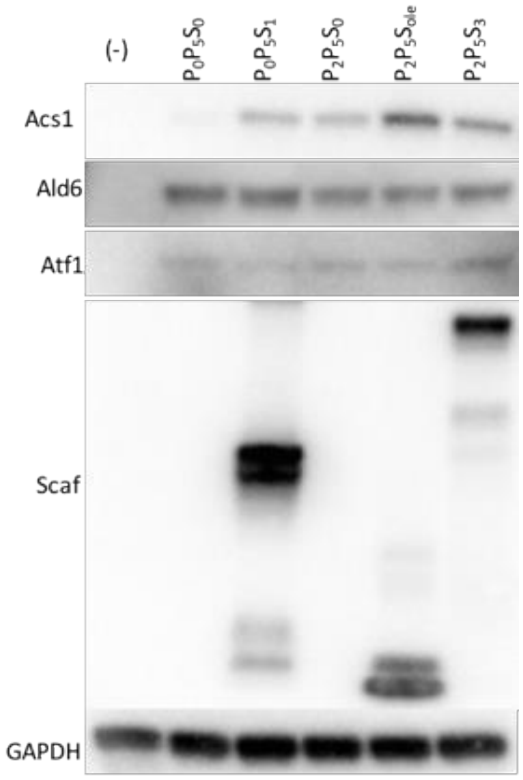

Figure S4.7. Western blot analysis of protein expression level for Ald6, Acs1, Atf1, and the scaffold. S_0, S_1, and S_3 represent no scaffold, oleosin-C_1-C_2, and oleosin-C_1-3C_2, respectively. S_{ole} is the oleosin-only control scaffold. anti-$(His)_6$, anti-HA, anti-myc, and anti-V5 antibodies were used for detection of Ald6-D_1, Acs1-D_2, Atf1, and scaffold. anti-GAPDH was used for loading control. 5 μg whole cell lysate was used for the analysis.

Table S4.2. Optical density of strains in the combinatorial library for flux optimization (Figure 4.4b of the text).

	Colony				
Construct	1	2	3	4	5
$P_1P_1S_1$	4.18	3.61	3.20	3.34	3.63
$P_1P_2S_1$	4.28	3.67	3.84	3.29	3.12
$P_1P_3S_1$	4.02	3.82	3.62	3.02	2.85
$P_1P_4S_1$	3.79	3.66	3.68	3.74	3.10
$P_1P_5S_1$	3.89	3.84	3.75	3.04	3.21
$P_1P_1S_2$	4.25	3.52	3.56	3.25	3.28
$P_1P_2S_2$	4.33	3.58	3.11	3.73	3.33
$P_1P_3S_2$	3.93	3.67	3.71	3.47	3.19
$P_1P_4S_2$	3.93	3.88	3.57	3.50	3.19
$P_1P_5S_2$	3.93	3.63	3.88	3.41	3.29
$P_1P_1S_3$	3.82	3.57	3.41	3.17	3.22
$P_1P_2S_3$	4.01	3.58	3.60	2.82	3.13
$P_1P_3S_3$	3.95	3.80	3.58	3.60	2.95
$P_1P_4S_3$	4.01	3.92	3.59	3.15	3.26
$P_1P_5S_3$	3.63	3.46	3.65	3.65	3.59
$P_2P_1S_1$	2.92	3.61	3.94	2.85	3.57
$P_2P_2S_1$	3.66	3.57	3.73	3.28	3.32
$P_2P_3S_1$	4.10	3.60	3.65	3.23	2.86
$P_2P_4S_1$	4.24	3.75	4.13	3.07	3.43
$P_2P_5S_1$	4.29	4.03	4.02	3.08	3.24
$P_2P_1S_2$	3.65	3.82	3.56	3.93	2.80
$P_2P_2S_2$	4.12	3.77	3.69	3.72	3.52
$P_2P_3S_2$	3.97	3.65	3.70	3.24	3.13
$P_2P_4S_2$	3.65	3.63	3.98	2.88	3.06
$P_2P_5S_2$	4.17	3.50	3.69	3.30	3.25
$P_2P_1S_3$	3.97	3.96	3.91	2.70	3.28
$P_2P_2S_3$	4.30	4.08	4.38	3.02	3.42
$P_2P_3S_3$	3.08	4.23	4.15	3.40	3.25
$P_2P_4S_3$	4.41	3.77	4.42	3.07	3.03
$P_2P_5S_3$	4.23	3.82	3.34	3.32	3.12
$P_3P_1S_1$	3.31	4.45	4.42	3.87	3.41
$P_3P_2S_1$	4.52	3.71	3.62	3.39	3.30
$P_3P_3S_1$	3.97	4.01	3.44	2.73	2.77
$P_3P_4S_1$	3.93	3.70	4.06	3.24	2.77
$P_3P_5S_1$	3.95	3.80	3.92	3.02	3.48
$P_3P_1S_2$	4.47	3.53	3.76	2.87	3.08
$P_3P_2S_2$	4.43	3.65	3.89	3.49	3.22
$P_3P_3S_2$	4.40	4.32	4.19	2.92	3.66
$P_3P_4S_2$	3.87	3.68	4.09	3.08	3.14
$P_3P_5S_2$	4.00	3.62	3.98	3.33	3.22
$P_3P_1S_3$	3.15	3.69	3.12	3.15	3.29
$P_3P_2S_3$	3.23	3.57	3.83	3.04	3.43
$P_3P_3S_3$	2.80	3.68	3.64	3.23	3.09
$P_3P_4S_3$	3.19	3.81	3.55	3.14	3.38
$P_3P_5S_3$	3.01	3.80	3.55	3.27	2.87
$P_4P_1S_1$	2.87	3.69	3.93	2.78	3.60
$P_4P_2S_1$	3.74	3.77	3.74	3.07	3.02
$P_4P_3S_1$	3.54	3.45	3.68	2.81	3.50
$P_4P_4S_1$	3.28	3.76	3.87	3.69	3.17
$P_4P_5S_1$	3.12	3.90	4.24	3.35	3.85
$P_4P_1S_2$	3.96	3.87	3.86	2.80	3.12
$P_4P_2S_2$	4.15	3.68	3.78	3.23	3.14
$P_4P_3S_2$	3.86	3.77	3.58	3.17	3.03
$P_4P_4S_2$	3.66	3.76	3.96	2.98	2.68
$P_4P_5S_2$	4.17	3.94	3.68	3.17	3.14
$P_4P_1S_3$	4.20	3.34	4.11	3.20	3.15
$P_4P_2S_3$	4.10	3.99	4.11	3.10	3.14
$P_4P_3S_3$	4.15	3.79	3.95	3.07	2.89
$P_4P_4S_3$	3.91	3.90	4.21	3.29	3.03
$P_4P_5S_3$	3.98	3.83	4.51	2.99	3.56
$P_0P_5S_1$	4.25	3.84	3.77	3.43	3.43

Chapter 5. Understanding Eht1 Endoplasmic Reticulum and Lipid Droplet Localization and Trafficking in *Saccharomyces cerevisiae*

5.1 Abstract

Lipid droplets (LDs) are ubiquitous organelles that play central roles in energy and lipid metabolism. They have a unique structure: a core of neutral lipids, composed of triacylglyceride (TAG) and sterol esters (SEs), surrounded by a phospholipid monolayer. LDs are also decorated with proteins that mediate important metabolic functions and inter-organelle communications. However, the mechanism of proteins targeting to LDs and the regulation of protein composition are not well understood and are still under investigation. Our protein of interest is Eht1, a medium chain fatty acid ester synthase from *Saccharomyces cerevisiae*. Our data shows that Eht1 localizes to the ER and subsequently to LDs; however, it lacks hydrophobic hairpin motifs, has no clear transmembrane domains (TMD), and there is no evidence of amphipathic terminal helices or other known LD targeting domains. The aim of this work is to understand the trafficking mechanism of Eht1 from endoplasmic reticulum (ER) to LDs in *S. cerevisiae*. Structure-function analysis suggests that both N- and C-termini are crucial for its membrane association. In addition, it suggests that the ER translocon may be related to the translocation process of Eht1 by gene knockdown and silencing analysis. Furthermore, to understand how Eht1 interactions with other proteins contribute to the trafficking, we conducted a series of immunoprecipitation experiments and identified

associated proteins by mass spectrometry. These studies begin to decipher the mechanism of translocation and protein trafficking to LDs.

5.2 Introduction

5.2.1 Lipid droplet structure and functions

Lipid droplets (LDs) have been the focus of many studies for they are closely related to obesity, type II diabetes, and cancer (1). They exist in eukaryotes (2-4) and even some of prokaryotes (5), functioning as the organelle for storage of neutral lipids. LDs are composed of a hydrophobic core of neutral lipids, sterol ester (STE) and triacylglyceride (TAG), and are surrounded by a phospholipid monolayer (6). There is a distinctive set of proteins decorating LDs, most of which are involved in lipid metabolism (6-8). Besides the lipid-related function, LDs contributes to some other functions, such as signaling (9,10), protein storage and degradation (11) and exchange of lipids between organelles (12).

5.2.2 LDs dynamic

LDs are being increasingly recognized as dynamic organelles that represent a frontier for cell biology (13). With respect to size, they range from 20 nm to 100 mm in diameter depending on cell types. Specifically for budding yeast, LDs are smaller than a micron, and the control of size requires the collaboration of Seipin-Ldb16 complex (14). In addition, the number, distribution, protein and lipid composition of LDs differ from cell types and physiological states (15,16).

LDs are often found in close juxtaposition to other organelles, such as peroxisomes (17), mitochondria (18), endosomes (19) and endoplasmic reticulum (20), which suggest that LDs might dynamically interact with these cellular organelles. Both microscopy and biochemical studies suggest that ER and LDs are connected tightly, and this is further supported by functional studies. The seipin-Ldb16 complex, as the key regulator of LDs morphogenesis in yeast, is found at ER-LD contact sites, which probably links neutral lipid synthesis with LD assembly (14).

5.2.3 Biogenesis of LDs

ER has been believed to have a guiding role in LD biogenesis and most of the enzymes involved in neutral lipids formation are localized on ER. However, the mechanism to explain how the neutral lipids accumulate and form LD remains to be elucidated. Several models have been proposed, including the "ER-budding model", the "Bicelle model" (21) and the "vesicular-budding" model (22). In the ER-budding model, it is proposed that the neutral lipids form a lens of oil in the ER bilayer and subsequently buds from the membrane, taking with phospholipids from the ER cytosolic leaflet (15). There is substantial evidence to support this model, but it has not been proved or observed directly (23,24).

5.2.4 Lipid droplet proteome

Proteins, as another important component of LDs, might require particular structure to bind LDs, for it has a monolayer membrane that is unique among all known cytoplasmic organelle. The study of protein composition of LDs is propelled by the well-established isolation methods via sucrose-gradient ultracentrifugation and advanced proteomic

technology analyzed by mass spectrometry. Hundreds of coating proteins have been identified and some of them have been further verified by biochemical, microscopic and functional methods. Among attempts for LD proteome studies of different cell types and organisms, several functional groups of proteins are present consistently and reproducibly, including lipid synthetic enzymes, membrane trafficking proteins, signaling proteins and proteins involved in protein degradation (6,8,11). Additionally, a variety of proteins are found in the hydrophobic core of LDs, such as the perilipin family proteins (25,26). However, the mechanism for proteins specifically localize to LDs remains to be determined.

5.2.5 Mechanisms for proteins targeting to LDs

Proteins targeting to LDs are sorted in two different classes. Class I proteins can access LDs from the ER either during LD formation or after formation via ER-LD contact site with an internal hydrophobic hairpin motif or N-terminal hydrophobic sequences. Class II can access to LDs surface from cytosol and bind through amphipathic helices or multiple amphipathic and hydrophobic helices (27). Some proteins that clearly target LDs are so far difficult to classify. For example, in yeast, two alcohol acetyl/acyltransferases (AATases), Atf1 and Atf2, localize to the ER and subsequently are sorted to LDs. Segments of the N- and C-terminal amphipathic helices are required for both ER and LDs association (28). The targeting mechanism of AATases is unknown, as is whether AATases target via Class I or Class II pathway.

5.2.6 AATase

AATase is responsible for producing short and medium chain (C2-C12) fatty acid ethyl esters (FAEEs) in yeast and fruits. These short and medium chain FAEEs contribute to the flavors of fruits and industrial fermented beverages. The natural physiological role of FAEEs as the secondary metabolites in *S. cerevisiae* is not well understood. And, the details about the metabolic pathway of FAEE biosynthesis remain to be elucidated. *In S. cerevisiae*, Atf1p and Atf2p are responsible for majority of short chain esters synthesis, while Eht1p and Eeb1p play a major role in medium chain esters. AATase activity in *S. cerevisiae* is repressed by oxygen and unsaturated acids and it has been suggested that it functions as a response to stress conditions (29). Previous studies suggest that AATase might be involved in cellular lipid metabolism and detoxification process (30-32). Understanding the localization and trafficking mechanism of this class of enzyme will enable, 1) engineered yeast that produces renewable biofuels and fine chemicals, 2) improved the flavor characteristic of fruits and wines by genetic modification, and 3) investigation in the LD biogenesis and trafficking.

Although evolutionally distinct from mammals, yeast *Saccharomyces cerevisiae* is an extensively studied model organism and has proven very valuable in understanding how proteins localize to lipid droplets. To address these questions, we focused on the protein localization and trafficking mechanism of acyl-coenzymeA:ethanol O-acyltransferase, particularly Eht1 and Eeb1, in *S. cerevisiae*. Eht1 and Eeb1 are responsible for medium-chain fatty acid ethyl ester biosynthesis and might be involved in the detoxification of fatty acids and ethanol during fermentation. Eht1 and Eeb1 are closely related and the

pair of paralogue arose from gene duplication(32). Fluorescence microscopy and fractionation study show that Eht1 and Eeb1 are membrane-associated proteins. Time course study shows that Eht1 and Eeb1 are initially localized to ER and subsequently sorted to LDs and mitochondria, respectively. A series of N- and C-terminal deletions and alanine-stretch scanning mutations was used to analyze the amino acid sequences of Eht1 necessary for LD localization. We demonstrate that both N- and C-terminal sequences are required, with N-terminal playing a major role. Through hydropathy-based analysis and transmembrane domain prediction of Eht1 and Eeb1, there is no transmembrane sequence internally or amphipathic helices on N- and C-termini. Without these two main known structures targeting proteins to LDs, it suggests that Eht1 might undergo an unknown translocation process from ER to LDs. This work begins to describe Eht1 trafficking and localization in yeast.

5.3 Material and Methods

Strains and culture conditions

All *E. coil* and *S. cerevisiae* strains used in this work are summarized in Table S1. All modified yeast strains were derived from BY4741 or BY4742 (33). *E. coli* DH5α used for molecular cloning. *E. coli* was grown in Luria Broth (LB) (Sigma) medium containing 50 μg mL^{-1} ampicillin (Fisher) for cloning experiment. *S. cerevisiae* strains without plasmids were grown in YPD complex medium containing 10 g/L yeast extract, 20 g/L peptone, and 20 g/L glucose. *S. cerevisiae* strains harboring plasmids were grown in the defined SC-URA medium containing 6.7 g/L yeast nitrogen (Bacton-Dickinson), 2

g/L synthetic dropout mix without uracil (Sigma), and 20 g/L glucose (Sigma). Manipulations were performed using a standard PEG/LiAC protocol (34). Solid media were prepared as above with 20 g/L agar.

Deletion strains were taken from the yeast deletion (35) or the DAmP (Decresed Abundance by mRNA Perturbation) (36) libraries, respectively. All deletion strains were verified using primers from within the endogenous open reading frame (ORF). The strains were cultured with 200 μg mL^{-1} G418 (Sigma).

Plasmids construction

The plasmids used in this study are listed in Table S2. Yeast genes, promoters, and terminators were amplified from genomic DNA. An overexpression cassette with C-terminal GFP tag driven by the constitutive yeast promoter phosphoglycerate kinase 1 (PGK1p) and terminated by PGK1t was constructed. The promoter and terminator were amplified from genomic DNA of BY4742 and cloned into pRS426. PGK1p was inserted using SacI and SacII sites. PGK1t was inserted using SpeI and KpnI sites, while GFP was inserted at NotI and SpeI sites. *EHT1*, *EEB1* and mutants to *EHT1* were amplified from BY4742 genomic DNA and cloned into PGK1 overexpressing cassette using SacII and NotI sites.

DsRed, amplified from pERGmDsRed (gift from J. Goodman, University of Texas Southwestern Medical School), was first inserted into pRS426 containing PGK1p-PGK1t at NotI and SpeI sites. LEU2, amplified from pRS315, was subsequently inserted between KpnI and EcoRV sites. This cassette was used to fuse DsRed to the 3' end of the

LD marker Erg6 and the mitochondria marker OM45 by PCR-based homologous recombination as previously described (28).

Fluorescence microscopy analysis

Cells were imaged using an Olympus BX51 microscope (UPlanFL 100X 1.30 oil-immersion objective lens, mercury lamp) and fluorescence micrographs were captured by a Q-Imaging Retiga Exi CCD camera. Images were processed using CellSens Dimension 1.7 software (Olympus). In all cases, at least three cell populations were analyzed and images representative of the cell populations are shown.

Subcellular fractionation and membrane topology assay

Fractionation on an Accudenz density gradient was performed essentially as described by Cowles et al. (37). One hundred optical density (OD) units of early log phase cells were harvested and transformed into spheroplasts by zymolyase 20 T (Seikagaku Corporation, Japan). Spheroplasts were resuspended in lysis buffer (0.25 M sorbitol-10 mM MES-Tris [pH=6.9]-0.2 mM EDTA) supplemented with a protease inhibitor cocktail (Roche), and lysed with a Dounce homogenizer by 40 strokes. The homogenates was precleared by centrigufation at 300 × *g* for 10 min, then separated into pellet and supernatant fractions by centrifugation at 13,000 × *g* for 20 min. All centrifugation steps were perfomed at 4 °C.

To determine the membrane association and topology (38), detergent and salt extractions of microsomal membranes were performed by incubating 50 μg of the microsomal fraction with 1% SDS, 1 M NaCl, or 0.1 M Na_2CO_3 in lysis buffer A for 30 min on ice. Samples were then centrifuged at 13,000 × *g* for 10 min, and proteins from

the pellet and supernatant fractions were precipitated by 10% TCA and analyzed by Western blotting. For the proteinase K protection experiment, 50 μg microsomal fractions were incubated with 0, 9, 14 or 28 μg/mL of proteinase K for 30 min on ice. The reaction was stopped by adding 5 mM PMSF, and proteins were precipitated by 10% TCA. The pellet was resuspended in sample buffer, boiled for 10 min, and subjected to SDS-polyacrylamide gel electrophoresis and Western blot analysis. Protein concentrations were determined by a commercially available assay (Pierce 660 nm Protein Assay, Thermo Fisher) and quantified with Nanodrop 2000c.

Western blot analysis

Western blots were performed using standard procedure. Briefly, proteins were loaded on Any kD™ Mini-PROTEAN® TGX™ Gel (Bio-Rad) and run at 200 V for 30 min. Samples were electrophoretically transferred to a PVDF membrane at 25 V overnight. Membranes were blocked with 5% non-fat milk in Tris buffer saline with TWEEN-20 (TBST) buffer for 1 h at room temperature, washed, and incubated with primary antibody in TBST with 1% non-fat milk for 1 h. Secondary antibody in TBST with 1% non-fat milk was applied, and incubated at room temperature for 0.5 h. After washing with TBST, Immobilon Western HRP Substrate (Millipore) was used for signal detection and UN-SCAN-IT gel 6.1 software was used to quantify band intensity. The following antibodies were used: rabbit anti-GFP (NB600-303; Novusbio), mouse anti-Myc (SC-40; Santa Cruz Biotech), rabbit anti-Kar2 (SC-33630, Santa Cruz Biotech), goat anti-rabbit IgG-HRP (65-6120; Invitrogen), goat anti-mouse IgG-HRP (31430; Thermo Fisher Scientific).

Immunoprecipitation and mass spectrometry

The spheroplasts were prepared and lysed with the Dounce homogenizer as described above. Detergent Triton X-100 or digitonin were added to final concentration 1% and incubate for 1h. The precleared lysates were incubated with equilibrated beads carrying GFP-binding protein (GFP-Trap_A; ChromoTek, Planegg-Martinsried, Germany) or Myc-binding protein (Myc-Trap_A; ChromoTek, Planegg-Martinsried, Germany; as negative control) for 1h at 4°C with mixing. After sedimentation, supernatant were removed and beads were washed 4 times with lysis buffer. The proteins on the beads were digested with trypsin overnight and analyzed by mass spectrometry.

qPCR

RNA was extracted from cells grown to stationary phase using the Yeastar RNA Isolation kit (Zymo Research), and residual DNA removed via DNase I digestion (NEB). The total RNA was converted to cDNA using the iScript Reverse Transcription Supermix (Biorad). Two μL of cDNA was subjected to qPCR using the SsoAdvanced Universal SYBR Green Supermix (Biorad) on a CFX Connect thermocycler (Biorad). Primers were designed using Primer3 according to manufacturer's specifications (39). Relative expression levels were determined using the Pfaffl method as previously described (40) and normalized to expression of TAF10.

Preparation of whole cell lysate

Yeast cells harboring expression plasmids were cultured to early stationary phase in 50 ml SD media without uracil in 250 ml baffled flasks. Cells were harvested by centrifugation at 3,500 rpm for 5 min at 4 °C and washed twice with 100 mM potassium

phosphate buffer (pH 7.4) containing 2 mM magnesium chloride. Equal volumes of wet cell pellets and 425-600 μm diameter acid-washed glass beads (Sigma-Aldrich) were added to a 15 mL tube and resuspended in 1 mL ice-cold lysis buffer (100mM potassium phosphate buffer, 2mM magnesium chloride, 2mM DTT, and protease inhibitor cocktail (Roche), pH7.4). Cells were disrupted by vortexing 10 times for 30 s. After each vortexing the suspension was kept on ice for 30 s. The beads were removed by centrifugation at 500g for 5 min at 4 °C and the supernatant was transferred to a pre-cooled 1.5 mL tube. Whole cell lysate protein concentrations were determined by a commercially available assay (Pierce 660 nm Protein Assay, Thermo Fisher).

AATase activity assay and screening

Alcohol-O-acetyl/acyltransferase activity was determined by monitoring NADH production from a coupled reaction with α-ketoglutarate dehydrogenase (α-KGDH). The reaction was performed at room temperature in 100 mM potassium phosphate buffer, pH 7.4. The assay solution contained final concentrations of 2 mM α-ketoglutarate (α-KG), 10 mM cystein, 2 mM NAD^+, 10 mM $MgCl_2$, and 0.03 U α-KGDH (Sigma-Aldrich). Whole cell lysate samples, pyrazole (15 mM final concentration), and alcohol (20 mM final concentration) were added to the assay solution. It has previously been reported that the order of substrate addition affects long chain AATase activity (25). The coupled enzyme reaction was initiated by adding 0.5 mM acetyl/acyl-CoA to the reaction solution. The assay was monitored by measuring the absorbance of NADH at 340 nm (ε_{340} = 6.22 $mM^{-1}cm^{-1}$) for 4 minutes. Screening experiments were performed in 96-well

microtiter plates with a final volume of 100 μL and the rate of NADH production was monitored with a BioTek Synergy H4 hybrid multi-mode microplate reader.

5.4 Results

5.4.1 Eht1 and Eeb1 are membrane-associated proteins

Eht1 and Eeb1 were tagged with C-terminal GFP to investigate their intracellular localization. They were overexpressed by the constitutive PGK1 promoter from a high copy number plasmid. Erg6 and OM45, as the lipid droplet and mitochondria marker proteins respectively, were chromosomally tagged with DsRed. Fluorescent microscopy images of cells expressing Eht1-GFP and Erg6-DsRed cultured in glucose medium revealed co-localization of GFP and DsRed fluorescence, indicating that Eht1 localized to LDs (Figure 1A). The co-localization of fluorescent signal from Eeb1-GFP and OM45-DsRed indicates that Eeb1 is localized to mitochondira. A time course study of the intracellular localization of Eht1 and Eeb1 at time points of 4, 10, 18 and 24 hours (Figure 1B) were performed to study their trafficking in cells. In lag and early log phase (4 and 10 hours respectively), C-terminally tagged Eht1 and Eeb1 showed clear ER structure. Subsequently, Eht1 and Eeb1 shift from ER to LDs (Eht1) or mitochondria (Eeb1) as cell progressed from late log phase (18h) to stationary phase (24h), suggesting that the translocation is growth dependent. To determine whether Eht1 and Eeb1 are indeed membrane associated at early log phase, as observed from fluorescent microscopy, their fractionation properties were examined by differential centrifugation (Figure 1C). Both of them were enriched in the 13,000 × *g* membrane pellet, Eht1 was

not detectable in cytosol and Eeb1 slightly showed in the cytosol, consistent with the membrane association of them.

5.4.2 N- and C-terminal amino acid sequences are required for membrane association of Eht1

To examine the possible mechanism of Eht1 LD association, we analyzed the intracellular localization of N- and C-terminal truncations of Eht1 during stationary phase (Figure 5.2). Wild type Eht1, Δ2-13, Δ2-21 and Δ429-451 truncates tagged with GFP were overexpressed by the constitutive PGK1 promoter from a high copy number plasmid. LD marker Erg6 was chromosomally tagged with DsRed and constantly expressed. Fluorescent microscopy analysis of cells co-expressing truncations tagged with C-terminal GFP and Erg6-DsRed cultured in glucose medium showed that the LD localization was not detected for truncations. Δ429-451 was unevenly distributed in the cytoplasm; Δ2-13 was partially localized to LDs and probably cell membrane while Δ2-21 was dispersed in the cytoplasm. These results suggested that the N- and C-terminal regions, consisting of amino acid residues 2-21 and 429-451 of Eht1, harbored a targeting determinant for Eht1.

Fluorescent images of Eht1 1-40 and 161-451 amino acid sequences fused with C terminal GFP at 4h and 24h (Figure S5.1A) showed that they were dispersed in cytosol or formed aggregates, suggesting that N- or C terminal region of Eht1 is not sufficient for targeting to ER or LDs. Internal truncations of Eht1, Δ81-160 and Δ41-160, are mislocated with LDs (Figure S5.1B), suggesting that the internal region from 40-160 amino acids of Eht1 might be involved in the membrane association.

5.4.3 N-terminus of Eht1 plays a major role in targeting to LDs

To examine the possible molecular mechanism of Eht1 LD localization, the N-terminal amino acid sequence of Eht1 and Eeb1 was aligned (Figure 5.3A). The result showed that 2-13 amino acids are different with identity for only two Prolines, 14-21 amino acids are exactly the same for Eht1 and Eeb1. To investigate the importance of N-terminal sequence of Eht1 for localization to LDs, we generated a mutant of Eeb1, named as Eeb1$^{\text{Eht1 2-13}}$ by replacing its N-terminal 2-13 amino acid sequence with Eht1's (Figure 5.3A). Fluorescent microscopy analysis of stationary cells co-expressing Eeb1$^{\text{Eht1 2-13}}$-GFP and Erg6-DsRed revealed that the mutant is localized to LDs (Figure 5.3B). Time course study of Eeb1$^{\text{Eht1 2-13}}$-GFP at different time points showed that Eeb1$^{\text{Eht1 2-13}}$-GFP origins from ER and then targets to LDs (Figure 5.3C). Another mutant of Eeb1, Eeb1$^{\text{Eht1 429-451}}$, is generated by replacing Eeb1 C-terminal 434-456 amino acid sequence with Eht1 C-terminal 429-451 amino acid sequence (Figure S5.2A). Fluorescent images of stationary cells co-expressing Eeb1$^{\text{Eht1 429-451}}$-GFP and Erg6-DsRed showed that the mutant is not localized to LDs and possibly targeted to mitochondria (Figure S5.2B). Time course study of Eeb1$^{\text{Eht1 429-451}}$-GFP at different time points revealed that Eeb1$^{\text{Eht1 429-451}}$-GFP origins from ER and then localizes to mitochondria (Figure S5.2C).

We next focused on this stretch of 21 amino acids on N-terminal of Eht1. Accordingly, we generated six substitution mutants of Eht1 by successive substitution of every four amino acid residues within this region. The intracellular localization of tetra-alanine scanning mutants of Eht1 was then examined by overexpressing in *S. cerevisiae* co-expressing Erg6-DsRed (Figure 5.3D). Remarkably, two of the tetra-alanine scanning

mutants, 14-17/A mutant (amino acid residues $H^{14}WGY^{17}$ substituted with $A^{14}AAA^{17}$) and 18-21/A mutant (amino acid residues $N^{18}GTV^{21}$ substituted with $A^{18}AAA^{21}$), showed cytosol-dispersed pattern at stationary phase. Other mutants showed significant co-localization with Erg6-DsRed analyzed by fluorescent microscopy images. Mutants 14-17/A and 18-21/A are dispersed in cytosol and lose the ER association as showed in Figure S5.3. These results strongly suggested that the N-terminal sequence of Eht1 has an important role on LD localization.

5.4.4 Hydropathy plot and membrane topology of Eht1

A hydropathy plot of Eht1 and Eeb1 was generated by the method of Kyte and Doolittle (Figure 4A). We chose to analyze the hydrophobicity of Eht1 and Eeb1 with a window size of 9 amino acids, as recent structural work on the signal peptide with SRP exhibited a binding interface within 8-20 hydrophobic residues (41). This plot suggested that Eht1 and Eeb1 do not have any possible transmembrane regions. Further analysis of the amino acid sequence of Eht1 and Eeb1 by algorithms used to predict membrane topology also suggested that either of them has any transmembrane domains (Figure 4B). Two of seven algorithms indicated that one or two transmembrane domains for Eht1 with low confidence, and one of the algorithms predicted a transmembrane domain for Eeb1 with low confidence. We showed that Eht1 is membrane-associated; however, both the hydropathy plot and transmembrane domain prediction algorithm indicated that there is no possible transmembrane domain for Eht1. Taken together, it suggested that Eht1 is a peripheral membrane protein.

To support this hypothesis, 13,000 × *g* membrane fractions from early log phase cells overexpressing Eht1-GFP was isolated and treated with chemicals that extract or solubilize proteins from membranes (Figure 4C). In samples incubated with buffer alone (Mock), Eht1 was found exclusively in the pellet (P) fraction. In the presence of detergent (1% SDS), Eht1 was completely solubilized. In contrast, in the presence of 1 M sodium chloride or 0.1 M sodium carbonate, which solubilize peripheral membrane proteins, Eht1 is partially solubilized, demonstrating that it is a peripheral membrane protein.

To determine the orientation of the N and C termini of Eht1 on ER, we performed protease protection assays. 13,000 × *g* membrane fractions from early log phase cells overexpressing Eht1 with N-terminal or C-terminal GFP tag were incubated with proteinase K and immunoblotted with anti-GFP, which recognizes the N- and C-termini of the expressed protein. In samples without treatment with proteinase K, Eht1 was detected by anti-GFP for both termini. In contrast, proteinase K treatment of membrane fractions destroyed both terminal epitopes, suggesting that the N and C termini are both exposed to the cytosol. To verify the integrity of the membrane fractions, samples were immunoblotted with an antibody against the ER luminal protein, Kar2. Kar2 was protected against proteolysis from proteinase K, indicating that the membrane fractions were intact. These results thus indicate that Eht1 is a peripheral membrane protein with N- and C-termini exposed to the cytosol on ER.

To refine Eht1 topological characterization, the accessibility of internal region of Eht1 to protease was examined. Therefore, Eht1 were tagged with GFP at their C terminus and myc tag between 13-14 amino acid or 160-161 amino acid (Figure S5.4A). Fluorescent

microscopy analysis at different time points (4h, 10h and 24h) revealed that 13-myc-14 and 160-myc-161 were initially localized to ER and subsequently translocated to LDs (Figure S5.4B), which is similar to the wildtype Eht1, suggesting that the structures are not disrupted by inserting myc tag internally. Both internal and C-terminal epitopes are sensitive of 13-myc-14 and 160-myc-161 are sensitive to protease digestion (Figure S5.4C), indicating that the internal region of Eht1 is also exposed to cytosol.

Also, the membrane association and topology of Eeb1 $^{Eht1\ 2\text{-}13}$ were characterized (Figure S5.5). Similar to Eht1 wildtype, Eeb1 $^{Eht1\ 2\text{-}13}$ is a membrane-associated protein with both termini exposed to the cytosol on ER.

5.4.5 Eht1 targeting to ER is related to translocons on ER

In *S. cerevisiae*, translocation occurs through two channels, the canonical translocon Sec61 and the alternative translocon Ssh1. The canonical Sec61 translocon mediates both co-and post-translational translocation by associated with different accessory factors. The nonessential *SBH1* gene encodes for the beta subunit of Sec61p ER translocation complex, and the nonessential *SEC72* gene encodes for an accessory factor required for the SRP-independent posttranslational translocation. The yeast genome contains a gene *SSH1* (Sec61 homolog), encoding a protein ~30% identical to Sec61p that is ER localized and associated with a homolog of Sbh1p, termed Sbh2p. This alternative translocon Ssh1 is active only in co-translational translocation. The strains were deleted for the non-essential genes (*SBH1*, *SEC72*, *SSH1*, and *SBH2*) and knockdown for the essential gene (*SEC61*). By imaging the wild type and knockout or knockdown strains overexpressing Eht1-GFP, we could examine whether the translocons are involved in Eht1 targeting to

ER and trafficking to LDs (Figure 5.5). Knockout of accessory factors (*SBH1*, *SEC72*, and *SBH2*) did affect the ER or LDs localization of Eht1. Eht1-GFP slightly dissociates from LDs to cytosol but maintains ER association with knockdown of *SEC61* or knockout of *SSH1*. In contrast, Eht1-GFP localization to ER is only affected by simultaneously knockdown of *SEC61* and knockout of *SSH1*. These results suggest that both translocons on ER might be involved in Eht1-GFP targeting to ER.

In addition, the gene knockout and silencing effect of common and alternative translocons were examined for Eeb1 and Eeb1$^{\text{Eht1 2-13}}$ localization and trafficking (Figure S5.6). Similar to Eht1 and significantly different from Eeb1, Eeb1$^{\text{Eht1 2-13}}$ localization and secretion is only affected by *SEC61* knockdown and *SSH1* knockout. It suggests that the N-terminal 2-21 amino acid sequence determines the interaction between Eht1 and translocons.

5.4.6 Identification of physical protein-protein interactions of Eht1 on ER

Immunoprecipitation combined with mass-spectrometry identified 48 proteins interacting with Eht1-GFP while it is localized on ER (Figure 5.6A). The proteins are classified based on their involvement and functions using the Saccharomyces Genome Database SGB (http://www.yeastgenome.org/) (Figure 5.6B, listed in Table S5.3). We identified proteins (14.6%) involved in metabolism, including lipid metabolism and amino acid/glyoxylate/carbohydrate metabolism. We also found numerous proteins (25.0%) related to protein trafficking and vesicle trafficking. We also identified ribosomal proteins and some translation factors (14.6%). Proteins involved in protein

posttranslational modification (10.4%) were also identified. Interestingly, four chaperones were identified.

To examine if these proteins interacting with Eht1 are required for its localization and trafficking, we chose 8 single gene mutants and conducted the screening for genes whose deletion affected the LD localization and secretion of Eht1. In this screen, each gene mutants was cultured for 36 hours and the fluorescent images were analyzed at different time points (t=4, 10, 24 and 36 hrs) (Figure 5.7). Overall, only *ERG5* knockout was found to retain the Eht1-GFP on ER membrane after 36 hrs culturing, indicating that it has defects in the translocation process.

5.4.7 Eeb1^{Mut} transcription, translation and function

Eeb1^{Mut} is generated by replacing Eeb1 N- and C-terminal amino acid sequences (2-13 and 434-456) with Eht1 N- and C-terminal amino acid sequences (2-13 and 429-451). Both Eeb1wt and Eeb1Mut were expressed driven by different strength constitutive promoters, including REV1p, TPI1p, PGK1p and TEF1p (REV1p<TPI1p<PGK1p<TEF1p), and the same terminator PGK1t. The transcription level of Eeb1^{wt} and Eeb1^{Mut} were examined and compared by qPCR, relative to TAF10. The translational level of Eeb1^{wt} and Eeb1^{Mut} were measured and quantified by western blot, normalized to GAPDH. The function of Eeb1wt and Eeb1Mut were determined by AATase enzymatic activity assay. The three-dimensional relationship between transcription, translation, and function of Eeb1^{wt} and Eeb1^{Mut} were compared as shown in Figure 5.8A, with detailed two-dimensional relationships were in Figure 5.8B, C and D. Eeb1^{wt} mRNA level is increased driven by stronger promoter; however, the protein

expression level and functional activity are consistently low under control four different promoters. Eeb1^{Mut} mRNA level is also increased with stronger promoter, and the protein expression level and functional activity are improved. In addition, Erg6 (LD marker protein) and OM45 (mitochondria marker protein) were chromosomally tagged with C-terminal DsRed to indicate the morphology of LDs and mitochondria. The fluorescent images of cells after 24 hrs culturing revealed normal morphology for both organelles.

5.5 Discussion

Our subcellular localization of GFP-tagged versions of Eht1 and Eeb1 indicates that Eht1 and Eeb1 are initially localized to ER and subsequently sorted to LDs and mitochondria, respectively. The biological function of these localizations remains unclear. Our possible explanation of this localization is its ability to detoxify fatty acids and ethanol by esterification. Free fatty acids and ethanol can inhibit cell growth and fermentation (42,43). It has previously been suggested that the primary metabolic role of AATases is to regenerate free CoAs from acetyl/acyl-CoAs that accumulate in yeast under anaerobic condition. Eht1 and Eeb1 have been reported as medium chain fatty acid ethyl ester synthases (44,45) and Eeb1 plays major role with Eht1 playing a minor role in *S. cerevisiae* (46). Eht1 is sorted to LDs to have accessibility to acyl-CoAs and ethanol in cytosol whereas Eeb1 is targeted to mitochondria to approach substrates in mitochondria. The products medium chain fatty acid ethyl esters can diffuse easily through membrane and be secreted to medium, further reducing the accumulation of toxic acid and shifting the equilibrium towards ester synthesis (47). LDs have been proposed to be sites for

protein sequestration functioning as chaperones to store proteins for later use (48). Histones H2A and H2B are unstable and would aggregate or be rapidly degraded without histone chaperones (49,50). However, they are rich on LDs without their normal binding partners (11), which suggests that LDs might function as an analogous chaperone function to store histones for possible largely demanding (48). Here, LDs might have the similar function to store Eht1 for immediately dealing with possible risk of toxic fatty acids or ethanol. However, the real physiological role of volatile ester synthesis is still not known. It is required to further improve our understanding of pathway of ester biosynthesis, regulation and biological functions.

Deletions of the N- and C-terminal regions of Eht1 were made to investigate the possible role of each terminus in membrane association and LD targeting. Truncation of residues 2-13 and 429-451 amino acids disrupted LD targeting and resulted in dispersed localization in cytosol, indicating the importance of these two regions in membrane association. N- or C-terminal regions fused to GFP (Figure S5.1A) are not able to localize the fluorescent protein to ER or LDs. We proposed that the termini of Eht1 are necessary but not sufficient for ER and LDs targeting. In addition, internal truncations Δ81-160 and Δ41-160 of Eht1 fused with GFP were mislocated (Figure S5.1B). But the 1-291 amino acid sequence of Eht1 is able to target the GFP to ER (Figure S5.1C), suggesting that the N-terminal and part of the internal region of Eht1 are required for ER association. Therefore in this case, it is possible that the internal regions within the protein may also be involved. It is similar to Atf1 and Atf2, which have been demonstrated that their N-

and C-terminal amphipathic helices are required but not sufficient for LD localization (28).

High sequence similarity but different localization at stationary phase between Eht1 and Eeb1 enable us to study the necessity of the N- or C-terminal of Eht1 for the targeting to ER and LDs. We have demonstrated that the mutant Eeb1$^{Eht1\ 2\text{-}13}$ undergoes same trafficking pathway as wildtype Eht1, from ER to LDs. However, replacement of the C-terminal region of Eeb1 does not target Eeb1$^{Eht1\ 429\text{-}451}$ to LDs instead of mitochondria. Taken together, it suggests that N-terminus of Eht1 plays a major role for localizing to LDs and ER. It is further demonstrated by alanine-stretch scanning of N-terminal sequence of Eht1. 7 amino acids, H^{14}WGYNGTV^{21}, might comprise an important targeting determinant for Eht1 in *S. cerevisiae*.

Our results thus far demonstrate the necessity of terminal regions for ER localization and LD targeting of Eht1, but they do not indicate a trafficking mechanism. We found that all the mutants of Eht1 targeting to LDs are always initially localized to ER, suggesting that the LD localization might be ER-dependent. Targeting to ER has been shown to occur co-translationally by the signal recognition particle (SRP) dependent (51-53) or SRP-independent (SND) (54) or post-translationally by the guided entry of tail-anchored proteins (GET) pathways (55,56). Three pathways work in parallel to facilitate proteins targeting to ER, where they undergo folding, processing, sorting and trafficking to subsequent endomembrane compartments. SND pathway acts as a backup targeting system and can compensate for the loss of both SRP and GET pathways. Three proteins, Snd1p, Snd2p and Snd3p, are involved in SND pathway; however, the mechanistic

details have yet been to be uncovered. Snd1p in cytosol is predicted to interact with ribosome to capture nascent substrate, Snd2p and Snd3p on ER membrane form a complex together with Sec61 translocon, might act as receptors in promoting substrate capture and handoff the translocon. By proximity-specific ribosome profiling analysis, the transcripts of Eht1 and Eeb1 was depleted on the ER membrane in cells from all three Δsnd strains, indicating that the SND machinery might have a role in targeting them to the ER surface as they are being translated. Our finding that knockout out of accessory factors involved in SRP or GET pathways did not affect Eht1 localization suggests that Eht1 localization to ER is not related to SRP or GET pathway. In addition, our protein-protein interaction analysis suggests that Snd2p might have physical interaction with Eht1, which further indicates that Eht1 might undergo co-translationally SND pathway to localize to ER. Furthermore, SND pathway can target diverse proteins with transmembrane domains dispersed throughout the entire protein range. However, the hydropathy plot and transmembrane domain prediction algorithms suggested that there is no transmembrane domain with high confidence for either Eht1 or Eeb1. It suggests that SND pathway could recognize the membrane proteins with TMD but also membrane-associated proteins lacking TMD. We found that Eht1p translocation from ER to LDs is only significantly affected by knockdown of common translocon and knockout of alternative translocon on ER. Sec71p has been reported to translocate across ER membrane via both translocons with preference to the Ssh1p translocon in yeast (57). It suggests that Eht1p, similar to Sec71p, is able to utilize the canonical Sec61 channel and the alternative Ssh1 channel.

LDs are found to be functionally connected to the ER membrane (58) and only large LDs have ability to grow in size (59). Biochemical studies demonstrated that ER membrane tightly associate with LDs and are not easily dissociated using ionic strength (60). Electron microscopy of early stage of LDs biogenesis showed that the nascent LDs for lens-like structures in the ER membrane (61). This connection between ER and LDs allows the efficient partitioning of membrane proteins between the two compartments. In addition, it has been demonstrated that proteins are able to access LDs from ER either during LD formation or after formation via ER-LD membrane bridges by an energy- and temperature-independent mechanism (24). With respect to the structure of Eht1, it would be interesting to examine how proteins can be accommodated both in ER lipid bilayer and LD monolayer. It is possible that protein conformation could be changed during the translocation process. Erg1p, a key enzyme of sterol biosynthesis in yeast, is localized to ER and LDs and this dual localization reflects a relationship between ER and LDs. But its enzymatic activity of squalene epoxidase was only detectable in the ER but not on LDs, indicating that the conformation in ER is different from that on LDs (62). Without conformational changes, there are alternative mechanisms to explain the dual localization. “Integral” LD proteins might use long hydrophobic regions to enter and exit the membrane on the same side of the lipid monolayer, such as oleosins (63), caleosins (64), and caveolins (65). “Surface” LD proteins have no long hydrophobic domains and their targeting involves redundant, discontinuous sequences, such as perilipin (66,67), HCV core proteins (68,69), and Atf1/2 (28). Lin et al. showed that the N- and C-terminal amphipathic helices of Atf1 and Atf2 are necessary but not sufficient for their LD

localization (28). It has also been reported that Atf2 localizes to the ER during exponential growth with two transmembrane domains, and both N- and C-termini are in the ER lumen (70). Different from Atf2, Eht1 is a peripheral membrane protein on ER with both termini exposed to cytosol. Eht1 is demonstrated as peripheral membrane protein on ER and is proposed to be surface LD protein without long hydrophobic regions. This membrane topology of Eht1 on ER results in a relatively weak membrane association, which might facilitate its trafficking from ER to LDs.

A conserved family of proteins, fat storage-inducing transmembrane (FIT) proteins, is required for proper budding of LDs from the ER (61). However, it is not clear that whether the protein trafficking from ER to LDs requires any proteins. Our immunoprecipitation and mass spectrometry analysis identified possible protein-protein interactions of Eht1. Of interest is that some of them are involved in protein trafficking and vesicle trafficking. The function of Atf1-COPI machinery in lipid droplet formation has been demonstrated and this function might be evolutionarily conserved in yeast and human cells (71). RET3, the subunit of COPI, was identified to have physical protein interaction with Eht1. It is possible that the COPI is also involved in the protein trafficking from ER to LDs. Two proteins related to protein traffic, SRP102 for SRP-dependent protein targeting and Sec62 for post-translational translocation, might form an unidentified complex with Snd proteins and translocons, which is responsible for proteins lacking TMD to be initially targeted to ER, such as Eht1p.

Metabolic engineering studies have focused on overexpressing enzymes by strong constitutive promoters to improve yield and productivity (72,73). The protein

transcription level is mainly determined by the promoter strength; however, post-translational processing of enzymes is another important factor for their functions, such as RNA-based control and protein-based control. RNA-based control includes translation initiation and mRNA stability, whereas the protein-based control includes regulating protein half-lives (74).

Fatty acid ethyl esters, are the secondary metabolites in yeast, do not participate in the central metabolic processes and their physiological roles remains to be elucidated. Secondary metabolite biosynthesis pathway always includes multiple enzymes encoded by secondary metabolism gene clusters, which are controlled by complex regulatory networking (75,76). By changing Eeb1's N- and C-terminal amino acid sequences, it improves $Eeb1^{Mut}$ expression level and function (Figure 5.8). It might because the protein trafficking pathway is changed and $Eeb1^{Mut}$ expression level and stability are improved by escaping from the regulatory networks. It provides another possible strategy to improve secondary metabolites production by changing the biocatalyst trafficking pathway and escaping from regulations.

5.6 References

1. Krahmer, N., Farese, R. V., Jr., and Walther, T. C. (2013) Balancing the fat: lipid droplets and human disease. *EMBO Mol Med* **5**, 973-983

2. Christiansen, K., and Jensen, P. K. (1972) Membrane-Bound Lipid Particles from Beef Heart - Chemical Composition and Structure. *Biochimica Et Biophysica Acta* **260**, 449-+

3. Clausen, M. K., Christiansen, K., Jensen, P. K., and Behnke, O. (1974) Isolation of Lipid Particles from Bakers-Yeast. *Febs Letters* **43**, 176-179

4. Gemmrich, A. R. (1981) Ultrastructural and Enzymatic Studies on the Development of Microbodies in Germinating Spores of the Fern Anemia-Phyllitidis. *Z Pflanzenphysiol* **102**, 69-80

5. Alvarez, H. M., and Steinbuchel, A. (2002) Triacylglycerols in prokaryotic microorganisms. *Appl Microbiol Biotechnol* **60**, 367-376

6. Grillitsch, K., Connerth, M., Kofeler, H., Arrey, T. N., Rietschel, B., Wagner, B., Karas, M., and Daum, G. (2011) Lipid particles/droplets of the yeast Saccharomyces cerevisiae revisited: lipidome meets proteome. *Biochim Biophys Acta* **1811**, 1165-1176

7. Athenstaedt, K., Zweytick, D., Jandrositz, A., Kohlwein, S. D., and Daum, G. (1999) Identification and characterization of major lipid particle proteins of the yeast Saccharomyces cerevisiae. *J Bacteriol* **181**, 6441-6448

8. Schmidt, C., Ploier, B., Koch, B., and Daum, G. (2013) Analysis of yeast lipid droplet proteome and lipidome. *Methods Cell Biol* **116**, 15-37

9. Meadows, J. W., Pitzer, B., Brockman, D. E., and Myatt, L. (2004) Adipophilin and signal transduction from lipid droplets in human fetal membranes. *J Soc Gynecol Invest* **11**, 77a-77a

10. Ren, J. H., Lin, C. P. C., Pathak, M. C., Temple, B. R. S., Nile, A. H., Mousley, C. J., Duncan, M. C., Eckert, D. M., Leiker, T. J., Ivanova, P. T., Myers, D. S., Murphy, R. C., Brown, H. A., Verdaasdonk, J., Bloom, K. S., Ortlund, E. A., Neiman, A. M., and Bankaitis, V. A. (2014) A phosphatidylinositol transfer protein integrates phosphoinositide signaling with lipid droplet metabolism to regulate a developmental program of nutrient stress-induced membrane biogenesis. *Molecular Biology of the Cell* **25**, 712-727

11. Cermelli, S., Guo, Y., Gross, S. P., and Welte, M. A. (2006) The lipid-droplet proteome reveals that droplets are a protein-storage depot. *Curr Biol* **16**, 1783-1795

12. Toulmay, A., and Prinz, W. A. (2011) Lipid transfer and signaling at organelle contact sites: the tip of the iceberg. *Curr Opin Cell Biol* **23**, 458-463

13. Farese, R. V., Jr., and Walther, T. C. (2009) Lipid droplets finally get a little R-E-S-P-E-C-T. *Cell* **139**, 855-860

14. Wang, C. W., Miao, Y. H., and Chang, Y. S. (2014) Control of lipid droplet size in budding yeast requires the collaboration between Fld1 and Ldb16. *J Cell Sci* **127**, 1214-1228

15. Guo, Y., Cordes, K. R., Farese, R. V., and Walther, T. C. (2009) Lipid droplets at a glance. *J Cell Sci* **122**, 749-752

16. Walther, T. C., and Farese, R. V. (2012) Lipid Droplets and Cellular Lipid Metabolism. *Annu Rev Biochem* **81**, 687-714

17. Binns, D., Januszewski, T., Chen, Y., Hill, J., Markin, V. S., Zhao, Y. M., Gilpin, C., Chapman, K. D., Anderson, R. G. W., and Goodman, J. M. (2006) An intimate collaboration between peroxisomes and lipid bodies. *J Cell Biol* **173**, 719-731

18. Wang, H., Sreenevasan, U., Hu, H., Saladino, A., Polster, B. M., Lund, L. M., Gong, D. W., Stanley, W. C., and Sztalryd, C. (2011) Perilipin 5, a lipid droplet-associated protein, provides physical and metabolic linkage to mitochondria. *Journal of Lipid Research* **52**, 2159-2168

19. Liu, P., Bartz, R., Zehmer, J. K., Ying, Y. S., Zhu, M., Serrero, G., and Anderson, R. G. (2007) Rab-regulated interaction of early endosomes with lipid droplets. *Biochim Biophys Acta* **1773**, 784-793

20. Jacquier, N., Choudhary, V., Mari, M., Toulmay, A., Reggiori, F., and Schneiter, R. (2011) Lipid droplets are functionally connected to the endoplasmic reticulum in Saccharomyces cerevisiae. *J Cell Sci* **124**, 2424-2437

21. Ploegh, H. L. (2007) A lipid-based model for the creation of an escape hatch from the endoplasmic reticulum. *Nature* **448**, 435-438

22. Walther, T. C., and Farese, R. V., Jr. (2009) The life of lipid droplets. *Biochim Biophys Acta* **1791**, 459-466

23. Salo, V. T., Belevich, I., Li, S., Karhinen, L., Vihinen, H., Vigouroux, C., Magre, J., Thiele, C., Holtta-Vuori, M., Jokitalo, E., and Ikonen, E. (2016) Seipin regulates ER-lipid droplet contacts and cargo delivery. *EMBO J* **35**, 2699-2716

24. Wilfling, F., Wang, H. J., Haas, J. T., Krahmer, N., Gould, T. J., Uchida, A., Cheng, J. X., Graham, M., Christiano, R., Frohlich, F., Liu, X. R., Buhman, K. K., Coleman, R. A., Bewersdorf, J., Farese, R. V., and Walther, T. C. (2013) Triacylglycerol Synthesis Enzymes Mediate Lipid Droplet Growth by Relocalizing from the ER to Lipid Droplets. *Dev Cell* **24**, 384-399

25. Robenek, H., Robenek, M. J., and Troyer, D. (2005) PAT family proteins pervade lipid droplet cores. *Journal of Lipid Research* **46**, 1331-1338

26. Tauchi-Sato, K., Ozeki, S., Houjou, T., Taguchi, R., and Fujimoto, T. (2002) The surface of lipid droplets is a phospholipid monolayer with a unique fatty acid composition. *Journal of Biological Chemistry* **277**, 44507-44512

27. Kory, N., Farese, R. V., Jr., and Walther, T. C. (2016) Targeting Fat: Mechanisms of Protein Localization to Lipid Droplets. *Trends Cell Biol* **26**, 535-546

28. Lin, J. L., and Wheeldon, I. (2014) Dual N- and C-Terminal Helices Are Required for Endoplasmic Reticulum and Lipid Droplet Association of Alcohol Acetyltransferases in Saccharomyces cerevisiae. *Plos One* **9**

29. Fujii, T., Kobayashi, O., Yoshimoto, H., Furukawa, S., and Tamai, Y. (1997) Effect of aeration and unsaturated fatty acids on expression of the Saccharomyces cerevisiae alcohol acetyltransferase gene. *Appl Environ Microbiol* **63**, 910-915

30. Mason, A. B., and Dufour, J. P. (2000) Alcohol acetyltransferases and the significance of ester synthesis in yeast. *Yeast* **16**, 1287-1298

31. Verstrepen, K. J., Van Laere, S. D., Vanderhaegen, B. M., Derdelinckx, G., Dufour, J. P., Pretorius, I. S., Winderickx, J., Thevelein, J. M., and Delvaux, F. R. (2003) Expression levels of the yeast alcohol acetyltransferase genes ATF1, Lg-ATF1, and ATF2 control the formation of a broad range of volatile esters. *Appl Environ Microbiol* **69**, 5228-5237

32. Saerens, S. M., Verstrepen, K. J., Van Laere, S. D., Voet, A. R., Van Dijck, P., Delvaux, F. R., and Thevelein, J. M. (2006) The Saccharomyces cerevisiae EHT1 and EEB1 genes encode novel enzymes with medium-chain fatty acid ethyl ester synthesis and hydrolysis capacity. *J Biol Chem* **281**, 4446-4456

33. Brachmann, C. B., Davies, A., Cost, G. J., Caputo, E., Li, J., Hieter, P., and Boeke, J. D. (1998) Designer deletion strains derived from Saccharomyces cerevisiae S288C: a useful set of strains and plasmids for PCR-mediated gene disruption and other applications. *Yeast* **14**, 115-132

34. Gietz, R. D., and Woods, R. A. (2002) Transformation of yeast by lithium acetate/single-stranded carrier DNA/polyethylene glycol method. *Guide to Yeast Genetics and Molecular and Cell Biology, Pt B* **350**, 87-96

35. Giaever, G., Chu, A. M., Ni, L., Connelly, C., Riles, L., Veronneau, S., Dow, S., Lucau-Danila, A., Anderson, K., Andre, B., Arkin, A. P., Astromoff, A., El-Bakkoury, M., Bangham, R., Benito, R., Brachat, S., Campanaro, S., Curtiss, M., Davis, K., Deutschbauer, A., Entian, K. D., Flaherty, P., Foury, F., Garfinkel, D. J., Gerstein, M., Gotte, D., Guldener, U., Hegemann, J. H., Hempel, S., Herman, Z., Jaramillo, D. F., Kelly, D. E., Kelly, S. L., Kotter, P., LaBonte, D., Lamb, D. C., Lan, N., Liang, H., Liao, H., Liu, L., Luo, C., Lussier, M., Mao, R., Menard, P., Ooi, S. L., Revuelta, J. L., Roberts, C. J., Rose, M., Ross-Macdonald, P., Scherens, B., Schimmack, G., Shafer, B., Shoemaker, D. D., Sookhai-Mahadeo, S., Storms, R. K., Strathern, J. N., Valle, G., Voet, M., Volckaert, G., Wang, C. Y., Ward, T. R., Wilhelmy, J., Winzeler, E. A., Yang, Y., Yen, G., Youngman, E., Yu, K., Bussey, H., Boeke, J. D., Snyder, M., Philippsen, P., Davis, R. W., and Johnston, M. (2002) Functional profiling of the Saccharomyces cerevisiae genome. *Nature* **418**, 387-391

36. Breslow, D. K., Cameron, D. M., Collins, S. R., Schuldiner, M., Stewart-Ornstein, J., Newman, H. W., Braun, S., Madhani, H. D., Krogan, N. J., and Weissman, J. S. (2008) A comprehensive strategy enabling high-resolution functional analysis of the yeast genome. *Nat Methods* **5**, 711-718

37. Cowles, C. R., Odorizzi, G., Payne, G. S., and Emr, S. D. (1997) The AP-3 adaptor complex is essential for cargo-selective transport to the yeast vacuole. *Cell* **91**, 109-118

38. Koffel, R., Tiwari, R., Falquet, L., and Schneiter, R. (2005) The Saccharomyces cerevisiae YLL012/YEH1, YLR020/YEH2, and TGL1 genes encode a novel family of membrane-anchored lipases that are required for steryl ester hydrolysis. *Mol Cell Biol* **25**, 1655-1668

39. Untergasser, A., Cutcutache, I., Koressaar, T., Ye, J., Faircloth, B. C., Remm, M., and Rozen, S. G. (2012) Primer3-new capabilities and interfaces. *Nucleic Acids Res* **40**

40. Pfaffl, M. W. (2001) A new mathematical model for relative quantification in real-time RT-PCR. *Nucleic Acids Res* **29**

41. Janda, C. Y., Li, J., Oubridge, C., Hernandez, H., Robinson, C. V., and Nagai, K. (2010) Recognition of a signal peptide by the signal recognition particle. *Nature* **465**, 507-510

42. Maiorella, B., Blanch, H. W., and Wilke, C. R. (1983) By-Product Inhibition Effects on Ethanolic Fermentation by Saccharomyces-Cerevisiae. *Biotechnology and Bioengineering* **25**, 103-121

43. Viegas, C. A., Rosa, M. F., Sacorreia, I., and Novais, J. M. (1989) Inhibition of Yeast Growth by Octanoic and Decanoic Acids Produced during Ethanolic Fermentation. *Appl Environ Microb* **55**, 21-28

44. Knight, M. J., Bull, I. D., and Curnow, P. (2014) The yeast enzyme Ehtl is an octanoyl-CoA:ethanol acyltransferase that also functions as a thioesterase. *Yeast* **31**, 463-474

45. Lin, J. L., Zhu, J., and Wheeldon, I. (2016) Rapid ester biosynthesis screening reveals a high activity alcohol-O-acyltransferase (AATase) from tomato fruit. *Biotechnol J* **11**, 700-707

46. Saerens, S. M. G., Verstrepen, K. J., Van Laere, S. D. M., Voet, A. R. D., Van Dijck, P., Delvaux, F. R., and Thevelein, J. M. (2006) The Saccharomyces cerevisiae EHT1 and EEB1 genes encode novel enzymes with medium-chain fatty acid ethyl ester synthesis and hydrolysis capacity. *Journal of Biological Chemistry* **281**, 4446-4456

47. Nordstrom, K. (1966) Formation of esters from acids by Brewer's yeast: formation from unsaturated acids. *Nature* **210**, 99-100

48. Welte, M. A. (2007) Proteins under new management: lipid droplets deliver. *Trends in Cell Biology* **17**, 363-369

49. Gunjan, A., Paik, J., and Verreault, A. (2006) The emergence of regulated histone proteolysis. *Curr Opin Genet Dev* **16**, 112-118

50. Jakel, S., Mingot, J. M., Schwarzmaier, P., Hartmann, E., and Gorlich, D. (2002) Importins fulfil a dual function as nuclear import receptors and cytoplasmic chaperones for exposed basic domains. *Embo Journal* **21**, 377-386

51. Young, B. P., Craven, R. A., Reid, P. J., Willer, M., and Stirling, C. J. (2001) Sec63p and Kar2p are required for the translocation of SRP-dependent precursors into the yeast endoplasmic reticulum in vivo. *Embo Journal* **20**, 262-271

52. Walter, P., and Johnson, A. E. (1994) Signal Sequence Recognition and Protein Targeting to the Endoplasmic-Reticulum Membrane. *Annu Rev Cell Biol* **10**, 87-119

53. Ng, D. T. W., Brown, J. D., and Walter, P. (1996) Signal sequences specify the targeting route to the endoplasmic reticulum membrane. *J Cell Biol* **134**, 269-278

54. Aviram, N., Ast, T., Costa, E. A., Arakel, E. C., Chuartzman, S. G., Jan, C. H., Hassdenteufel, S., Dudek, J., Jung, M., Schorr, S., Zimmermann, R., Schwappach, B., Weissman, J. S., and Schuldiner, M. (2016) The SND proteins constitute an alternative targeting route to the endoplasmic reticulum. *Nature* **540**, 134-138

55. Jonikas, M. C., Collins, S. R., Denic, V., Oh, E., Quan, E. M., Schmid, V., Weibezahn, J., Schwappach, B., Walter, P., Weissman, J. S., and Schuldiner, M. (2009) Comprehensive Characterization of Genes Required for Protein Folding in the Endoplasmic Reticulum. *Science* **323**, 1693-1697

56. Schuldiner, M., Metz, J., Schmid, V., Denic, V., Rakwalska, M., Schmitt, H. D., Schwappach, B., and Weissman, J. S. (2008) The GET complex mediates insertion of tail-anchored proteins into the ER membrane. *Cell* **134**, 634-645

57. Spiller, M. P., and Stirling, C. J. (2011) Preferential Targeting of a Signal Recognition Particle-dependent Precursor to the Ssh1p Translocon in Yeast. *Journal of Biological Chemistry* **286**, 21953-21960

58. Jacquier, N., Choudhary, V., Mari, M., Toulmay, A., Reggiori, F., and Schneiter, R. (2011) Lipid droplets are functionally connected to the endoplasmic reticulum in Saccharomyces cerevisiae. *J Cell Sci* **124**, 2424-2437

59. Ozeki, S., Cheng, J. L., Tauchi-Sato, K., Hatano, N., Taniguchi, H., and Fujimoto, T. (2005) Rab18 localizes to lipid droplets and induces their close apposition to the endoplasmic reticulum-derived membrane. *J Cell Sci* **118**, 2601-2611

60. Zhang, S. Y., Wang, Y., Cui, L. J., Deng, Y. Q., Xu, S. M., Yu, J. H., Cichello, S., Serrero, G., Ying, Y. S., and Liu, P. S. (2016) Morphologically and Functionally Distinct Lipid Droplet Subpopulations. *Sci Rep-Uk* **6**

61. Choudhary, V., Ojha, N., Golden, A., and Prinz, W. A. (2015) A conserved family of proteins facilitates nascent lipid droplet budding from the ER. *J Cell Biol* **211**, 261-271

62. Leber, R., Landl, K., Zinser, E., Ahorn, H., Spok, A., Kohlwein, S. D., Turnowsky, F., and Daum, G. (1998) Dual localization of squalene epoxidase, Erg1p, in yeast reflects a relationship between the endoplasmic reticulum and lipid particles. *Molecular Biology of the Cell* **9**, 375-386

63. Li, M., Murphy, D. J., Lee, K. H. K., Wilson, R., Smith, L. J., Clark, D. C., and Sung, J. Y. (2002) Purification and structural characterization of the central hydrophobic domain of oleosin. *Journal of Biological Chemistry* **277**, 37888-37895

64. Naested, H., Frandsen, G. I., Jauh, G. Y., Hernandez-Pinzon, I., Nielsen, H. B., Murphy, D. J., Rogers, J. C., and Mundy, J. (2000) Caleosins: Ca2+-binding proteins associated with lipid bodies. *Plant Mol Biol* **44**, 463-476

65. Ostermeyer, A. G., Ramcharan, L. T., Zeng, Y. C., Lunlin, D. M., and Brown, D. A. (2004) Role of the hydrophobic domain in targeting caveolin-1 to lipid droplets. *J Cell Biol* **164**, 69-78

66. Rowe, E. R., Mimmack, M. L., Barbosa, A. D., Haider, A., Isaac, I., Ouberai, M. M., Thiam, A. R., Patel, S., Saudek, V., Siniossoglou, S., and Savage, D. B. (2016) Conserved Amphipathic Helices Mediate Lipid Droplet Targeting of Perilipins 1-3. *Journal of Biological Chemistry* **291**, 6664-6678

67. Garcia, A., Sekowski, A., Subramanian, V., and Brasaemle, D. L. (2003) The central domain is required to target and anchor perilipin A to lipid droplets. *Journal of Biological Chemistry* **278**, 625-635

68. Tanaka, T., Kuroda, K., Ikeda, M., Wakita, T., Kato, N., and Makishima, M. (2013) Hepatitis C virus NS4B targets lipid droplets through hydrophobic residues in the amphipathic helices. *Journal of Lipid Research* **54**, 881-892

69. Boulant, S., Montserret, R., Hope, R. G., Ratinier, M., Targett-Adams, P., Lavergne, J. P., Penin, F., and McLauchlan, J. (2006) Structural determinants that target the hepatitis C virus core protein to lipid droplets. *Journal of Biological Chemistry* **281**, 22236-22247

70. Tiwari, R., Koffel, R., and Schneiter, R. (2007) An acetylation/deacetylation cycle controls the export of sterols and steroids from S. cerevisiae. *EMBO J* **26**, 5109-5119

71. Guo, Y., Walther, T. C., Rao, M., Stuurman, N., Goshima, G., Terayama, K., Wong, J. S., Vale, R. D., Walter, P., and Farese, R. V. (2008) Functional genomic screen reveals genes involved in lipid-droplet formation and utilization. *Nature* **453**, 657-661

72. Blazeck, J., and Alper, H. S. (2013) Promoter engineering: recent advances in controlling transcription at the most fundamental level. *Biotechnol J* **8**, 46-58

73. Alper, H., Fischer, C., Nevoigt, E., and Stephanopoulos, G. (2005) Tuning genetic control through promoter engineering. *P Natl Acad Sci USA* **102**, 12678-12683

74. Siddiqui, M. S., Thodey, K., Trenchard, I., and Smolke, C. D. (2012) Advancing secondary metabolite biosynthesis in yeast with synthetic biology tools. *Fems Yeast Res* **12**, 144-170

75. Keller, N. P., Turner, G., and Bennett, J. W. (2005) Fungal secondary metabolism - from biochemistry to genomics. *Nat Rev Microbiol* **3**, 937-947

76. Brakhage, A. A. (2013) Regulation of fungal secondary metabolism. *Nat Rev Microbiol* **11**, 21-32

5.7 Figures

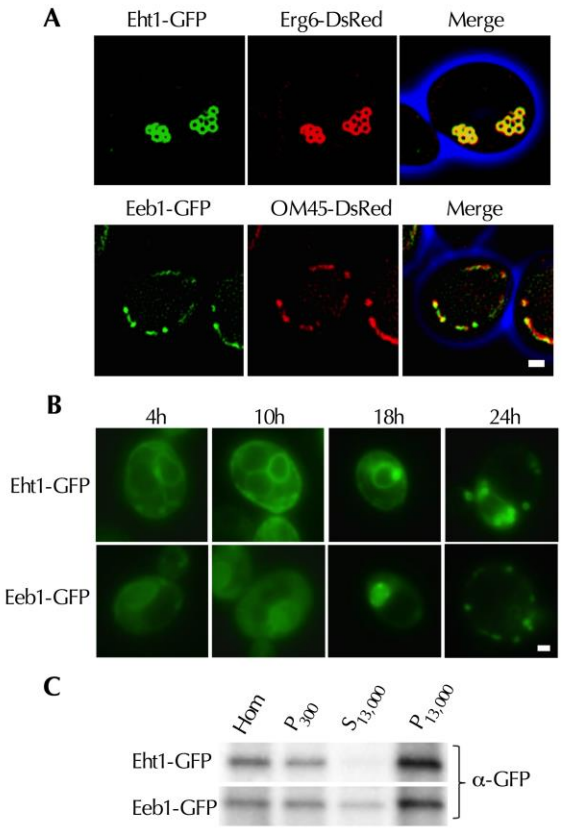

Figure 5.1. Eht1 and Eeb1 are membrane-associated proteins. (A) Fluorescent microscopy images of selected stationary phase cells cultured in glucose media co-expressing Eht1-GFP or Eeb1-GFP and LD marker Erg6-DsRed or mitochondria marker OM45-DsRed. Eht1-GFP and Eeb1-GFP signal is shown in green and Erg6-DsRed and OM45-DsRed is shown in red. The merged image shows the phase contrast image false colored in blue. Co-localization of green and red is indicated by yellow and demonstrates Eht1-GFP localization to LDs and Eeb1-GFP localization to mitochondria. (B) Time course study of intracellular localization of Eht1 and Eeb1. Cells were first grown to stationary phase followed by dilution in fresh media. Cells were harvested and analyzed at different time points (t=4, 10, 18, and 24 hrs). (C) Western blot analysis of subcellular fractions. Homogenates (Hom) from cells expressing the GFP-tagged were fractionated by differential centrifugation to yield 300 × *g* (P_{300}), 13,000 × *g* ($P_{13,000}$) membrane pellets and cytosolic supernatants ($S_{13,000}$). Ten-microgram samples of proteins from each fraction were separated by electrophoresis, blotted, and probed with anti-GFP antibody.

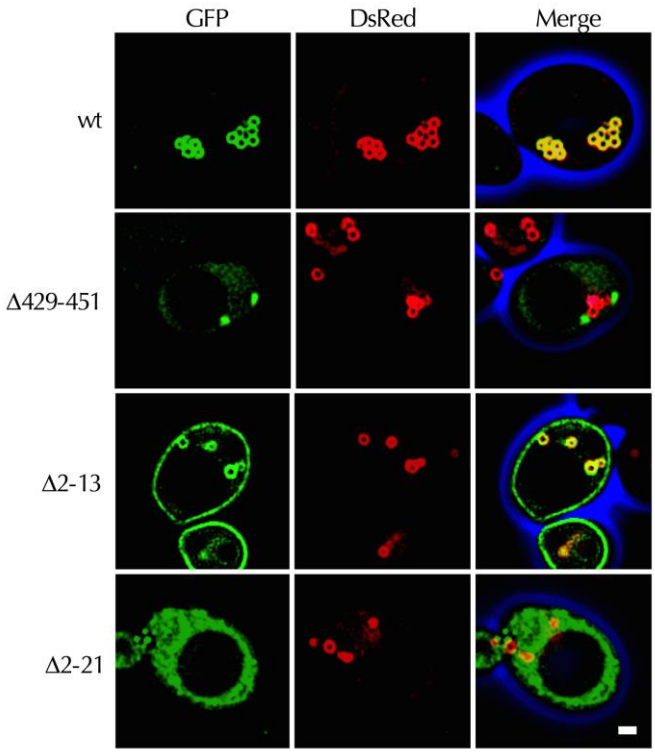

Figure 5.2. Fluorescent microscopy images of stationary phase cells overexpressing Eht1-GFP and truncations with co-expression of the LD marker Erg6-DsRed. GFP signal is shown in green and Erg6-DsRed is shown in red. The merged image shows the phase contrast image false colored in blue. Truncation from N- or C-terminus eliminates LD localization. Scale bar, 1 μm.

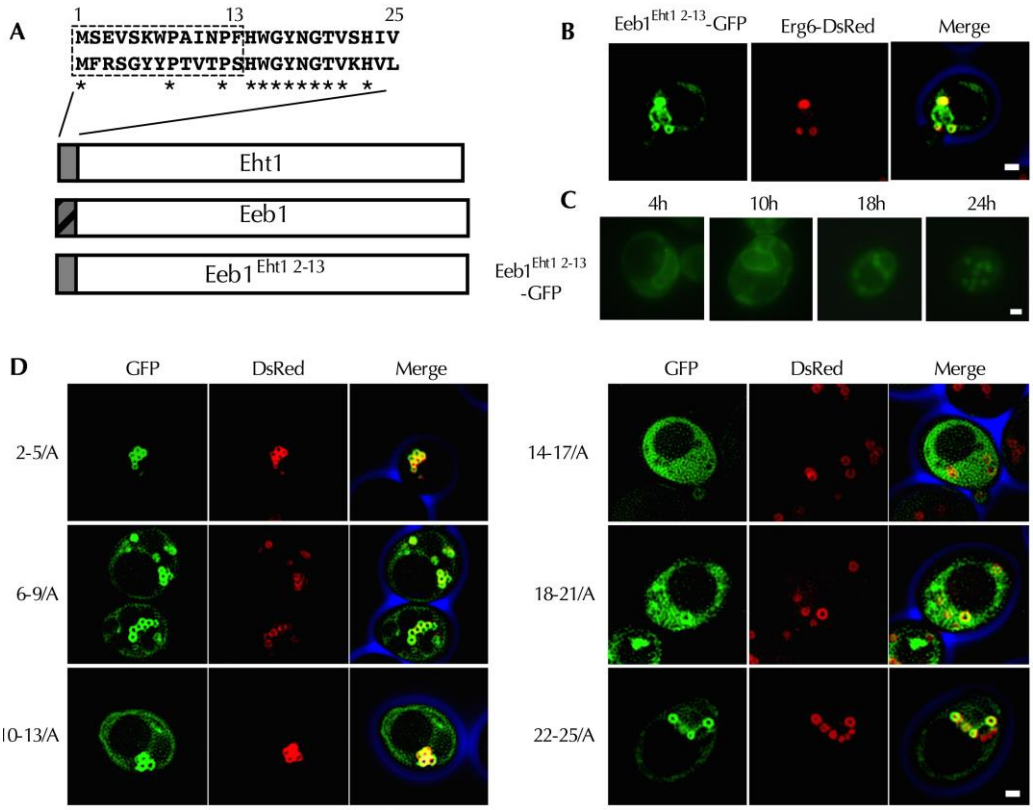

Figure 5.3. N-terminus of Eht1 plays a major role in targeting to LDs. (A) Amino acid sequence alignment of the N-terminus of Eht1 and Eeb1. Numbers above show the amino acid site and the stars below indicate the sequence identity. A mutant of Eeb1 named as Eeb1$^{Eht1\ 2\text{-}13}$ is generated by replacement of N-terminal 2-13 amino acids of Eeb1 with that of Eht1. The residues are indicated by dashed line box. (B) Fluorescent microscopy images of stationary phase cells overexpressing Eeb1$^{Eht1\ 2\text{-}13}$-GFP (shown as green) and co-expressing LD marker Erg6-DsRed (shown as red). The merged image shows the phase contrast image false colored in blue. Eeb1$^{Eht1\ 2\text{-}13}$-GFP is co-localized with Erg6, suggesting that it is targeted to LDs. Scale bar, 1 μm. (C) Time course study of intracellular localization of Eeb1$^{Eht1\ 2\text{-}13}$. Cells were first grown to stationary phase followed by dilution in fresh media. Cells were harvested and analyzed at different time points (t=4, 10, 18, and 24 hrs). Eeb1$^{Eht1\ 2\text{-}13}$ is initially localized to ER and subsequently sorted to LDs. Scale bar, 1 μm. (D) Fluorescent microscopy images of stationary phase cells overexpressing tetra-alanine scanning mutants-GFP (shown as green) and co-expressing LD marker Erg6-DsRed (shown as red). The merged image shows the phase contrast image false colored in blue. Scale bar, 1 μm.

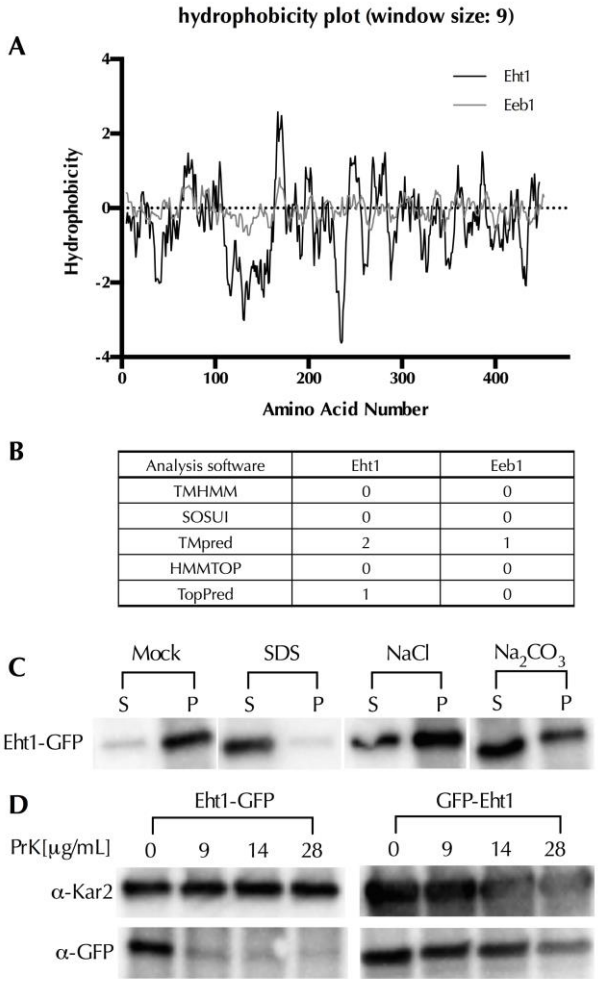

Analysis software	Eht1	Eeb1
TMHMM	0	0
SOSUI	0	0
TMpred	2	1
HMMTOP	0	0
TopPred	1	0

Figure 5.4. Hydropathy plot and membrane topology of Eht1. (A) Hydrophobicity plot and Eht1 and Eeb1. A hydrophobicity plot of Eht1 and Eeb1 was generated by the method of Kyte and Doolittle using a window of 9 amino acids. (B) Predicted transmembrane domains (TMD) for Eht1 and Eeb1. (C) Eht1 is a peripheral membrane protein. Early log phase cells overexpressing Eht1-GFP was grown in SD-U medium, cells were broken with Dounce homogenizer, and membranes were pelleted by centrifugation at 13,000 × *g*. 50 μg of protein from the membrane pellet was incubated for 30 min at 4°C with 1 M NaCl, 0.1 M Na_2CO_3, 1% SDS, or buffer alone (Mock) and then centrifuged at 13,000 × *g* for 30 min to yield soluble (S) and pellet (P) fractions. Proteins were precipitated by TCA, and 10 μg was separated by electrophoresis and probed for the presence of GFP epitope with and anti-GFP antibody. (D) Protease sensitivity of the N- or C-terminal GFP on Eht1. 50 μg of proteins from the 13,000 × *g* membrane pellet was incubated with the indicated proteinase K (PrK) concentrations for 30 min on ice. Proteins were precipitated by TCA, and 10 μg was separated by electrophoresis and probed for the presence of the GFP epitope or for Kar2, respectively.

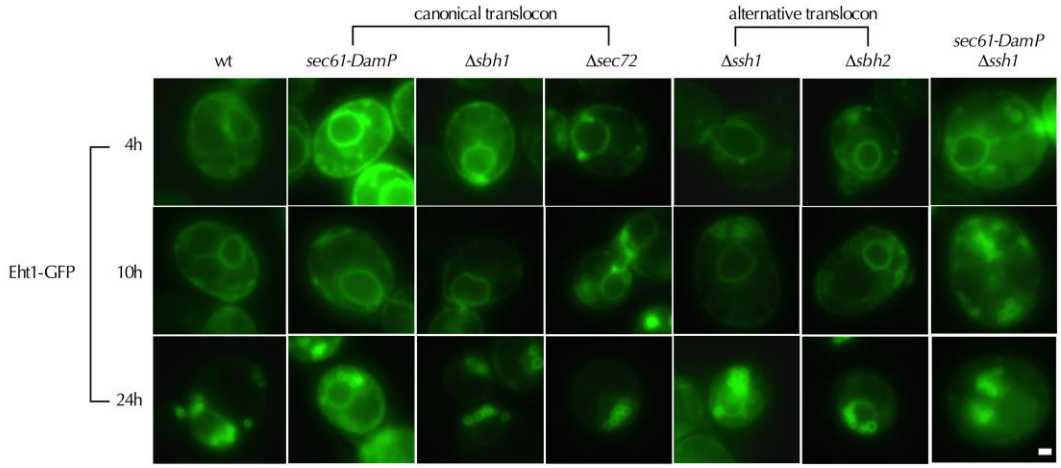

Figure 5.5. Eht1 targeting to ER is related to translocons on ER. C-terminal fluorescently tagged GFP protein Eht1 was imaged with knockdown of essential gene *SEC61* (encoding for canonical translocon) or knockout of nonessential gene *SBH1* and *SEC72* (encoding for canonical translocon) and *SBH2* (encoding for alternative translocon), at different time points, 4, 10 and 24 hrs. Scale bar, 1 μm.

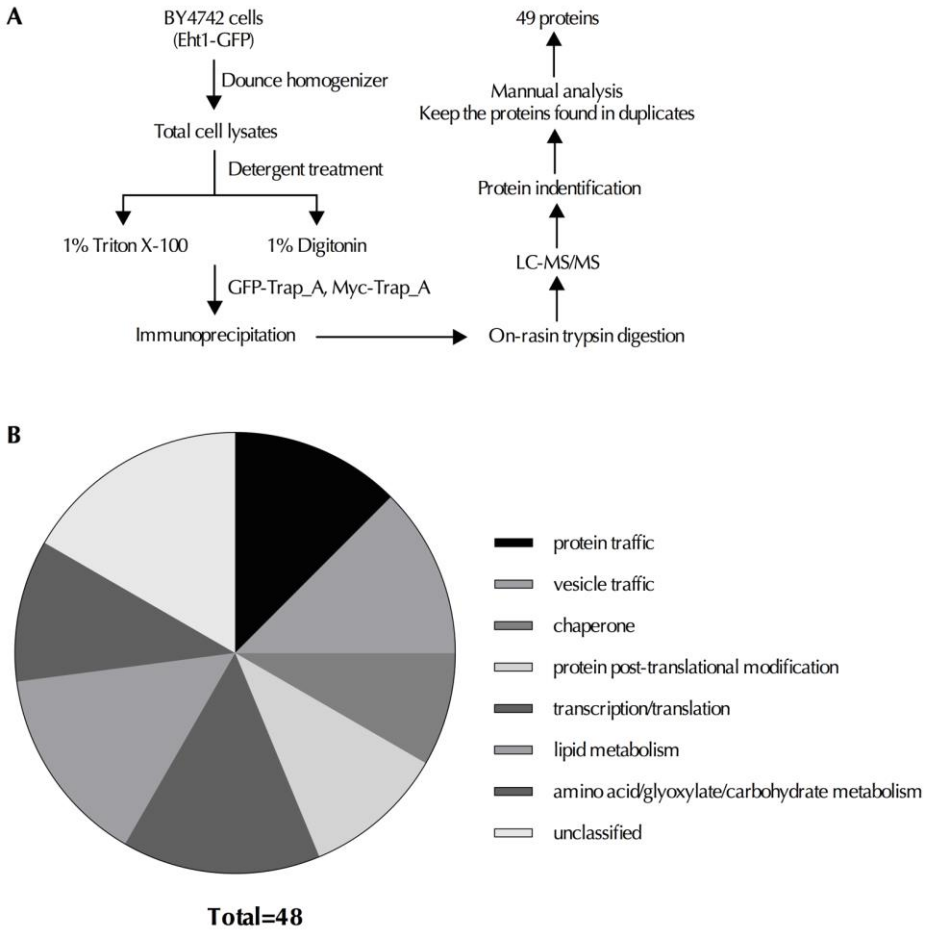

Figure 5.6. Identification of proteins interacting with Eht1 on ER. (A) Flow diagram for analyzing the protein-protein interactions of Eht1-GFP by immunoprecipitation and mass spectrometry. (B) The 49 proteins interacting with Eht1-GFP on ER were classified into 6 main groups according to the Saccharomyces Genome Database SGB (http://www.yeastgenome.org/).

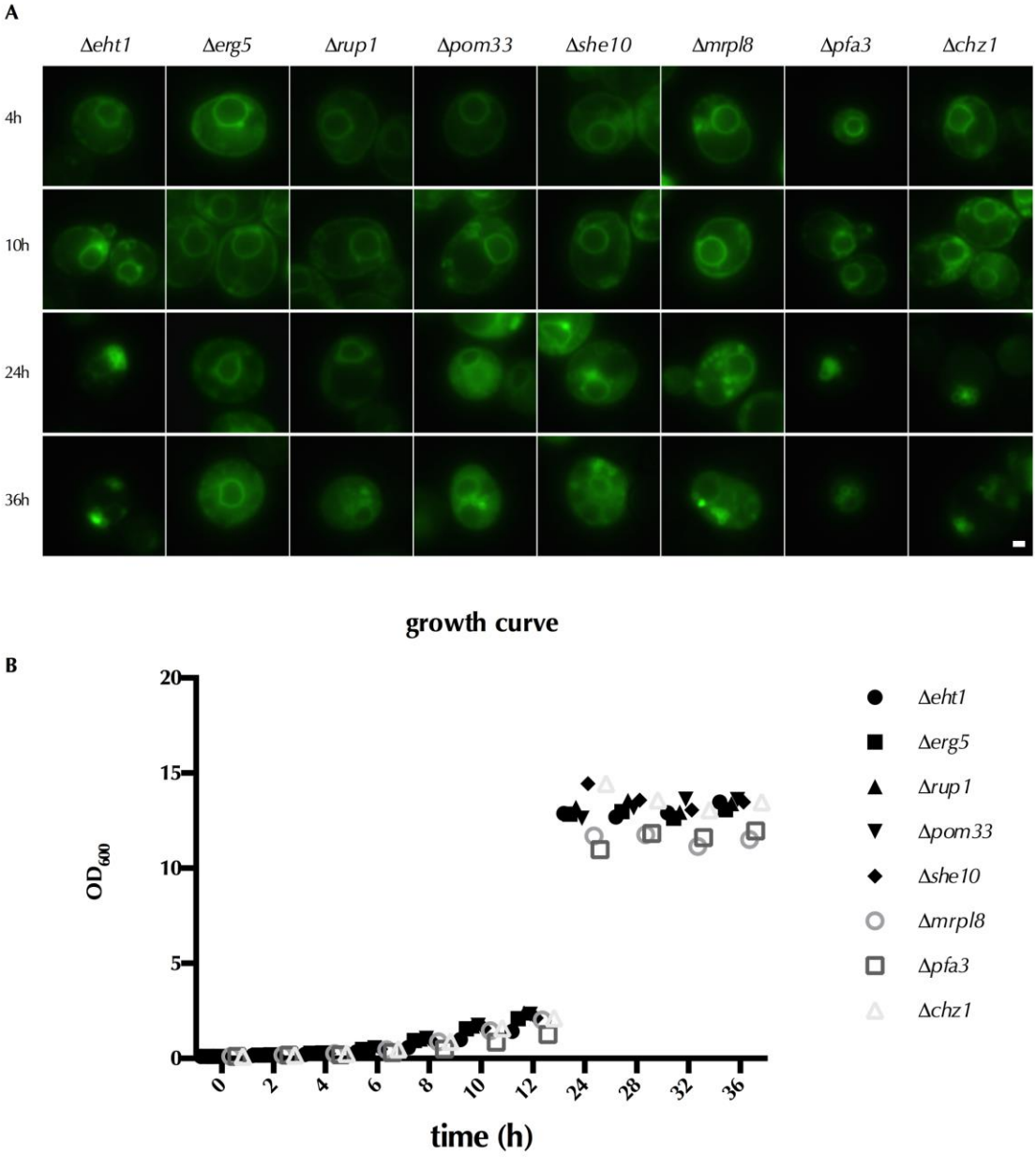

Figure 5.7. Effect of gene deletion on the localization and trafficking of Eht1. (A) Fluorescent images of Eht1-GFP on the background of gene knockouts at different time points (4h, 10h, 24h and 36h). Scale bar, 1 μm. (B) Growth curve of gene knockout strains harboring plasmids to overexpress Eht1-GFP.

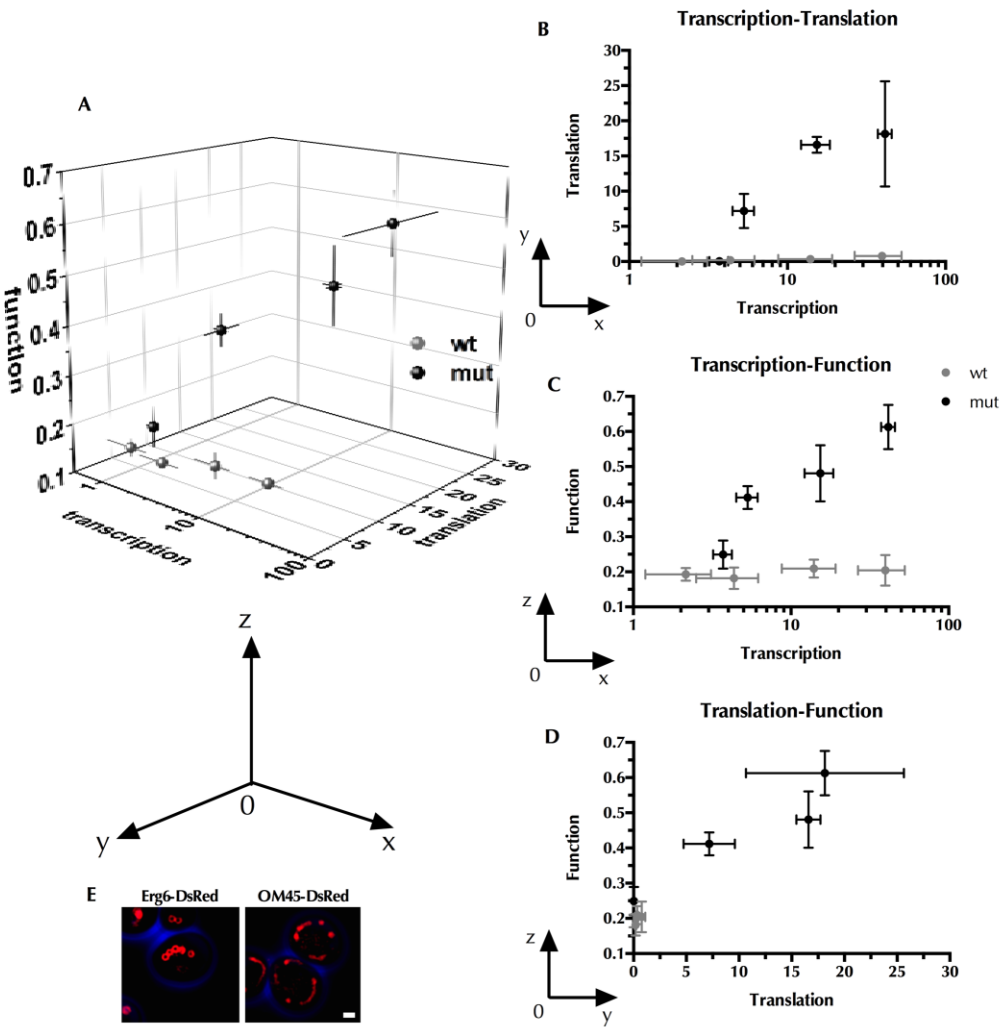

Figure 5.8. Eeb1^{wt} and Eeb1^{mut} transcription, translation and function relationship. (A) 3D plot of transcription (x axis), translation (y axis) and function (z axis) of Eeb1^{wt} and Eeb1^{mut}. (B), (C) and (D) showed 2D plot of transcription, translation and function relationship, respectively. (E) Fluorescent images of LD and mitochondira morphology. Erg6 (LD marker protein) and OM45 (mitochondria marker protein) are fused with DsRed, shown as red color. Blue color showed the phase contrast of cells. Scale bar, 1 μm.

5.8 Supporting Information

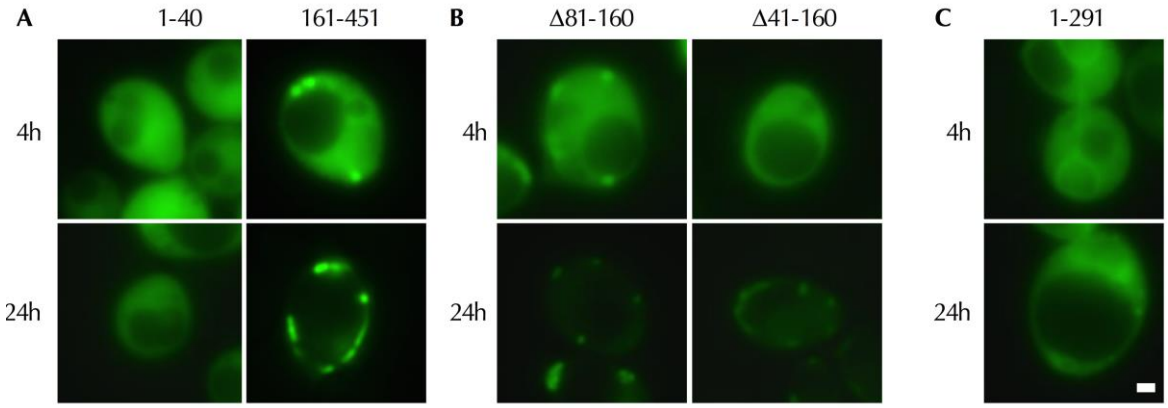

Figure S5.1. Fluorescent microscopy images of Eht1 truncations intracellular localization. (A) Eht1 N- or C-terminal sequence, 1-40 amino acids and 161-451 amino acids; (B) Eht1 internal truncations, from 80-160 amino acids and 40-160 amino acids; (C) Eht1 N terminal sequence, from 1-291 amino acid, are fused with C terminal GFP to indicate their intracellular localization at time points (4h and 24h). Cells were first grown to stationary phase followed by dilution in fresh media. Scale bar, 1 μm.

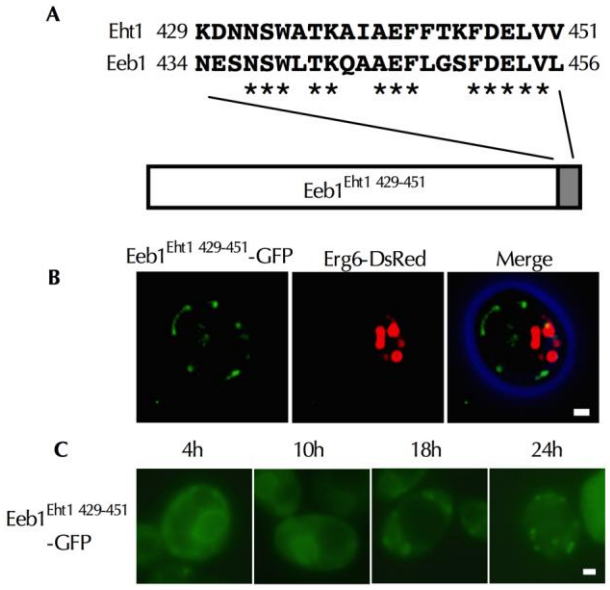

Figure S5.2. Intracellular localization and trafficking of Eeb1$^{Eht1\,429-451}$-GFP. (A) Amino acid sequence alignment of the C-terminus of Eht1 and Eeb1. Numbers show the amino acid site and the stars below indicate the sequence identity. A mutant of Eeb1 named as Eeb1$^{Eht1\,429-451}$ is generated by replacement of C-terminal 434-456 amino acids of Eeb1 with C-terminal 429-451 amino acids of Eht1. (B) Fluorescent microscopy images of stationary phase cells overexpressing Eeb1$^{Eht1\,429-451}$ -GFP (shown as green) and co-expressing LD marker Erg6-DsRed (shown as red). The merged image shows the phase contrast image false colored in blue. Eeb1$^{Eht1\,429-451}$ -GFP is not co-localized with Erg6, suggesting that it is not targeted to LDs. Scale bar, 1 μm. (C) Time course study of intracellular localization of Eeb1$^{Eht1\,429-451}$. Cells were first grown to stationary phase followed by dilution in fresh media. Cells were harvested and analyzed at different time points (t=4, 10, 18, and 24 hrs). Eeb1$^{Eht1\,429-451}$ is initially localized to ER and possibly is targeted to mitochondira. Scale bar, 1 μm.

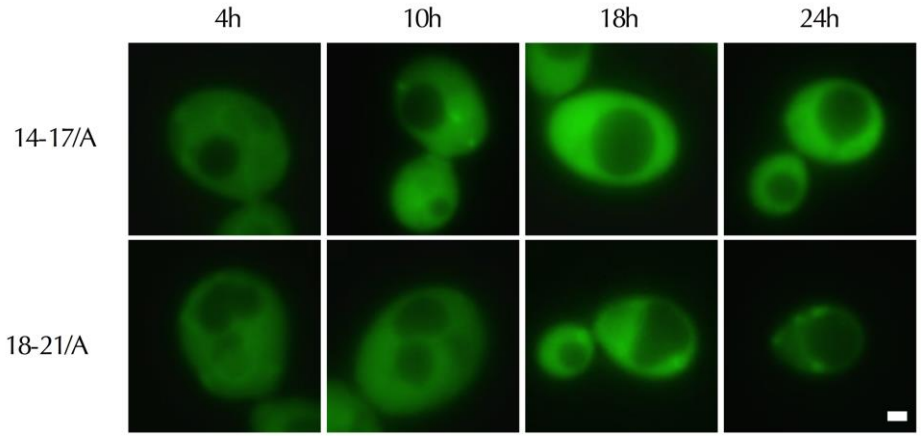

Figure S5.3. Time course study of intracellular localization of Eht1 14-17/A and 18-21/A. Cells were first grown to stationary phase followed by dilution in fresh media. Cells were harvested and analyzed at different time points (t=4, 10, 18, and 24 hrs). The ER and LD association is lost for both Eht1 14-17/A and 18-21/A. Scale bar, 1 μm.

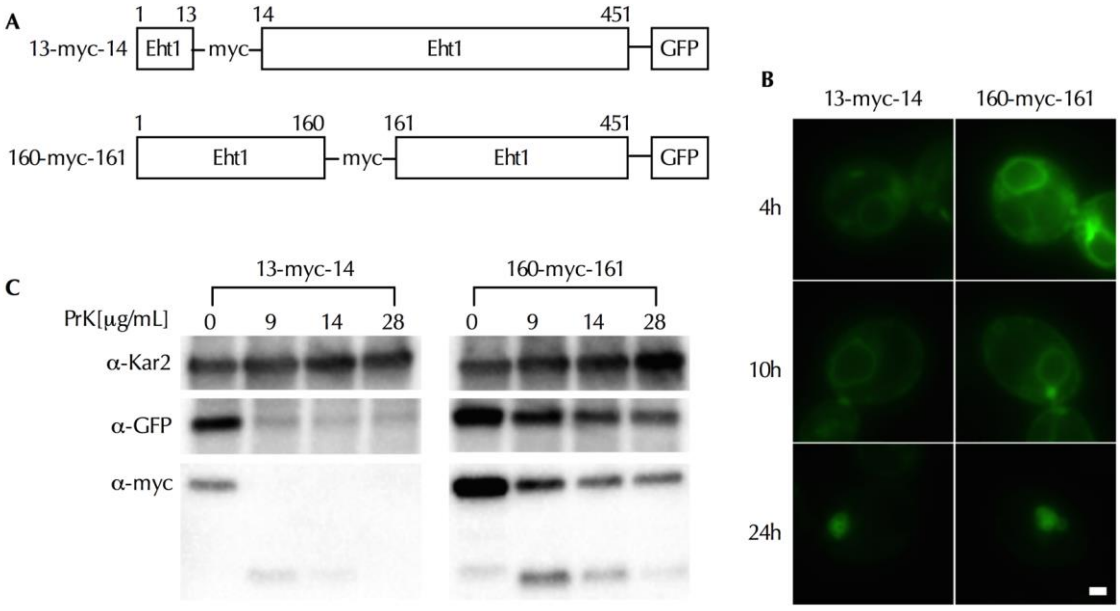

Figure S5.4. Intracellular trafficking and membrane topology assay of Eht1 13-myc-14 and 160-myc-161. (A) A myc tag is added between Eht1 13 and 14 amino acids or Eht1 160-161 amino acids, and a GFP tag is fused on C terminus. (B) Time course study of intracellular localization of Eht1 13-myc-14 and 160-myc-161. Cells were first grown to stationary phase followed by dilution in fresh media. Cells were harvested and analyzed at different time points (t=4, 10, 18, and 24 hrs). Both 13-myc-14 and 160-myc-161 remain the ER and LD association, similar to Eht1 wild type, suggesting that their structure is disrupted. Scale bar, 1 μm. (C) Protease sensitivity of the epitopes on Eht1 13-myc-14 and 160-myc-161. 50 μg of proteins from the 13,000 × *g* membrane pellet was incubated with the indicated proteinase K (PrK) concentrations for 30 min on ice. Proteins were precipitated by TCA, and 10 μg was separated by electrophoresis and probed for the presence of the myc and GFP epitope or for Kar2, respectively.

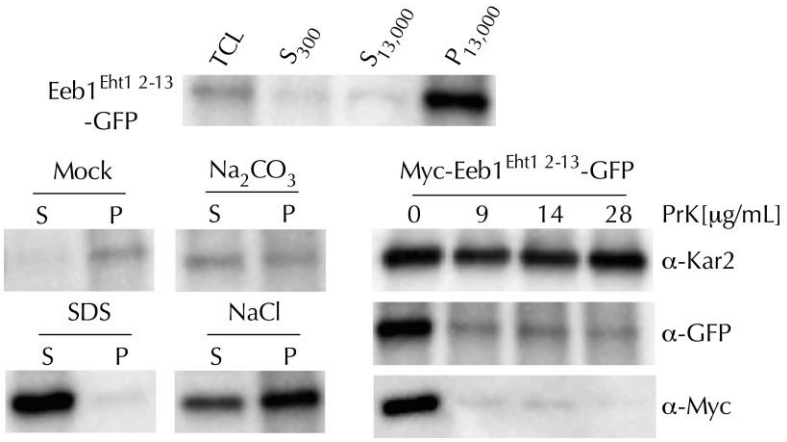

Figure S5.5. Membrane association and topology assay of Eeb1 $^{Eht1\ 2-13}$. Eeb1 $^{Eht1\ 2-13}$ is a peripheral membrane protein. Early log phase cells overexpressing Eeb1 $^{Eht1\ 2-13}$-GFP was grown in SD-U medium, cells were broken with Dounce homogenizer, and membranes were pelleted by centrifugation at 13,000 × *g*. 50 μg of protein from the membrane pellet was incubated for 30 min at 4°C with 1 M NaCl, 0.1 M Na_2CO_3, 1% SDS, or buffer alone (Mock) and then centrifuged at 13,000 × *g* for 30 min to yield soluble (S) and pellet (P) fractions. Proteins were precipitated by TCA, and 10 μg was separated by electrophoresis and probed for the presence of GFP epitope with and anti-GFP antibody. Protease sensitivity of the N-myc or C-terminal GFP epitopes on Eeb1 $^{Eht1\ 2-13}$ was performed. 50 μg of proteins from the 13,000 × *g* membrane pellet was incubated with the indicated proteinase K (PrK) concentrations for 30 min on ice. Proteins were precipitated by TCA, and 10 μg was separated by electrophoresis and probed for the presence of the myc and GFP epitope or for Kar2, respectively.

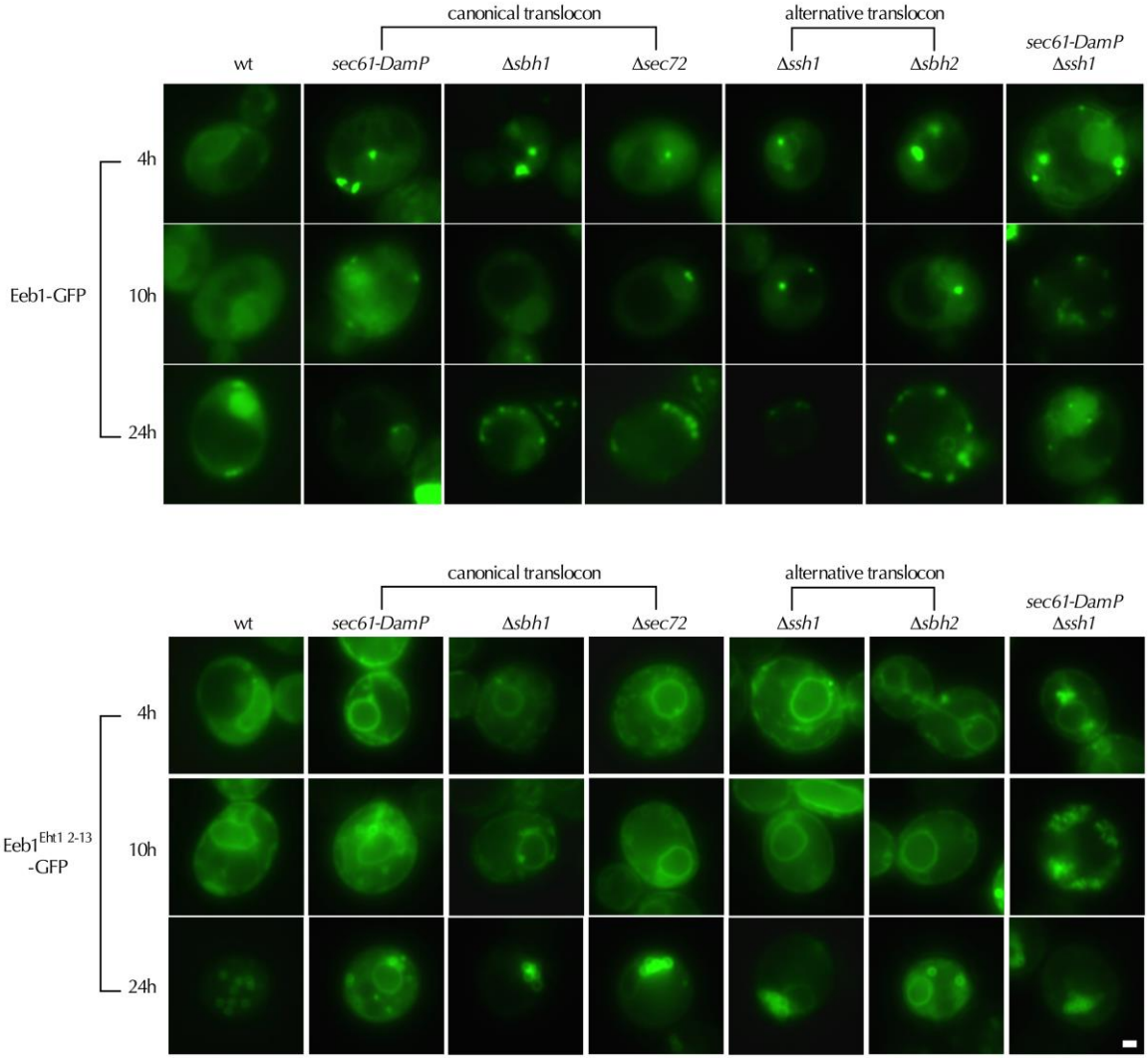

Figure S5.6. Eeb1$^{\text{Eht1 2-13}}$ targeting to ER is related to translocons on ER. C-terminal fluorescently tagged GFP proteins Eeb1 and Eeb1$^{\text{Eht1 2-13}}$ were imaged with knockdown of essential gene *SEC61* (encoding for canonical translocon) or knockout of nonessential gene *SBH1* and *SEC72* (encoding for canonical translocon) and *SBH2* (encoding for alternative translocon), at different time points, 4, 10 and 24 hrs. Scale bar, 1 μm.

Table S5.1. Strains used in this study.

Strains	Genotype	Source
E. coli		
DH5α	*F– Φ80lacZΔM15 Δ(lacZYA-argF) U169 recA1 endA1 hsdR17 (rK–, mK+) phoA supE44 λ– thi-1 gyrA96 relA1*	Life technologies
S. cerevisiae		
BY4742	*MATα his3Δ1 leu2Δ0 lys2Δ0 ura3Δ0*	GE healthcare
YS218	*MATα his3Δ1 leu2Δ0 lys2Δ0 ura3Δ0 ERG6::DsRed*	Lin and Wheeldon
YS578	*MATα his3Δ1 leu2Δ0 lys2Δ0 ura3Δ0 OM45::DsRed*	this study
YS702	*MATa his3Δ1 leu2Δ0 lys2Δ0 ura3Δ0 sec61-DAmP::KanR*	GE healthcare
YS732	*MATα his3Δ1 leu2Δ0 lys2Δ0 ura3Δ0 Δssh1-DAmP::KanR*	GE healthcare
YS733	*MATα his3Δ1 leu2Δ0 lys2Δ0 ura3Δ0 Δsbh1-DAmP::KanR*	GE healthcare
YS734	*MATα his3Δ1 leu2Δ0 lys2Δ0 ura3Δ0 Δsbh2-DAmP::KanR*	GE healthcare
YS735	*MATα his3Δ1 leu2Δ0 lys2Δ0 ura3Δ0 Δsec72-DAmP::KanR*	GE healthcare
YS790	*MATa his3Δ1 leu2Δ0 lys2Δ0 ura3Δ0 sec61-DAmP::KanR Δssh1::LEU2*	this study

Table S5.2. Plasmids used in this study.

Plasmid	Description	Source
pEHT1	pRS426-P_{PGK1}-EHT1-GFP-T_{PGK1}	this study
pEHT2	pRS426-P_{PGK1}-EHT1 (13-451AA)-GFP-T_{PGK1}	this study
pEHT3	pRS426-P_{PGK1}-EHT1 (22-451AA)-GFP-T_{PGK1}	this study
pEHT4	pRS426-P_{PGK1}-EHT1 (1-428AA)-GFP-T_{PGK1}	this study
pEHT5	pRS426-P_{PGK1}-EHT1 (2-5AA mutate into alanines)-GFP-T_{PGK1}	this study
pEHT6	pRS426-P_{PGK1}-EHT1 (6-9AA mutate into alanines)-GFP-T_{PGK1}	this study
pEHT7	pRS426-P_{PGK1}-EHT1 (10-13AA mutate into alanines)-GFP-T_{PGK1}	this study
pEHT8	pRS426-P_{PGK1}-EHT1 (14-17AA mutate into alanines)-GFP-T_{PGK1}	this study
pEHT9	pRS426-P_{PGK1}-EHT1 (18-21AA mutate into alanines)-GFP-T_{PGK1}	this study
pEHT10	pRS426-P_{PGK1}-EHT1 (22-25AA mutate into alanines)-GFP-T_{PGK1}	this study
pEHT11	pRS426-P_{PGK1}-GFP-EHT1-T_{PGK1}	this study
pEHT12	pRS426-P_{PGK1}-Eht1 (1-13AA)-myc-Eht1 (14-451AA)-GFP-T_{PGK1}	this study
pEHT13	pRS426-P_{PGK1}-Eht1 (1-160AA)-myc-Eht1 (161-451AA)-GFP-T_{PGK1}	this study
pEHT14	pRS426-P_{PGK1}-Eht1 (1-40AA)-GFP-T_{PGK1}	this study
pEHT15	pRS426-P_{PGK1}-Eht1 (1-80AA)-Eht1 (161-451AA)-GFP-T_{PGK1}	this study
pEHT16	pRS426-P_{PGK1}-Eht1 (1-40AA)-Eht1 (161-451AA)-GFP-T_{PGK1}	this study
pEHT17	pRS426-P_{PGK1}-Eht1 (161-451AA)-GFP-T_{PGK1}	this study
pEHT18	pRS426-P_{PGK1}-Eht1 (1-291AA)-GFP-T_{PGK1}	this study
pEEB1	pRS426-P_{PGK1}-EEB1-GFP-T_{PGK1}	this study
pEEB2	pRS426-P_{PGK1}-EHT1 (1-13AA)-EEB1 (14-456AA)-GFP-T_{PGK1}	this study
pEEB3	pRS426-P_{PGK1}-EEB1 (1-433AA)-EHT1 (429-451AA)-GFP-T_{PGK1}	this study
pEEB4	pRS426-P_{PGK1}-EHT1 (1-13AA)-EEB1 (14-433AA)-EHT1 (429-451AA)-GFP-T_{PGK1}	this study
pEEB5	pRS316-P_{REV1}-EEB1-GFP-T_{PGK1}	this study
pEEB6	pRS316-P_{TPI1}-EEB1-GFP-T_{PGK1}	this study
pEEB7	pRS316-P_{PGK1}-EEB1-GFP-T_{PGK1}	this study
pEEB8	pRS316-P_{TEF1}-EEB1-GFP-T_{PGK1}	this study
pEEB9	pRS316-P_{REV1}-EHT1 (1-13AA)-EEB1 (14-433AA)-EHT1 (429-451AA)-GFP-T_{PGK1}	this study
pEEB10	pRS316-P_{TPI1}-EHT1 (1-13AA)-EEB1 (14-433AA)-EHT1 (429-451AA)-GFP-T_{PGK1}	this study
pEEB11	pRS316-P_{PGK1}-EHT1 (1-13AA)-EEB1 (14-433AA)-EHT1 (429-451AA)-GFP-T_{PGK1}	this study
pEEB12	pRS316-P_{TEF1}-EHT1 (1-13AA)-EEB1 (14-433AA)-EHT1 (429-451AA)-GFP-T_{PGK1}	this study

Table S5.3. Proteins interact with Eht1-GFP on ER identified by immunoprecipitation and mass spectrometry. PTM: post-translational modification.

Gene name	Systematic name	Essential gene	Function	Cellular component
EHT1	YBR177C	-		
SHE10	YGL228W	-	unclassified	ER
RET3	YPL010W	-	vesicle traffic	Golgi; ER
NAS2	YIL007C	-	PTM	cytoplasm, nucleus
ERG28	YER044C	-	lipid metabolism	ER
ERG5	YMR015C	-	lipid metabolism	ER
RUP1	YOR138C	-	PTM	cytoplasm, nucleus
HRD3	YLR207W	-	PTM	ER membrane
OSH6	YKR003W	-	lipid metabolism	cortical ER
LAC1	YKL008C	-	lipid metabolism	ER
CHZ1	YER030W	-	chaperone	nucleus
GOR1	YNL274C	-	glyoxylate metabolism	cytoplasm, nucleus, mitochondrion
MNN9	YPL050C	-	glyoxylate metabolism	ER, cis-Golgi
ARP4	YJL081C	-	transcription	nucleus
ERP4	YOR016C	-	vesicle traffic	ER
AVT3	YKL146W	-	amino acid metabolism	fungal type vacuole membrane
GGC1	YDL198C	-	unclassified	mitochondrial inner memberane
VPS24	YKL041W	-	protein traffic	cytoplasm
ORF unchara cterized	YDR090C	-	transcription/ translation	membrane
MAK5	YBR142W	-	translation	nucleus
LOA1	YPR139C	-	lipid metabolism	ER, lipid droplet
ATP17	YDR377W	-	unclassified	mitochondrion
RIX1	YHR197W	+	transcription	cytosol, nucleus
MOB1	YIL106W	-	PTM	cytoplasm, nucleus
LEO1	YOR123C	-	transcription	nucleus
SHR3	YDL212W	-	chaperone	ER
ENV10	YLR065C	-	protein traffic	ER
IPP1	YBR011C	-	unclassified	cytoplasm,

SDH3	YKL141W	-	protein traffic	nucleus mitochondrial inner memberane
SRP102	YKL154W	-	protein traffic	ER
GPH1	YPR160W	-	carboxylate metabolism	cytoplasm
Sec62	YPL094C	+	protein traffic	ER
IRC24	YIR036C	-	unclassified	cytoplasm
YTM1	YOR272W	-	translation	nucleus
RFT1	YBL020W	+	lipid metabolism	ER
SEC9	YGR009C	-	vesicle traffic	plasma membrane
MOT2	YER068W	-	PTM	cytoplasm
ENV9	YOR246C	-	vesicle traffic	LD
YMR1	YJR110W	-	protein traffic	cytoplasm
MRPL8	YJL063C	-	translation	mitochondrion
PFA3	YNL326C	-	vesicle traffic	fungal type vacuole membrane
POM33	YLL023C	-	unclassified	ER
SUR2	YDR297W	-	lipid metabolism	ER membrane
MTC5	YDR128W	-	unclassified	fungal type vacuole membrane
VMA22	YHR060W	-	chaperone	ER
SSQ1	YLR369W	-	chaperone	mitochonrial matrix
VTC1	YER072W	-	vesicle traffic	ER, vacuolar membrane
DYN1	YKR054C	-	unclassified	cytoplasm
ERR2	YPL281C	-	amino acid metabolism	unknown

Chapter 6 Summary

Volatile esters have distinct aromas and flavors, and are produced during fruit ripening and beverage fermentation. Short and medium chain fatty acid esters are widely applied in food, dairy, cosmetic and pharmaceuticals industries. Industrial production of these chemicals has been an effort of metabolic engineering in the last decade. It has been successfully achieved in microbial cell factories, such as *E. coli* and yeast. However, the yield, titer and productivity are not high and remain to be improved. The physiological role and metabolic pathways of volatile esters production in yeast also are not well known. In yeast, alcohol-O-acetyl/acyltransferase is responsible for short and medium chain fatty acid ethyl ester production, catalyzing the condensation of ethanol and acetyl/acyl-CoAs. The overall goal of this thesis is to understand and engineer AATases in yeast. New fundamental understandings of AATases and new biotechnologies will help accelerate the progress of industrial production of FAEEs. With respect to this, several scientific questions and engineering strategies are addressed and developed in this thesis.

Compared to the natural extraction and Fisher esterification synthesis, an attractive approach to produce short and medium chain FAEEs is by microbial cell factories. In chapter 2, six AATases from yeast and fruit tomato were evaluated with respect to activity, intracellular localization, and expression level in two most common microbial cell factories, *S. cerevisiae* and *E. coli*. The results provide important information on the biochemical properties of AATases under homologous and heterologous expressions. All

AATases formed aggregates with low specific enzymatic activity when expressed in *E. coli*. In addition, the membrane association observed in *S. cerevisiae* was lost in *E. coli*, which could partially explain the low function is *E. coli*. Therefore, we demonstrate that *S. cerevisiae* is a better microbial host to produce short and medium chain FAEEs compared to *E. coli*.

To discover and protein engineer highly active AATases, an effective screening method is required. However, traditional measurement methods, such as gas chromatography (GC) and thin-layer chromatography (TLC), are low throughput and time consuming. To overcome this, we have developed a rapid and high throughput screening method for AATases activity and substrate specificity in Chapter 3. The produced CoA-SH by AATase is coverted to succinyl-CoA by a-KGDH with other saturated substrates. The rate of produced NADH from NAD^+ is measured by following the absorbance at 340nm. This spectrophotometer based coupled enzyme assay is applied to screen a library of AATases for fatty acid ethyl ester synthesis. Atf from *Solanum lycopersicum* was discovered to be active towards short and medium chain acyl-CoAs and different alcohols, with preference to hexanoyl-CoA and 1-pentanol. Therefore, this assay will help accelerate the protein engineering and new enzyme discovery of AATase.

In Chapter 4, the concepts of substrate channeling and enzyme-colocalization were applied to increase efficiency and yield of ethyl acetate synthesis pathway in *S. cerevisiae*. We design a protein scaffold based on the plant LD targeting protein oleosin, and cohesin/dockerin protein-protein interaction pairs (OCD). The upstream enzymes of ester biosynthesis pathway, Acs1 and Ald6 are naturally localized to

cytosol/mitochondria and cytosol, respectively. By this OCD scaffold, Acs1 and Ald6 were recruited and relocalized to the outer surface of LDs, the localization of terminal step, Atf1. This produces a clustered three-step pathway on LDs membrane that channels key intermediates between enzymes. The multiple enzymes colocalization was demonstrated by Förster Resonance Energy Transfer (FRET) and the effect of substrate channeling wass demonstrated by *in vitro* kinetic analysis. We further optimized the scaffold and pathway expression levels and the production rate of ethyl acetate *in vivo* increased ~ 2-fold. Colocalization of multiple enzymes on LDs is a possible strategy for engineering synthetic metabolic pathways on membranes.

In addition to engineering AATase, we find that AATases, Atf1, Atf2 and Eht1, are membrane-associated proteins and localized on LDs during stationary phase in *S. cerevisiae*. LDs have been the focus of many studies for they play crucial role in energy and lipid metabolism. They are composed of a core neutral lipids and a monolayer of phospholipids. Proteome studies identify a distinctive set of proteins decorating LDs. However, lots of questions about LDs remain to be elucidated. For example, what is the mechanism of LD biogenesis? How do proteins specifically target to LDs? And what is the physiological role of LDs besides lipid metabolism and storage? In this thesis, we focus on one class of enzymes, AATase, to understand the LDs localization and trafficking.

In Chapter 5, structure-function analysis and a protein-protein interaction study were performed. Eht1 and Eeb1 are responsible for medium chain fatty acid esters production in *S. cerevisiae*, and the pair of paralogues arose from genome duplication. They are

closely related, with 58% sequence identity and 73% sequence similarity at amino acid sequence level. Eht1 and Eeb1 are initially localized to ER membrane and subsequently sorted to LDs and mitochondria, respectively. Truncations from either N- or C-termini disrupt the membrane association of Eht1, indicating that both terminal regions are important. However, N- and C-terminal amino acid sequences are not able to target GFP to ER or LDs, suggesting that the internal region might be also involved. As another function recovery study example, the N- or C-terminal region of Eeb1 was replaced with the amino acid sequences of Eht1. Eeb1$^{\text{Eht1 2-13}}$ localized to LDs instead of mitochondria by N-terminal amino acid sequence replacement, whereas Eeb1$^{\text{Eht1 429-451}}$ remains mitochondria localization. Furthermore, the alanine-stretch screening of N-terminal region of Eht1 suggests that the 14-21 amino acids are the most important region.

Membrane-associated proteins always contain the hydrophobic transmembrane domains. However, our hydropathy analysis suggests that there are no transmembrane domains with high confidence for Eht1 and Eeb1. Membrane topology assay experimentally shows that they are peripheral membrane proteins on ER.

An interesting finding is that the LD targeting Eht1 and its mutants are always initially targeted to ER. It suggests that the translocons might be involved in the Eht1 trafficking process from ER to LDs. To answer this question, the knockout and gene silencing experiments are performed for Eht1, Eeb1 and Eeb1$^{\text{Eht1 2-13}}$. Knockdown of *SEC61* (encoding for common translocon) or knockout *SSH1* (encoding for alternative translocon) does not affect the ER targeting and LD localization of Eht1 and Eeb1 $^{\text{Eht1 2-13}}$. Also, the knockout of accessory factor genes does not have any effect for $^{\text{Eht1 2-13}}$ ER

targeting and translocation to LDs. The significant effect is only observed when *SEC61* is knockdown and *SSH1* is knockout. These results suggest that both translocons might be related to Eht1 ER targeting and sorting process to LD.

It has been reported that proteins are involved in the lipid trafficking from ER to LDs. We hypothesize that proteins might also be involved in the protein trafficking from ER to LDs. Therefore, immunoprecipitation and mass spectrometry were performed to study the physical protein-protein interaction of Eht1 on ER. 48 proteins of high confidence were identified to have interactions with Eht1. We found 12 proteins related to protein trafficking and vesicle trafficking. One of interest is Snd2p, which is a key component of SND (SRP-independent) pathway. From Aviram's study, it is suggested that Eht1 and Eeb1 undergo SND pathway to be targeted to ER, a conclusion that supports our result. Some accessory factors related to the common translocon on ER were also identified in the screen. With these results, we choose some of the genes encoding for the Eht1 interacting proteins and knock them out. The localization and trafficking of Eht1-GFP were examined with these gene knockout strains. We demonstrated that *ERG5* knockout blocks the translocation of Eht1p from ER, suggesting that Erg5p might be related to the secretion of Eht1p. Knockout of *ERG5* affects the morphology of LDs, the amount of LDs increases while size decreases. This opens to an interesting question, is Erg5p specific for Eht1p or is it general for AATase or even for a broad range of proteins lacking TMD but associated with LD? And also, is this effect directly resulted from Erg5p or it is because of the changed morphology of LD?

Returning to the respect of AATase activity *in vivo*, it has been demonstrated that the overexpression of Eht1 or Eeb1 does not increase FAEE synthesis. It could be explained by the limited accessibility of substrates, especially acyl-CoAs. However, from our study, we found that after changing the N- and C-terminal amino acid sequences, the protein expression level and enzymatic activity of Eeb1 increase while the transcription level decreases. This might because the changed trafficking pathway stabilizes $Eeb1^{Mut}$ and prevents it from degradation. The different protein loading capacity of mitochondria and LDs could be an alternative explanation.

In this thesis, we have demonstrated that *S. cerevisiae* is a better microbial cell factory for short and medium chain FAEE production. We have developed a rapid and high throughput screening method for discovery and protein engineering of AATase. In addition, we developed and analyzed a protein scaffold to co-localize pathway enzymes on LDs to improve the pathway production rate and yield based on the concept of protein colocalization and substrate channeling. Furthermore, we open up to understand the AATase LD localization and protein trafficking mechanism. Taken together, this thesis spans from understanding of AATases biochemical properties and trafficking mechanisms to metabolic and pathway engineering of short and medium chain FAEEs production in *S. cerevisiae*.